Maximilian Maierhofer, BSc

Porphyrin Based Complexes with Enhanced Spectral Properties for Oxygen Sensing

MASTER THESIS

to achieve the university degree of

Master of Science (MSc)

Master's degree programme: Chemistry

submitted to

Graz University of Technology

Supervisor
Ass. Prof. kand. Sergey Borisov

Institute of Analytical Chemistry and Food Chemistry

Graz, March, 2017

Невозможно всё время выигрывать, но зато возможно проигрывать.

Abstract

The aim of this thesis was the investigation of new pathways leading to long-wavelength absorbing phosphorescent metalloporphyrins suitable for oxygen sensing. In this work a new phthalocyanine dye based on a carbazole precursor was synthesized. This dye showed a significantly red shifted absorption as well as emission spectra compared to the reference Zinc-tetra-tert-butyl-phthalocyanine (Zn-TtBu-Pc). Furthermore, two new benzoporphyrin dyes could be synthesized via Friedel-Crafts acylation of platinum(II)/palladium(II) meso-tetra(4-fluorophenyl)-tetrabenzoporphyrin (Pt/Pd-TPTBPF). These two dyes show similar luminescent lifetimes and increased quantum yields compared to the references platinum(II)/palladium(II) meso-tetraphenyl-tetrabenzoporphyrine (Pt/Pd-TPTBP). Additionally, platinum(II) meso-tetra(4-tert-butyl-phenyl)-tetrabromobenzoporphyrin (Pt-TPTtBuBPBr) was modified by Sonogashira coupling at the β-position leading to a new Pt(II) porphyrin complex. For the formation of J-aggregates the synthesis of highly soluble porphyrin and phthalocyanine dyes was attempted. Moreover the modification of a phenanthroline based chelate complex ($Pt(Ph_2N_2O_2)dpp$) was attempted by the introduction of a push-pull moiety at the N_2O_2 chelate ligand, which was expected to lead to a bathochromic shift of absorption spectra and an increased brightness.

Kurzfassung

Das Hauptziel dieser Arbeit war die Erschließung neuer Synthesestrategien von langwellig-absorbierenden und phosphoreszierenden Metalloporphyrinen, welche für Sauerstoffmessungen anwendbar sind. Im Zuge dieser Arbeit wurde ein neuer Phthalocyanin Farbstoff, welcher ein modifiziertes Carbazol als Hauptbaustein besitzt, synthetisiert. Im Vergleich zu Zink-tetra-tert-butyl-phthalocyanin (Zn-TtBu-Pc) verfügt dieser Farbstoff über ein signifikant langwellig verschobenes Absorptions- sowie Emissionsspektrum. Mittels Friedel-Crafts Acylierung von Platin(II)/Palladium(II) meso-tetra(4-fluorophenyl)-tetrabenzoporphyrin (Pt/Pd-TPTBPF) konnten zwei neue Benzoporphyrin-Farbstoffe synthetisiert werden. Diese zeigen im Vergleich mit den jeweiligen Platin(II)/Palladium(II) meso-tetraphenyl-tetrabenzoporphyrin (Pt/Pd-TPTBP) Referenzen ähnliche Phosphoreszenz-Lebenszeiten, sowie erhöhte Quantenausbeuten. Zusätzlich wurde Platin(II) meso-tetra(4-tert-butyl-phenyl)-tetrabromobenzoporphyrin (Pt-TPTtBuBPBr) via Sonogashira Kupplungsreaktion an den β-Positionen des Porphyrinkerns erweitert. Für die Bildung von J-Aggregaten wären gut lösliche Porphyrin- und Phthalocyanin-Farbstoffe getestet worden. Zuletzt wurde versucht ein Phenanthrolin basierter Chelat Komplex ($Pt(Ph_2N_2O_2)dpp$) mittels der Einführung einer Donor-Akzeptor Gruppe am N_2O_2 Chelat Liganden zu erweitern. Diese Modifikation soll das Absorptionsmaximum des Komplexes weiter in Richtung des roten Bereichs verschieben, sowie dessen Helligkeit erhöhen.

EIDESSTATTLICHE ERKLÄRUNG

Ich erkläre an Eides statt, dass ich die vorliegende Arbeit selbstständig verfasst, andere als die angegebenen Quellen/Hilfsmittel nicht benutzt, und die den benutzten Quellen wörtlich und inhaltlich entnommenen Stellen als solche kenntlich gemacht habe. Das in TUGRAZonline hochgeladene Textdokument ist mit der vorliegenden Masterarbeit identisch.

AFFIDAVIT

I declare that I have authored this thesis independently, that I have not used other than the declared sources/resources, and that I have explicitly indicated all material which has been quoted either literally or by content from the sources used. The text document uploaded to TUGRAZonline is identical to the present master's thesis.

10. März, 2017

Datum/Date

Unterschrift/Signature

Danksagung

Сергей, огромное спасибо, что когда у меня возникали вопросы или же я не знал в каком направлении двигаться дальше, всегда, в любое время, в любой день, независимо от того где Вы находились, Вы давали мне конкретные и полезные советы. Ещё раз, огромное Вам спасибо за оказаную поддержку и помощь, и интересную совместную работу!
Danke Ingo für die Möglichkeit in einer so lustigen und gut zusammenarbeitenden Arbeitsgruppe meine Masterarbeit machen zu können.
Wenn ich hier jetzt alle einzelnen Personen aufzählen würde, die ein großes Dankeschön an diesem Institut verdienen, würde ich mit meiner Masterarbeit wohl heuer nicht mehr fertig werden. Daher ein rießengroßes Dankeschön an das gesamte Team des Instituts für die echt tolle Stimmung, egal ob während der Arbeit im Labor, in den Kaffee bzw. Kuchenpausen oder beim Mittagessen. Auch das ein oder andere Feierabend-Bier blieb uns zum Glück nicht verwehrt. Die gemeinsamen *Social Events* wie Wandertopfkochen, Beach Volleyball oder Biathlon sind immer ein Hit mit euch. Daher freue ich mich auf die kommenden drei spannenden Jahre mit euch allen.
Peter, als mein Quasibetreuer, sollte ich allerdings nicht vergessen dir extra zu danken, deswegen Danke für Rat und Tat; du warst stets bemüht mir meine nervigen Fragen beantworten zu können.
Ebenso möchte ich mich bei meinen Studienkollegen bedanken, welche diesen Weg seit dem WS 2011 mit mir gegangen sind. Es war mir zumeist eine Freude mit euch diesen Weg gehen zu dürfen.
Ohne meine Familie wäre ich natürlich gar nicht in der Lage diese Arbeit zu verfassen, denn ihr habt mich immer unterstützt, egal was ich gemacht habe, ob sportlich oder schulisch und auch später bei der Wahl meines Studiums hatte ich freie Hand. Mama, Papa und Sebi, ich danke euch von ganzem Herzen für alles, was ihr für mich auf euch nehmt. Jessi, Danke, dass du immer für mich da bist, egal ob es stressige oder ruhige Zeiten sind, du hältst mich immer aus und erdest mich wenn ich es brauche.
Des Weiteren möchte ich meinem Gymnasiallehrer Herrn Tobias Fröhlich danken, dass er schon zu Schulzeiten den Forschertrieb in mir weckte, ohne Sie hätte ich vielleicht gar nicht die naturwissenschaftliche Richtung eingeschlagen.

Maximilian Maierhofer, BSc Graz, March, 2017

Contents

1 Introduction

Oxygen is an essential agent for life on our planet. Thus measurements of this chemical species are very important in many fields of our daily life.
On one hand, there are some classical methods: Winkler titration [1] and amperometric measurement [2]. But also measurement via thermoluminescence [3] or via chemiluminescence [4] are possible.
The Clark electrode, for example, is robust and commonly used. Nevertheless it has some disadvantages. It is bulky and the traditional methods are limited by oxygen consumption during the utilization time, comparatively long response times and electrical interferences. The electrode can also be poisoned by sample constituents.
On the other hand, oxygen concentration can also be measured optically with the help of sensors. On the contrary optical oxygen sensors do not suffer from electrical interferences, have the advantages of selectivity, are stable against ambient or scattered light, mostly inexpensive and easy to miniaturize, minimally invasive or non-invasive [5], can be used as films, fibers and even nanoparticles. Nanoparticles have usually an improved photostability and have less toxicity than molecular dyes [6].
Nanoparticles furthermore have very small dimensions so that they can enter cells [7] to measure e.g. the oxygen concentration in a living cell [8]. Another application for an optical oxygen sensor in the clinical field can be the analysis of gas in the bloodstream and the vascular system of a patient [9, 10]. Furthermore oxygen sensing in breath gas (respiratory diagnosis) and imaging of oxygen in skin can be performed [11]. Further fields of application can be found in environmental and marine analysis, molecular biotechnology, bioprocess control (contactless sensing in a bioreactor), food packaging and industrial production monitoring like the brewing industry or wine production [12]. Additionally, optical oxygen sensors can be used for difficult applications where other systems like the electrochemical sensors are not suitable. Here one has to mention fiber optic sensors which can measure over large distances and in spite of strong electromagnetic fields. Optical oxygen sensors are also suitable for sensing over large areas (skin, aerodynamics, marine ground profiles) [11].

The most common class of optical oxygen sensors is based on Pt(II) or Pd(II) metalloporphyrin macrocycles. These have some advantages such as good sensitivity and strong phosphorescence which will be described later. Furthermore different classes of porphyrins exist such as metalloporphyrins, benzoporphyrins, naphthoporphyrins and even hybrid classes, which have very promising optical properties such as strong phosphorescence, large Stoke's shift and high

molar absorption coefficients [12]. Due to many different synthetic modifications properties like solubility, photostability, absorption wavelength, etc can be tuned, enabling various fields of application. Some examples are photovoltaic and solar-cells[13], technology, medicine [14] and catalysis [15].

Phthalocyanines have a similar ground structure as porphyrins and are also very variable in their design. Additionally they show high chemical and thermal stability and are even more photostable than benzoporphyrins [12] [16]. Their spectral properties make them interesting for certain application fields in industry and biomedicine. Some of them are already applied in nonlinear optics [17, 18], gas sensing [19], catalysis [20], liquid crystals [21] and photosensitization [22, 23]. Phthalocyanine derivatives have also several applications as sensitizers in photodynamic therapy (PDT).

2 Theoretical Background

This chapter is mostly based on references [24–27]. Other references will be cited separately.

2.1 Luminescence

Luminescence is the emission of photons (ultraviolet, visible or infrared) which is based on relaxation of electronically excited molecules. By a source of energy an electron is excited from its ground state (S_0) to an electronically higher level (excited state, e.g. S_1). After this it relaxes from its excited state to its ground state. Due to this the electron loses energy either by electromagnetic radiation or by heat. This generated radiation is called luminescence. The most important type of luminescence is photoluminescence which occurs after excitation with light. It is one possible effect emerging from the interplay of light and matter. Specific cases of photoluminescence are either called fluorescence if the relaxation is spin-allowed or phosphorescence, a spin-forbidden process (described in section 2.1.5 on page 7). These two cases are not the only pathways of de-excitation processes after the absorption of a photon by a molecule. Also internal conversion (IC), intersystem crossing (ISC) and intramolecular charge transfer or conformational changes are potential pathways. A molecule that absorbs a photon from the VIS range is usually called dye or luminophore.

2.1.1 Absorption of light

A molecule in its ground state can absorb a photon of discrete energy (very fast process takes about $10^{-15}\,s$). This energy is equal to the energy difference between its ground state and its excited states. Both orbitals involved are the highest occupied molecular orbital (HOMO) and the lowest unoccupied molecular orbital (LUMO). Thus an electron from the LUMO is lifted to the energetically higher HOMO. Generally this excitation can happen from a sigma (σ), pi (π) or non-bonding orbital (n) to their appropriate antibonding orbitals σ^* or π^*. This is the common order for these electronic transitions:

$$n \rightarrow \pi^* < \pi \rightarrow \pi^* < n \rightarrow \sigma^* < \sigma \rightarrow \pi^* < \sigma \rightarrow \sigma^* \tag{2.1}$$

Usually the raise of a sigma electron needs plenty of energy (light from the far UV) so these

transitions are less important in spectrometric analysis. For transitions from n or π to π^* generally energy from light in the UV-visible light is needed. The absorbane at a specific wavelength can be expressed with the Beer-Lambert Law:

$$A = log\left(\frac{I_0}{I}\right) = \epsilon \cdot c \cdot d \tag{2.2}$$

A	absorbance
I_0/I	intensity of light entering/leaving the absorbing medium
ϵ	molar absorption coefficient $\left[\frac{l}{mol*cm}\right]$
c	concentration of absorbing species $\left[\frac{mol}{l}\right]$
d	thickness of absorbing medium [cm]

In a fully occupied orbital there are two electrons with opposite spins ($+\frac{1}{2}$ and $-\frac{1}{2}$). If one of these electrons is transferred to an energetically higher molecular orbital (MO), the spin of this electron is not changed in principle, so that the sum of the spins is still zero.

Whether the multiplicities ($M = 2S + 1$) of the ground and the excited state are 1, both are named as singlet state (e.g. S_0, S_1). If it occurs that the spin of an electron changes within the conversion so that in the energetically higher state are two electrons with the same spin. Due to this, the total spin quantum number is now 1 and the multiplicity 3. Such state is called triplet state (T_0) because it corresponds to three states of equal energy.

2.1.2 Franck-Condon principle

In addition to the named references in section 2.1 sections 2.1.2 - 2.1.4 are also based on reference [28]. Corresponding to the Born-Oppenheimer approximation the movement of the nuclei is very low compared to the fluctuation of electrons. The promotion of an electron from its ground state to its excited state takes about $10^{-15}\,s$, whereas molecular vibrations require $10^{-10} - 10^{-12}\,s$.

Therefore electronic transition nuclei do not change their position, so that the atoms have the same interspace between each other in both states. According to the Boltzmann distribution, most of the molecules are in the lowest energy-level of the ground state at room temperature. As figure 2.1 on page 5 shows, the energy curve (y-axes) as function of nuclear configuration (x-axes). This function describes a vertical transition from ground to excited state.

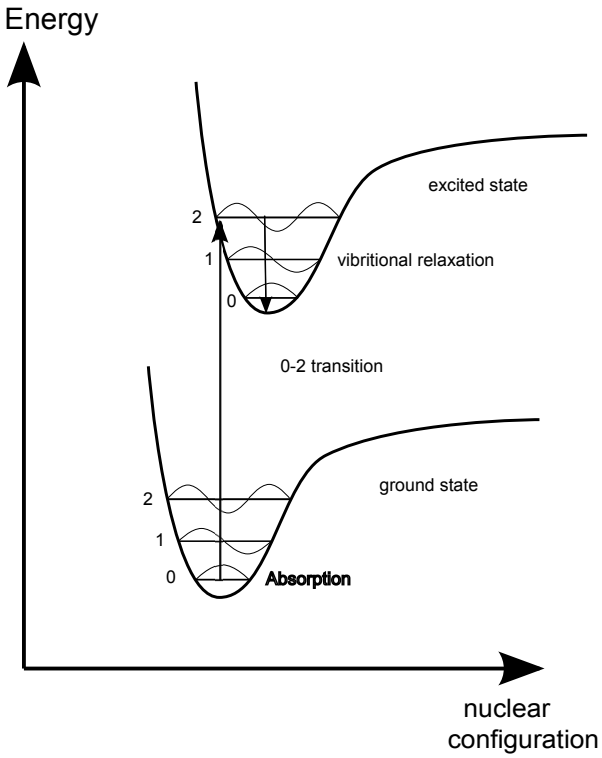

Figure 2.1: Franck-Condon Principle

2.1.3 Characteristics of fluorescence emission

Selection rules

There are two major selection rules for electron transitions: Transitions can be *spin-forbidden* and *symmetry-forbidden* which decreases their probability of occurrence. Spin-forbidden transitions are between states of different multiplicities (e.g. from singlet to triplet state and vice versa). Transitions can, in addition to that, be forbidden for symmetry reasons. Here it depends on the overlap and the symmetry of the involved orbitals. Based on molecular vibrations some symmetry forbidden transitions can become possible.

Perrin-Jablonski diagram

The Perrin-Jablonski diagram (see figure 2.2 on page 6) shows possible processes. Absorption and the so called intrinsic pathways of de-excitation which are intersystem crossing, internal conversion, fluorescence, phosphorescence, delayed phosphorescence and triplet-triplet transitions.

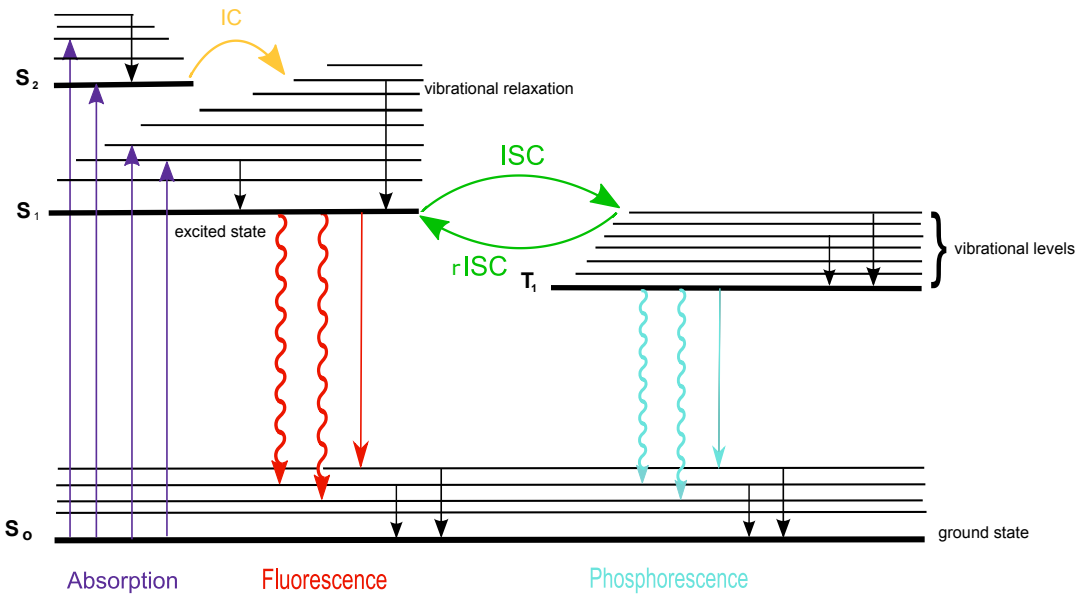

Figure 2.2: Jablonski diagram

The ground state is titled as S_0, excited singlet state as S_1, or S_2, excited triplet state as T_1. According to Hunds rule, the triplet state has a lower energy than the singlet state. Each state has its own vibrational levels. As mentioned before, absorption is a transition of an electron from S_0 to S_1/S_2. After the absorption of a photon the electron can undergo several de-excitation processes. These can either be radiative or non-radiative.

2.1.4 Non-radiative processes

Internal Conversion (IC)

IC occurs between states of the same multiplicity (spin-allowed) and from a higher to a lower vibrational level (e.g. S_1 to S_0). This action can be followed by a vibrational relaxation for the lowest vibrational level of the particular lower electronic state. IC from S_2 to S_1 is observed with a time-scale of about $10^{-13} - 10^{-11}\,s$. The energy gap between S_1 and S_0 is higher and therefore IC between these two states is slower so other transitions like fluorescence and ISC with following phosphorescence can be observed.

Intersystem Crossing (ISC)

ISC is a transition between two isoenergetic vibrational levels of electronic states with various multiplicities (e.g. S_1 to T_1). Subsequent vibrational relaxation brings a molecule to its lowest vibrational level of T_1. As mentioned in 2.1.3, a change of multiplicity is a change of spin and therefore this transition is spin-forbidden. Spin-orbit coupling can be large enough to allow ISC. This is favored at the presence of heavy atoms like Br or Pb. ISC can compete with other

phenomena like fluorescence and internal conversion because its time-rate is with $10^{-7} - 10^{-9}\,s$ fast enough.

reverse Intersystem Crossing (rISC)

If the energy gap between T_1 and S_1 is small, another process can occur besides IC and phosphorescence. This process is called reverse intersystem crossing. Due to the fact that this transition is thermally activated its occurrence increases with increasing temperature. But for reaching the S_1 level there is another possibility; the triplet-triplet annihilation (see delayed fluorescence).

2.1.5 Radiative processes

Fluorescence

The emission of a photon during the transition from S_1 to any vibrational level of S_0 is called fluorescence. Its characteristics do not depend on the excitation wavelength as this process results from the emission of S_1. Usually emitted light has a lower energy than the light which was needed for absorption so that the fluorescence spectrum is shifted bathochromically comparing to the absorption spectrum. This difference between absorption and fluorescence is called *Stokes shift*. The emission of a photon takes about 10^{-9} s.

Phosphorescence

Phosphorescence is a radiative de-excitation process, which can only occur after ISC. This requires a transition from T_1 to S_0. During the transition there is a change of multiplicity; therefore it is a spin-forbidden process and a slow one ($10^{-6} - 1\,s$). Nevertheless it is often observed at low temperatures and in a rigid matrix. Due to spin-orbit coupling which is favored by heavy atoms, this transition can be observed. For the specific compounds at RT or 77 K the spectrum of phosphorescence is located at longer wavelengths than the fluorescence spectrum. This is due to the fact, that the energy of the lowest vibrational level of T_1 is lower than the energy of S_1 (Hunds rule).

Delayed Fluorescence

There are diffrent types of delayed fluorescence. Similar to fluorescence the E-type of delayed fluorescence is also from S_1 to S_0, but it can only happen after ISC (S_1 to T_1) and afterwards reverse ISC (rISC, T_1 to S_1). The spectrum is identical to that of fluorescence but the lifetime of the luminescence is significantly longer than in normal fluorescence. The efficiency of rISC rises with increasing temperature. Also the energy gap between S_1 and T_1 has to be very small. Another type of delayed fluorescence is triplet-triplet annihilation (P-type, spin-allowed). For this two excited molecules (T_1) have to collide and thereby one of them is transferred to the S_1 state while the other molecule relaxes to its ground state.

2.1.6 Lifetime

If a molecule absorbs a photon, it rises from S_0 to an excited state like S_1. After that it can undergo radiative (e.g. fluorescence) or non-radiative deactivation processes (IC or ISC). This happens not immediately, so that the molecule remains a specific time in its excited state (e.g. S_1 or T_1). This time is called lifetime of the excited state τ. The rate constant k of this deactivation processes can be described by kinetics of the first order.

$$k = k_{non-radiative} + k_{radiative} \tag{2.3}$$

$$-\frac{d[A^*]}{dt} = \frac{k}{[A^*]} \tag{2.4}$$

[A*]	concentration of species A in excited state $\left[\frac{mol}{l}\right]$
t	time [s]
$k_{radiative}$/k_r	rate constant for radiative deactivation from S_1 to S_0

$$\tau_s = \frac{t}{k} \tag{2.5}$$

τ_s lifetime of excited state

The integration of the differential equation (2.4) leads to the resulting equation (2.6).

$$[A_t^*] = [A_0^*] \cdot e^{-\frac{t}{\tau}} \tag{2.6}$$

From the last equation we can deflect that the fluorescence intensity decreases exponentially if there is no excitation anymore. Usual lifetimes are for S_1 $10^{-10} - 10^{-7}\,s$ and for T_1 about $10^{-6} - 1\,s$.

2.1.7 Quantum yield

In reality not every excited molecule emits a corresponding photon by a radiative transition due to the fact that non-radiative deactivation processes compete with fluorescence and phosphorescence. This is defined by the fluorescence quantum yield Φ_F. The quantum yield of fluorescence is the quotient of emitted photons to absorbed photons. Φ_F can be described with the following equation:

$$\Phi_F = k_r \cdot \tau_s = \frac{\tau_s}{\tau_r} \tag{2.7}$$

Φ_F quantum yield
τ_r radiative lifetime

If the temperature increases, the fluorescence quantum yield usually decreases because non-radiative transitions occur easier with increasing temperature (thermal agitation).

2.1.8 Luminescence quenching

Quenching is a bimolecular radiationless de-excitation process involving an excited molecule (M^*) and a quencher (Q). Possible photophysical interactions are collision with a heavy atom or paramagnetic species, excimer/exciplex formation, proton, electron or energy transfer. Two main quenching types will be described in the following. These two are called static quenching and dynamic quenching.

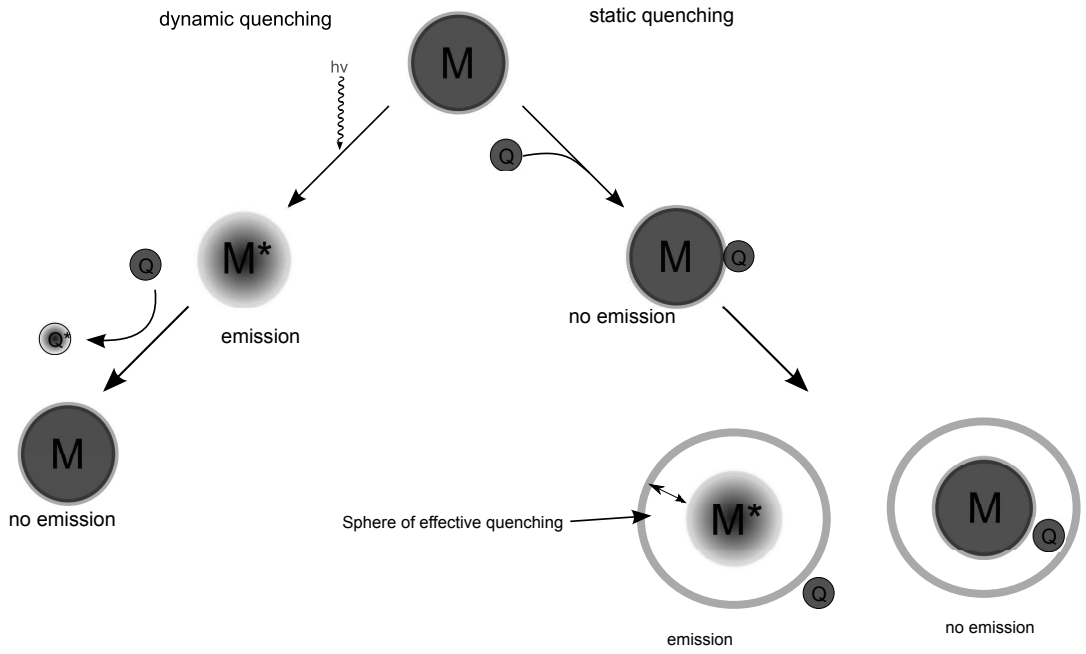

Figure 2.3: Dynamic and static quenching mechanism

Static quenching

For static quenching a non-fluorescence complex MQ has to be formed. This can happen on two main pathways.Either this complex is formed by M and Q in their ground states or it occurs because of the existence of a sphere for efficient quenching. The second process is possible if the distance between Q and M^* is small enough for quenching (see figure 2.3). Nevertheless these two pathways decrease the concentration of the luminophore. Static quenching does not affect the lifetime of the uncomplexed fluorophore M by quencher in contrast to the dynamic quenching.

Dynamic quenching

Here the quencher Q collides with the luminophore in its excited state M* and, due to an energy transfer from M* to Q, the luminescence is quenched. Dynamic quenching is a diffusion controlled non-radiative process. A longer lifetime of the excited state increases the probability of quenching. The rate constant is lifetime-dependent and the lifetime of the luminophore is reduced in presence of a quencher molecule. If Q and M* are identical molecules, the process is called self-quenching.

2.1.9 Stern-Volmer kinetics

The kinetics of dynamic quenching can be described by the Stern-Volmer-equation (see equation 2.8) where the $\frac{I_0}{I}$ and $\frac{\tau_0}{\tau}$ are both described by the Stern-Volmer equation. These two quotients increase, in an optimal case, linear to the concentration of Q and K_{SV} describes the slope of the curve. This equation is almost always valid for measurements in solution.

$$\frac{I_0}{I} = \frac{\tau_0}{\tau} = 1 + k_q \cdot \tau_0 \cdot [Q] = 1 + K_{SV} \cdot [Q] \tag{2.8}$$

I_0, τ_0	fluorescence intensity and decay time in absence of Q
I, τ	fluorescence intensity and decay time in presence of Q
$[Q]$	concentration of quencher molecule
K_{SV}	Stern-Volmer constant

2.1.10 Two-Site Model

Equation 2.8 is suitable for solutions but for further applications it is mostly necessary to embed the dye into a matrix. Here, not all dye molecules are identical accessible and therefore there are different domains in a sensor matrix. Due to this fact there are different quenching coefficients. Therefore Stern-Volmer plots show superimposed non-linear curves. For these systems it is necessary to include a second Stern-Volmer constant K^2_{SV} as well as a factor f which describes the dye distribution between the different sections (see 2.9).

$$\frac{I}{I_0} = \frac{f}{1 + K^1_{SV} \cdot p_{O_2}} + \frac{1 - f}{1 + K^2_{SV} \cdot p_{O_2}} \tag{2.9}$$

Here f is the fraction of the total emission for the first site and K^1_{SV} and K^2_{SV} are the Stern-Volmer quenching constants (equal to K_{SV} in equation 2.8) for the two sites. The two sites are representing two different environments in the sensor matrix [29].

2.2 Optical sensors and optical oxygen sensors

In 1990 Wolfbeis defined the term chemical sensor as the following: *"Chemical sensors are small-sized devices comprising a recognition element, a transduction element, and a signal processor capable of continuously and reversibly reporting a chemical concentration." [30]* Basically a sensor consists of the transduction platform and a following signal processing which yields the measured analyte concentration (see figure 2.4). In optical sensors the transducer has typically its specific optical transduction (e.g. absorption, fluorescence or phosphorescence) [31].

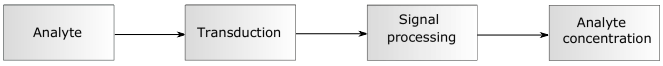

Figure 2.4: Functional principle of a sensor

Optical sensors can be divided roughly into two categories: intrinsic and extrinsic sensors. Intrinsic sensors monitor the optical characteristics of the analyte. Extrinsic optical sensors operate differently; here the sensors have to produce a signal resulting of an interaction between analyte and indicator because the analyte itself does not provide an optical signal which can be detected. This interaction can either be of physically or chemically nature. The signal is translated from a chemical/physical one to an electric one. Optical oxygen sensors do work by the principle of dynamic quenching which can be described by Stern-Volmer kinetics. Here the luminescence of the dye (fluorescence or phosphorescence) is quenched by molecular triplet oxygen. The oxygen concentration can be measured by intensity or lifetime based measurement techniques. To avoid cross-sensitivity to other analytes, the sensing material is dissolved in a polymer (matrix, permeable for oxygen) [5], so that the thin polymer layer acts as a barrier for ions or metals. Because of this there is less contamination by disturbing compounds. Moreover, (nano)particles can be used instead of a polymer film.

2.2.1 Advantages of optical oxygen sensors

As mentioned in the introduction, there are some other techniques to measure oxygen-concentration (e.g. Winkler tiration, Clark electrode). There are various reasons why optical oxygen sensors have advantages on other systems; on one hand it is not a diffusion-controlled technique such as the Clark electrode [2]. On the other hand e.g. a titration (Winkler titration) [1] is very slow and time-consuming; this is not the case with optical oxygen sensors. Nevertheless the Clark electrode is the conventional method but is more and more replaced by optical oxygen sensors. Also the classical Clark electrode is not suitable for measurement in very low oxygen concentrations. The most important advantage of an optical oxygen sensor is that they do not consume oxygen which makes them applicable for trace oxygen measurements [12] and are not affected by electric interferences [32]. Also they are inexpensive and can be miniaturized easily. This extends their fields of application to noninvasive and remote measurements. The sensitivity of optical oxygen sensors can be tuned by variation of dye and corresponding polymer [33].

2.2.2 Principle of an optical oxygen sensor

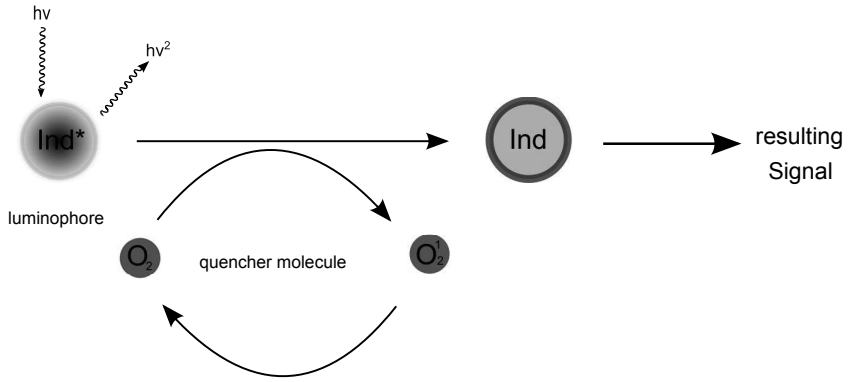

Figure 2.5: Principle of an optical oxygen sensor

The principle of optical oxygen sensors is based on a process of dynamic quenching (see 2.3 on page 9) of the used luminophore with oxygen (see figure 2.5). Generally the efficiency of dynamic quenching is depending on the lifetime of the excited state (see section 2.1.6 on page 8). Usually the luminophore is dissolved in a polymer matrix which is permeable to oxygen (see section 2.3.1 on page 14), so oxygen- and dye-molecules are able to interact.

Moreover the matrix serves as a permeation-selective barrier; thereby no other undesirable species can permeate inside to affect. As explained above, quenching results in a decrease of the luminescent lifetime. The mathematical interrelationship between lifetime and concentration is described with the Stern-Volmer-equation (see equation 2.8 on page 10). This equation is valid for the ideal case with totally homogeneous environment (dye solution). In most polymers, this is not the case. For this scenario another equation (two-site model, see 2.9 on page 10) is suitable which includes the effects of a heterogeneous environment.

Sensitivity of an optical oxygen sensor

Another important factor is the sensitivity of a sensor. Two main factors are very important for the development of a new oxygen sensor. First, the luminophore itself is very fundamental because the lifetime and the luminescence depend on its structure and type of this molecule. Generally longer τ leads to higher sensitivity. In addition to this, the gas permeability of the chosen matrix (see section 2.3.1 on page 14) is also important to determine the characteristics of the sensor. According to the desired properties of the sensor these two building blocks can be tuned so that the sensitivity is optimal for a specific application.

2.2.3 Measuring methods

Different methods of read out exist to measure oxygen concentrations. The first method is measuring of the luminescence intensity. This technique suffers from several drawbacks. Photobleaching of the dye, different dye concentrations or scattering and light source fluctuations affect the results. To overcome these drawbacks luminescence lifetime based read out methods are used. This can either be performed in time or in frequency domain. Here no special ratiometric fluorophores are necessary and the measurement is independent of intensity or fluorophore amount. By using the first method the dye is excited by a pulse of light. Then the time dependent decay is measured whereby the lifetime can be calculated. As example of frequency domain measurement method phase-fluorimetry (schematically shown in figure 2.6) is the most important measurement method. The used light for excitation is modulated at a specific frequency. The emitted light of the dye shows the same frequency but with a certain delay compared to the excitation light. This phase difference can be measured and is called phase shift ϕ.

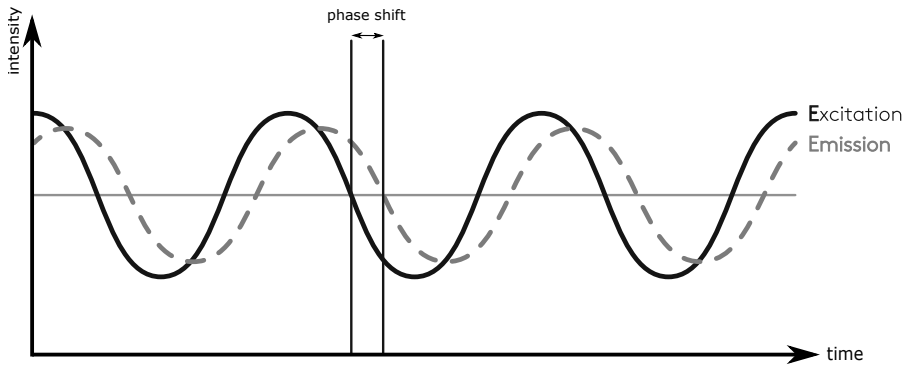

Figure 2.6: Principle of phase-fluorimetry

Equation 2.10 shows the relationship between τ, ϕ and f:

$$\tau = \frac{\tan(\phi)}{2\pi f} \tag{2.10}$$

ϕ phase shift [°]
τ phase shift lifetime [s]
f excitation frequency [Hz]

2.3 Matrices

A main assignment of a matrix is to prevent the luminophore of leaching. This can either be attained by covalent binding of the dye to the matrix or just by dissolution of a hydrophobic dye in a hydrophobic matrix. Another important function is to act as a solvent for luminophore and additives which allows diffusion. Also the selectivity and sensitivity of the sensor can be regulated by choosing different matrices.

A matrix prevents the luminophore against light interferences [34]. The speed of bleaching of the luminophore can be slowed down by using different matrices/solvents. In many cases the sensor, is fixed at the end of an optical fiber but also planar foils for imaging with a CCD camera are common. Usually these are either sol-gel glasses [35] like SiO_2 or TiO_2 or polymers like PS, PMMA and as plasticizer PVC.

The response time for sol-gel matrices are significantly lower [24]. Nevertheless other groups of polymers have also a very important role in this field. Silicone polymers, organic glassy polymers, fluoropolymers and cellulose derivative polymers can act as well as matrices in optical oxygen sensing [36].

2.3.1 Matrix permeability

In any case the chosen matrix must be permeable to oxygen to tune sensitivity of a sensor. This property is given by the oxygen permeability coefficient P [cm^3 (STP) cm^{-2} scmHg] (see equation 2.11).

$$P = S \cdot D \tag{2.11}$$

P is the product of diffusion constant D [cm^2s^{-1}] and solubility S [cm^3 (STP) cm^{-3} cmHg] [5]. These data for some usual matrices are given in table 2.1.

Table 2.1: Different properties of polymers for optical oxygen sensing

Polymer	$\mathbf{P \cdot (10^{13})}$	$\mathbf{D \cdot (10^{6})}$	$\mathbf{S \cdot (10^{6})}$	**reference**
poly(1-trimethylsily-1-propyne)	7700	47	170	[37]
poly(dimethylsiloxane)	695	40	24	[38]
poly(2,2,2-trifluoroethylmethacrylate)	32	15	0.27	[39]
poly(isobutylmethacrylate)	20	-	-	[5]
ethylcellulose	11.0	0.64	1.73	[40]
poly(methylmethacrylate)	0.116	1.4	-	[40]
cellulose acetate	0.585	-	-	[40]
cellulose acetobutyrate	3.56	-	-	[38]
polystyrene	2.63	-	-	[38]
poly(vinyl chloride)	0.034	-	-	[40]

2.3.2 Classification and requirements of polymers

As mentioned in the previous part of this section, the dye and its additives should dissolve in the polymer very well. The polymer should be chemically and physically/mechanically stable and, for biological applications, non-toxic. Furthermore a polymer has to be stable at higher temperatures and against ambient light. There should not be an intrinsic color/luminescence. For measurements it has to be transparent in the dispositive spectral range [34].

Silicon rubbers

These polymers are very usual especially for highly sensitive sensors because of their high P and chemical stability [5, 41]. For some poly(dimethyl siloxane)s it is reported that here oxygen has a very high P and S (see table 2.1) [38] but most dyes tend to aggregate inside these silicone rubbers.

Organic glassy polymers

Polystyrene, poly(methyl methacrylate), poly(isobutyl methacrylate) and poly(vinyl chloride) belong to this group. Polystyrene is often used with metalloporphyrins and $Ru(dpp)^{3+}$ [42]. The oxygen permeability coefficient and the solubility of oxygen is lower than in fluoropolymers and silicon polymers but this group provides mechanical strength even at thin layers [5].

Fluoropolymers

This group of polymers has two significant advantages; on the one hand P for oxygen is high and on the other hand these polymers are very resistant against irradiation and are also chemically resistant. That is due to their strong and short C-F bonds within the molecules [5]. Also aggregation can be prevented by fluorinated dyes.

Cellulose derivative polymers

Two main representatives are ethyl cellulose and cellulose acetate. These show usually high mechanical strength in thin films [5]. Their properties are also described in table 2.1. Another polymer to be mentioned here is a derivative of cellulose with tributyl phosphate (TBP) as plasticizer because this species has a high oxygen permeability coefficient. That is why cellulose acetate with TBP films is popular at optical oxygen sensing applications. Examples for this are very sensitive optical oxygen sensors based on Pd^{2+} or Pt^{2+} porphyrin complexes which were reported by Mills 1997 [33].

2.4 Indicators for oxygen sensors

2.4.1 Characteristics of an optimal indicator

Primarily reference [12] is used for this section, all other references are provided separately. In this chapter some important parameters an indicator should have are listed up:

- An indicator should have a large Stokes shift so that excitation and emission light can easily be separated.

- Responsible for the brightness of an indicator are a high molar absorption coefficient and high quantum yield. The higher the brightness of an indicator the less amount is needed to build up a sensor. This allows the preparation of thin layers leading to short response times, while simultaneously minimizing the risk of aggregation.

- For the sensitivity of a sensor the lifetime of an indicator dye is essential. This corresponds to the fact that a longer lifetime of a dye molecule increases the chance of a collision with a quencher molecule.

- The dye should have high solubility in a polymer matrix so that the luminophore is distributed nearly homogeneously. Usually the solubility of a dye in apolar matrices can be improved by insertion of bulky substituents like long alkyl chains.

- Another important point is the chemical and the photostability of the luminophore; e.g. Pt(II) and Pd(II) with highly fluorinated tetra(pentafluorophenyl)porphyrin ligand are known as one of the most photostable (due to electron withdrawing fluorine groups) indicators reported so far [43]. This is necessary to get constant data even at high light intensities or long measurement times.

- For biological and medical applications it is very important to use species which are non-toxic. The toxicity of an indicator can be significantly reduced by encapsulation in a polymer but the phototoxicity caused by singlet oxygen cannot be eliminated only partly.

- Besides these parameters shown above, an indicator should be cheap and the sensor assembling as simple as possible.

2.4.2 Classification of commonly used indicators

In the following two chapters several dye classes are explained which exist for oxygen sensing applications.

Absroption-based indicators

In this class there are two groups of indicators; *reversible* and *irreversible* probes.

Irreversible setups are used e.g. in food packaging. Here the species produces a visible color change to indicate a change in the composition of the head-space gas. For example methylene blue is one used molecule for an irreversible application [44]. Commonly known and used reversible systems consist of several organometallic compounds [45]. Another molecule which can bind reversibly to oxygen is a very important one in our human body: hemoglobin is responsible for the oxygen transport from blood to muscle cells.

Luminescent-based indicators: Polycyclic aromatic hydrocarbons

The most popular class of indicators is luminescence-based and includes several groups. The oldest group, which should be mentioned here, are the polycyclic aromatic hydrocarbons (PAHs). It consists of pyrene and its derivatives, decacyclene and other PAHs (e.g. perylene dibutyrate see 2.7 [46]).

This group of indicators has usually short luminescent lifetimes wherefore they should be dissolved in a very gas permeable matrix. The disadvantage here is that the luminophore is often badly soluble in the matrix. Nevertheless they have high quantum yields but also low molar absorption coefficients. That is why their brightness is relatively low and this group of indicators is not so significant anymore.

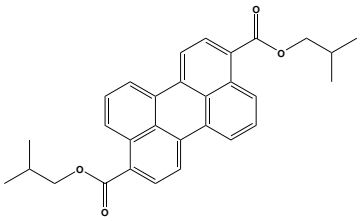

(a) perylene dibutyrate

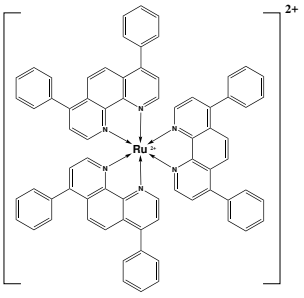

(b) $Ru(dpp)_3{}^{2+}$

Figure 2.7: Representative dyes for polycyclic aromatic hydrocarbons and transistion metal polypyridyl complexes

Transistion metal polypyridyl complexes

The second group contains transition metal polypyridyl complexes. Their central metal ions are usually Ru(II), Os(II) or Re(II). Generally the indicators of this group suffer from the fact that they are very easily influenced by temperature, that they have just a moderate molar absorption coefficient and also a relatively short lifetime of several microseconds.

Another problem is that the absorption wavelength of Ru(II)-complexes is in the blue part of the spectrum, wherefore this group of indicators cannot be used for many applications. However, Ru-polypyridyl complexes (e.g. $[Ru(dpp)_3]^{2+}$ see figure 2.7) have a very high Stokes shift and are photostable.

In addition to this, they can be tuned, but spectral variations are limited. Nevertheless these indicators are very popular in oxygen sensing. The last problem to be mentioned with this species is that usually the complexes are ionic molecules and the counter ion is inorganic. Due to this, the inorganic counter ion for the complex has to be exchanged with an organic ion to be soluble in hydrophobic matrices [47, 48].

2.5 Porphyrins and phthalocyanines

The most important group of luminescent indicators are metalloporphyrins with Pt(II) or Pd(II) as central ions. They have some advantages such as strong phosphorescence at room temperature, moderate to high molar molar absorption coefficients and large Stokes shifts.

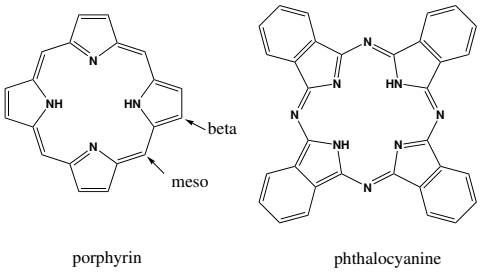

Figure 2.8: Structure of an unsubstituted porphyrin (l) and phthalocyanine (r)

But what are porphyrins? These macrocyclic compounds (see figure 2.8) are of natural origin and probably one of the most important pigments in nature. Four pyrroles and four methine carbons build up a square planar 18 π-aromatic ring structure [49]. These compounds are involved in many different processes occurring in nature like oxygen transport, fatty acid oxidation, cell respiration and even in light harvesting reactions [14, 50, 51]. Another interesting group are phthalocyanines (Pc, see figure 2.8). This group has the same ground structure as a benzoporphyrins (see figure 2.9 on page 20) but here nitrogen atoms act as bridging atoms. Both groups have the advantages of being structurally robust and showing chemical stability as well as intense absorption and emission behavior. Also their optical properties can be tuned over a wide range by extending their electronic π-system. For specific applications the ground structure can be modified via different substitutions at the ring system and choosing other central metals (like platinum, palladium, zinc, iridium,...) [12, 49]. Phthalocyanines have diverse application fields in industry, biomedicine and are important colorants. Some of them are applied in nonlinear optics [17, 18], gas sensing [19], catalysis [20], liquid crystals [21] and photo-sensitization [22, 23]. Here one has to mention that phthalocyanine derivatives have several applications as sensitizers in photodynamic therapy (PDT) as well. This method is a suitable tool to indicate cancer cell death. The sensitizer molecules are activated with a light of certain wavelength and generate free radicals like singlet oxygen[52, 53]. Besides this some unsymmetrically substituted phthalocyanine complexes show cell penetrating properties [54].

To sum up one can say that porphyrins are one of the most popular dye classes. Metalloporphyrins have very strong phosphorescence even at room (M=Pt(II), Pd(II)), large Stoke's shifts and also high molar absorption coefficients [12]. As mentioned in table 2.1 on page 14, polystyrene, polyvinyl chloride and ethyl cellulose derivatives are common polymeric matrices

for oxygen measurement applications with this dye class. Porphyrins have been studied over a long time and it has been shown that their properties can be tuned via different modifications.

First, the porphyrin core unit can be modified by attaching different aromatic fragments which leads to an extension of the electronic π system resulting in a bathochromic shift of absorption/emission spectra [33]. Second, if there are solubility problems one can attach bulky substituents to the core so that the pophyrins planarity is manipulated [55]. Third, for further modification one can introduce good leaving groups like chlorine or bromine. Besides the use of these groups for further substitution they alter the electronic and optical properties of the dyes [14].

Due to this variety of tuning possibilities there are several applications in various areas for porphyrin based complexes. Some examples are solar energy conversion [56], catalysis [15], photovoltaic cells [57], thin-film transistors [58], light emitting diodes [59] and not to forget the big field of optical sensors [12, 14]. Like phthalocyanines porphyrins are important in medicine in PDT to act as sensitizers [60, 61].

A typical absorption spectrum of a metalloporphyrin shows two significant areas: the Soret-band at lower wavelength (higher energy of excitation) and the Q-bands at longer wavelength (lower energy of excitation). Due to lower efficiency of spin-orbit coupling, Pd(II)-complexes have longer lifetimes (microsecond to millisecond) than Pt(II)-species [62, 63]. Pt(II) complexes have lifetimes up to tens of μs and about 2-3 times higher quantum yields compared to the corresponding Pd(II) complexes. Nevertheless Pd(II) complexes show rather intense phosphorescence which is red shifted compared to the corresponding Pt(II) species [64]. Besides this the metallation step in synthesis for a Pd(II) dye is much easier than for the Pt(II) structural analog, due to its smaller atomic radius [13]. PtTFPP has to be mentioned as one of the most important dye for oxygen measurements in the last century. This dye replaced others such as PtOEP due to its higher photostability. The fluorinated phenyl substituents decrease the electron density at the ring system (electron withdrawing effect, EWG) reducing the reactivity of the dye with singlet oxygen [43] leading to a significant increase of the photostability.

Furthermore several Ir(III) metalloporphyrin systems for oxygen sensing were published [65]. But most of these indicators show absorption and emission in the UV-Vis region and therefore suffer from mainly three drawbacks limiting their field of applications. First, if there is excitation in the UV-Vis region a high background signal in biological tissue is created due to the autofluorescence of several fluorescent compounds as NAD, chlorophyll and FAD. Second, in scattering probes like in marine applications these UV-Vis dyes are hardly suitable for oxygen measurements. Third, they can not be taken for implantable sensors because blood absorbs in the visible region very efficiently [12].

To eliminate these influences the π-system of the porphyrin can be extended. So tetrabenzo-porphyrin (TBP, see section 2.5.1 on page 21) compounds are created which can be excitated with red light and emit in the NIR [66, 67]. Due to the bathochromic shift of the absorption- and emission spectra, measurements in scattering probes are also possible (e.g. in tissues).

2.5.1 Near infrared indicators

Infrared light (IR) is the electromagnetic radiation which has a wavelength of 700 nm up to 1 mm. This part of the spectrum is divided into three sub areas; near-IR, mid- and far-IR. Besides the above named advantages for biological applications this region of the spectrum is also very interesting for photovoltaic and solar-cell applications. Nearly 50% of the sun's energy arriving on our planet is located in the NIR region [13]. So it is clear that more effective light harvesting applications have to be a goal for the future of organic solar cells [68]. Due to minimal autofluorescence of biological probes in the range of the optical window (700-900 nm) indicators which absorb and emit in this area are an important issue [13, 68]. The third big advantage of having red light excitable indicators is that they are compatible with red laser diodes over 600 nm [69]. These are less expensive compared to other light sources.

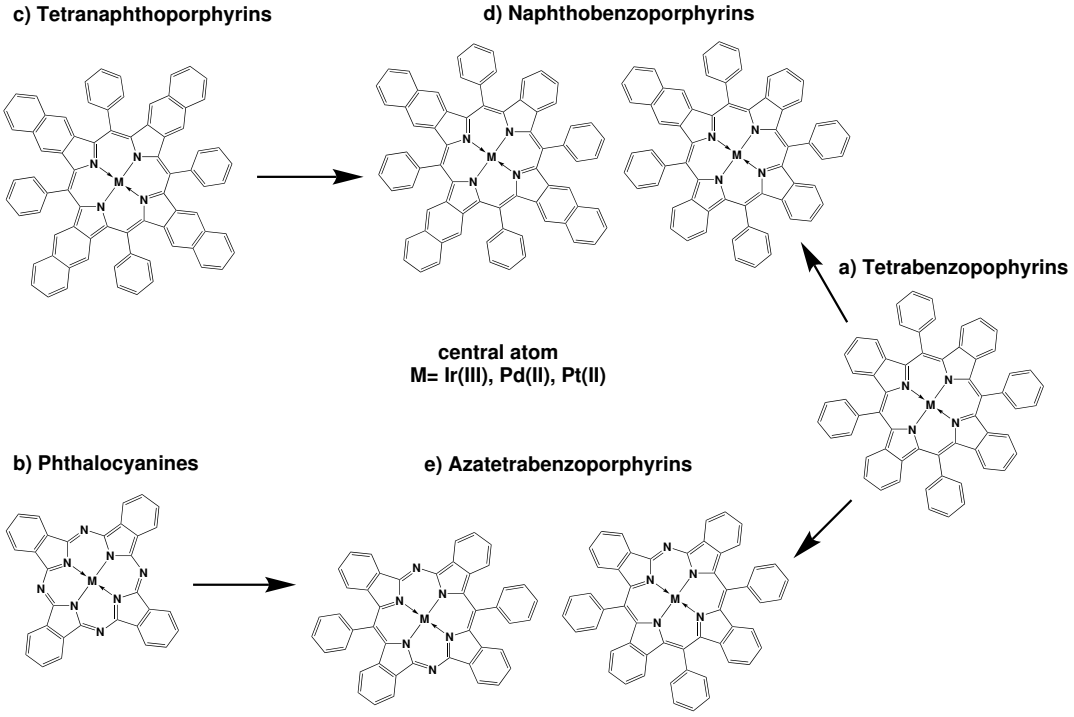

Figure 2.9: Overview NIR indicators

In the following chapters an overview of the indicators shown in figure 2.9 is given. How can a bathochromic shift be achieved by tuning the porphyrin dyes? This question was of much importance for the research in the last years, wherefore many different strategies have been explored. Some expamples are listed in the following.

Oxidation of the porphyrin macrocycle to lactone [70] or ketone groups [64], manipulation of the porphyrin core so that the electronic system and the solubility changes [71], reduction of the tetrapyrol macrocycle (e.g. to chlorine) [72], also introducing meso-alkynyl groups [73]. Another possibility is to extend the core of the porphyrin unit by aromatic fragments [74]. This

can be done via different synthetic methods [14, 75, 76]. It seems that the most important synthetic modification of the porphyrin to gain a bathochromically shift is the attachment of aromatic moieties at the β-pyrrole position [71, 77, 78]. This leads for example to tetrabenzo- (TBP) or tetranaphthoporphyrins (TNP, see compounds **a** and **c** figure 2.9 on page 20). Adding aromatic species to the meso position (see figure 2.8 on page 18) was also investigated. However this did not lead to the desired bathochromical shift due to the fact that the phenyl rings do not strongly influence the π-system of the porphyrin [13].

The rigid dye suffers from low solubility and aggregation problems but these can be overcome by adding phenyl groups at the meso position [13, 78] or bulky-groups like tert-butyl groups [71]. This results in a non-planar system of the substituents whereas the macrocycle remains planar. Adding fluorinated groups (EWG, fluorophenyl derivatives) as well as phenyl gropus at the meso position does not only increase the solubility but shows also higher photostability and furthermore shifts the absorption- and emission spectra to higher wavelengths [67, 69].

The bathochromic shift depends on the HOMO-LUMO energy gap. It is an essential parameter for optical and electronic properties of the dye [13, 79]. Therefore a closer look on the substituents is important. EWG (e.g. $-CF_3$) stabilize the HOMO, resulting in less electron density at the center leading to a bathochromic shift. EDG like $-$OMe do show the opposite effect [13]. Further examples leading to a bathochromic shift are the introduction of polarizable heteroatoms (e.g. O, S) [80] or the extension of the π-system of the ligands. Here one has to be careful because increasing chain length can lead to a decrease of the phosphorescence [6].

Within the last years many different applications of π-extended porhyrin dyes where published. They find use as optical oxygen sensors, NIR OLEDs and also in bioimaging [13].

Benzo- and naphthoporphyrins

This dye class was first synthesized in 1938 by the group of Helberger [81] and after around 10 years also Linstead and co-workers presented a route for this synthesis [82]. These compounds are applied in a wide range including technology, medicine [14] and catalysis [15] to name a few of them. Benzoporphyrins have the same ground structure as porphyrins but with fused benzene rings on the pyrrole position (see figure 2.10 on page 22). The absorption spectrum looks similar to that of porphyrins but is shifted bathochromically so that especially the Q-band has a wide range of its maximum (600-650 nm). As a representative of this dye class one can choose tetraphenyltetrabenzoporphyrins (e.g. PtTPTBP, see compound **a** in figure 2.9 on page 20). These dyes are bright have high quantum yields (50% for Pt(II) and 18% for Pd(II)) and a red shifted emission (770 nm). Additionally, they have excellent photostability even though it is not as good as PtTFPP [67, 83].

For applications in long term measurements or when high light intensity are an issue photostability is an important parameter one has to consider [84]. Photo-degeneration is in most cases induced by singlet oxygen which is produced via quenching. These dyes may also generate cytotoxic free radicals caused by radiation with light of a specific wavelength [85]. The

fluorination of the meso positioned phenyl rings (with EWGs) leads to higher photostability [69]. A drawback of this dye class is their moderate solubility of their ground structure. To overcome this drawback attachment of bulky substituents in meso position and/or phenyl rings can be done [86]. This leads to a better solubility whereby aggregation can be prevented [55]. After introduction of the benzoporphyrin dye into a suitable matrix (e.g. polystyrene) Pt(II) complexes are suitable for oxygen measurements up to 100% air saturation. The corresponding Pd(II) derivatives find applications in oxygen trace measurements [12].

Tetraphenyltetrabenzoporphyrin (TPTBP) dyes can be excited with red light, show emission in the near-infrared and are able to produce singlet oxygen. Therefore they have several applications in medicine like for treatment of cancer cells with PDT (see section 2.5 on page 18) [14]. For further specific biological applications like oxygen measurements in tissue the dye have to be either permeable or impermeable for biological membranes. Red and NIR emission is necessary as the excitation light has to penetrate biological tissue. Also they must not be toxic/phototoxic [87]. To achieve the desired modification/encapsulation of the dye for specific applications different methods exist.

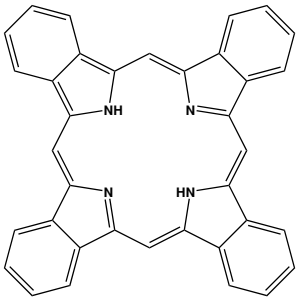

(a) benzoporphyrin

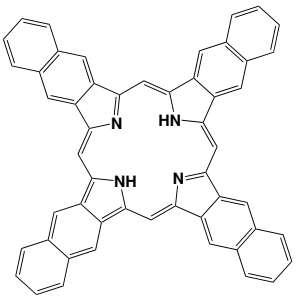

(b) naphthoporphyrin

Figure 2.10: Representative ground structures of benzo- and naphthoporphyrins

First, metalloporphyrins can be encapsulated into poly(arylglycine) dendrimers. These compounds can fold in aqueous medium and therefore tune the sensitivity and dynamic range of a sensor. For reducing the toxicity PEG residues are used. An important example for this method is oxyphor G2 (in vivo measurement in rat brains) [12, 87]. Second, also very popular is an encapsulation of the dye in nanoparticles, PEBBLEs (*probes encapsulated by biologically localized embedding*) [88]. These nanoparticles have a very small radius compared to the volume of a biological cell and can therefore be used in minimally invasive sensing applications [12, 89].

Other applications for TBPs can be found in material science. Some examples are optical limiters [90], liquid crystals [91], or sensitizers in photovoltaic cells [92].

As one can see in figure 2.10 naphthoporphyrins have the same ground structure as benzoporphyrins but have an additional benzene ring fused at the β-pyrrole position (called naphtha moiety). With these moieties a bathochromic shift of the Q-band over about 20 nm is achieved for each naphtha building block [12, 84], the Soret band nearly stays the same. Tetranaphthaporphyrins (TNPs) do show intense and narrow transitions which are in the NIR window of tissue [71, 77]. Besides this effect adding naphtha moieties also decreases significantly the photostability and the quantum yields [59, 66]. Due to these drawbacks and also their low solubility and high tendency for aggregation their applications are limited [71, 84]. To overcome

the drawback of low solubility tetraarylation at the meso position is a common solution. This forces the dye into a non-planar structure [77].

Hybrid porphyrin dyes

In this section a short overview about hybrid porphyrin complexes will be given. First, there are hybrid benzo- and naphthoporphyrin complexes to mention (see compounds **d** figure 2.9 on page 20). These species should combine the advantages of both classes; benzo- and naphthoporphyrins. The *tailor-made* NIR absorbing complexes are synthesized via condensation of external aromatic moieties. The new dyes have absorption bands in the red region (around 630-690 nm) and their emission range from 815 to 882 nm. If they are modified by extension of their π-system the lifetimes and quantum yields decrease as well as their oxygen sensitivity and photobleaching increases. One possible application for these hybrid species is a simultaneous measurement of glucose and oxygen [84]. To prevent photobleaching introduction of halogen substituents at the ligands can be a solution [12].

Second, hybrid azatetrabenzoporphyrins have to be mentioned. This class is a hybrid between phthalocyanines and tetrabenzoporphyrins (see compounds **e** figure 2.9 on page 20). These dyes should again combine the advantages of both origin classes, TBPs and Pcs. Pcs are stable (chemically, thermally and photostable), compounds but they do not have high quantum yields (QY$\backsimeq$1%) concerning their Pt(II) and Pd(II) derivatives [12, 16, 93]. That makes them not suitable for many applications in oxygen sensing [86]. With their phenyl rings attached at the meso position the hybrid complexes have better solubility as Pcs and TBPs. As in the former explained classes also the solubility of these dyes can be increased by introduction of bulky groups at the meso position [94]. Azatetrabenzoporphyrins have a comparable photostability as PtTFPP and a better one compared to TPTBP. Their luminescent properties show a red shifted emission of about 80 nm also the Q-band is shifted bathochromically whereas the Soret band has a hypsochromic shift [86] (all compared to TPTBP). Recently, Huang et al published that Pt(II) azatetrabenzoporphyrin dyes are suitable for applications as NIR-OLED (*organic light emitting diode*) [95].

2.6 J-aggregates

What are J-aggregates? Such structures are ordered clusters of organic molecules which are coherently coupled to each other. These clusters have different spectral properties compared to their monomers [96–98]. How can J-aggregates be characterized? First, they have very narrow absorption spectra which are usually drastically red shifted compared to the monomer spectra (up to 100 nm) [99]. Second, due to different packing types two or more narrow absorption bands can be observed [96]. Third, their absorbance is drastically increased compared to the monomers, whereas the fluorescence spectra have small Stoke's shifts (around 10 nm) [98]. Emission quantum yields are very high but the lifetimes are usually shorter (picoseconds)

compared to the monomers [100]. J-aggregates are self-organized one dimensional formations of several molecules which are aligned parallel to the line through their centers in a *head-to-tail* or *shifted plates* formation. This arrangement model is called *staircase*-type conformation and here the transition dipoles are ordered in one line leading to stronger electronic coupling of emitting monomers [101]. Corresponding to inhomogeneous distribution of energies the absorption and fluorescence bands of J-aggregates are narrower compared to the monomers [99].

The most famous class which is reported to form J-aggregates are cyanine dyes. They have two main groups in their structure. On the one side they have a donor and on the other side an acceptor moiety. These are coupled via polymethine chains (see **a** in figure 2.11). Nevertheless J-aggregates can also be formed by other molecules like squaraine, merocyanine and also tetrapyrole dyes [98]. meso-Tetrakis(p-sulfonatphenyl)porphyrin (TSPP) is a famous example for a porphyrin dye to form J-aggregates [103]). Corresponding to this and the fact that J-aggregates can shift very wide to the red part of the spectrum it may also be possible for benzoporphyrin or phthalocyanine complexes to form J-aggregates which fit for applications concerning the optical window (see section 2.5.1 on page 20).

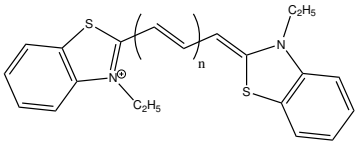

(a) Example of a cyanine dye

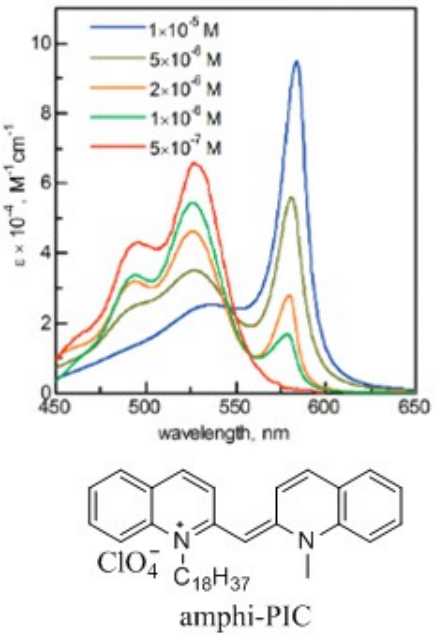

(b) Absorption dependency of amphi-PIC with different dye concentration, adopted from [102]

Figure 2.11: Example of a cyanine dye and the concentration dependency of J-aggregates for amphi-PIC

Which parameters affect the self-assembly of J-aggregates? Studies have been done which investigated different parameters in solution like solvent polarity, salinity and temperature [104, 105]. First, the self-assembly process can be indicated by changing the dye solution from organic to aqueous medium [106]. Second, an higher salinity supports also aggregation [107]. The third parameter is pH, increasing the pH value leads to the formation of regularly structured J-aggregates [108]. Also the dye concentration has a big influence on J-aggregates formation (see sharp bond formation **b** in figure 2.11)

There are many applications already existing for J-aggregates. One of them is the field of light-harvesting devices. An example for these are photovoltaic cells based on organic sensitizer dyes. Here the dye is absorbed at nanoporous TiO_2 (electrode). Li et al. have already shown that a formation of J-aggregates is possible using porphyrins [109]. Synthesis of benzoporphyrins forming J-aggregates with a respective

bathochromic shift would enable application of those indicators as sensitizer dyes in light-harvesting devices.

2.7 Organic reactions

In this section two main reactions will be described which were used within this masterthesis for modification of existing porphyrin dyes. These reactions should lead to a bathochromic shift of the dyes.

2.7.1 Sonogashira reaction

This reaction is a convenient cross-coupling reaction which was first published by Sonogashira et al. in 1975. It is used to form carbon-carbon bonds between a terminal alkine and a vinyl- or aryl-halide [110]. As shown in figure 2.12 a palladium catalyst, a copper(I) catalyst and an amine base (e.g. Et_3N) are necessary. The mechanism can be described as the following. First, in situ generation of Pd(0) catalyst and generation of coordination space via loss of two ligands. Followed by an oxidative addition reaction (R'X). Third, trans-metallation step, leads to substitution of X by the second building block. Fourth, after cis/-trans isomerization, generation of desired product via reductive elimination and regeneration of palladium catalyst [110, 111].

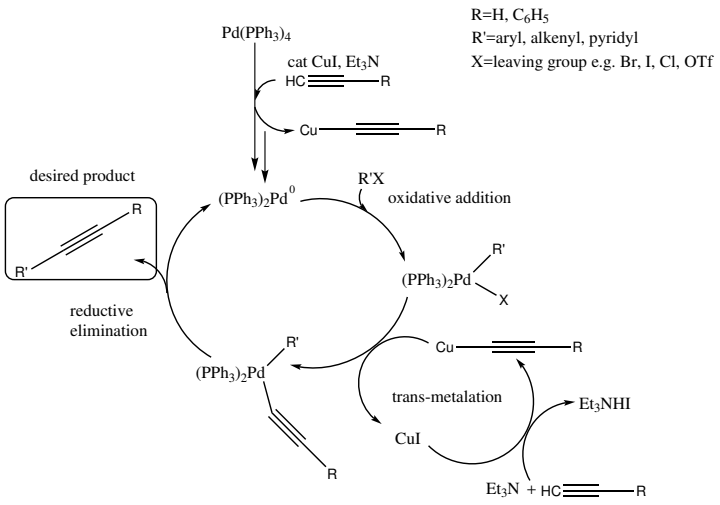

Figure 2.12: Schematic overview of the mechanism of the Sonogashira cross-coupling reaction

Already in the late 1990s different groups studied the electronic modulation of porphyrins with arylethynyl groups in meso position. They coupled the arylethynyl moieties at position 5 and 15 to existing Zn(II) porphyrin dyes. This modification leads to a significant red shift of the spectra compared to the unsubstituted complex [112]. Shultz and his group published a Sonogashira based modification for coupling of two porphyrin complexes to a bisporphyrin species. Here again the meso position of the porphyrin core was used as linking position [113]. Aim of this master thesis was to investigate the influence of the substitution of alkine groups (e.g. phenylacetylene) at the β position of an existing porphyrin dye and if this also results in a significant change in the spectral properties or if this hardly affects the π-system of the dye.

2.7.2 Friedel-Crafts reaction

This acylation reaction can be used to synthesize an aromatic ketone via reaction of an aromatic substrate molecule with an acyl containing secondary building block. It was first published in 1877 by Friedel and Crafts [114]. This reaction is catalyzed by strong Lewis acids (e.g. $FeCl_3$, $AlCl_3$, $TiCl_4$) or strong protic acids (e.g. HF or H_2SO_4) [115]. In figure 2.13 the reaction mechanism of such an acylation reaction is shown schematically. After activation of the acyl building block (R=Cl, RCOO; see I) the aromatic substrate can attack the electrophilic carbon. After loss of the hydrogen atom and the addition of the Lewis acid (in this case $AlCl_3$, see II) the product is generated by quenching with water (see III).

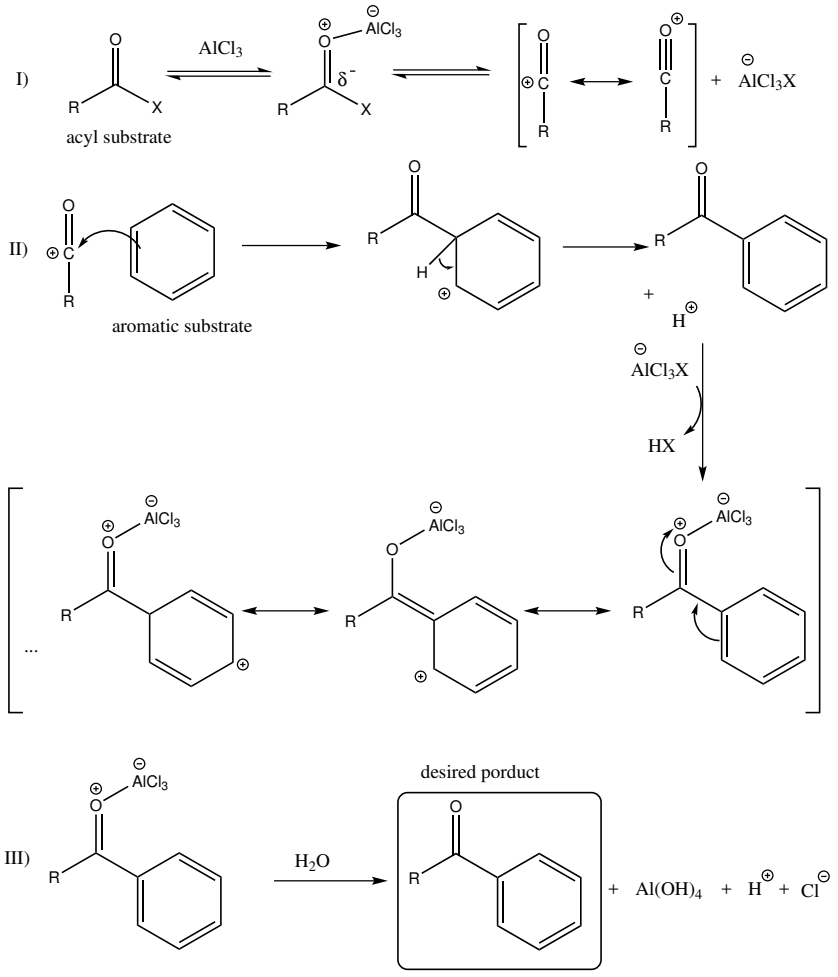

Figure 2.13: Schematic overview of the mechanism of Friedel-Crafts acylation reaction

In this mastethesis we wanted to take a closer look on the impact of a coupled aromatic acyl component to an existing porphyrin dye at the beta position (see figure 2.5 on page 18) and if such a substitution alters the spectral properties of the dye significantly.

3 Materials and Methods

3.1 Chemicals

Table 3.1: List of used chemicals

Chemical	Supplier	CAS-Number
Pottasium carbonate	Merck	584-08-7
Iodomethane	Acros organics	74-88-4
Sodium hydride	Sigma-Aldrich	7646-69-7
3-(Dibutylamino)phenol	TCI Europe	43141-69-1
Bromine	Sigma-Aldrich	7726-95-6
Sodium thiosulfate pentahydrate	Sigma-Aldrich	10102-17-7
2-(Chloromethyl)benzoyl chloride	Sigma-Aldrich	42908-86-1
Aluminum chloride	Fluka Analytical	7446-70-0
2-Bromobenzoylchloride	Alfa Aesar	7154-66-7
α, $\acute{\alpha}$-Dibromo-o-xylene	TCI	91-13-4
2,3-Dichloro-5,6-dicyano-p-benzoquinone	Sigma-Aldrich	84-58-2
1-Dodecylamine	Fluka Analytical	124-22-1
α, α, $\acute{\alpha}$, $\acute{\alpha}$-Tetrabromo-o-xylene	Alfa Aesar	13209-15-9
Phthaldialdehyde	Alfa Aesar	643-79-8
Propionic acid	Sigma-Aldrich	79-09-4
Ethyl pyruvate	Alfa Aesar	617-35-6
Iron(II)-sulfate heptahydrate	Roth	7782-63-0
Sulfuric acid	Roth	7664-93-9
Hydrogen peroxide	Roth	7722-84-1
Ammonia solution, 7 N in methanol	Arcos Organics	7664-41-7
Pottasium cyanide	Merck	151-50-8
Phosphorous(V)oxychloride	Sigma-Aldrich	10025-87
Thionyl chloride	Fluka	7719-09-7
Palladium(II)acetate	Sigma-Aldrich	3375-31-3
Palladium(II)chloride	ABCR	7647-10-1
Sodium iodide	Sigma-Aldrich	7681-82-5
Pottasium iodide	Roth	7681-11-0

Continued on next page

Table 3.1 – continued from previous page

Chemical	Supplier	CAS-Number
Sodium tert-butoxide	Sigma-Aldrich	865-48-5
Diisobutylaluminum hydride solution	Sigma-Aldrich	1191-15-7
Iodine	ABCR	7553-56-2
Ammonium hydroxide solution	Merck	1336-21-6
Benzamide	Acros organics	55-21-0
Indole	TCI	120-72-9
1-Iodobutane	ABCR	542-69-8
4-Bromo-3-methoxyaniline	Acros organics	19056-40-7
4,7-Diphenyl-1,10-phenanthroline	ABCR	1662-01-7
Lithium	Acros organics	7439-93-2
Manganese (IV) oxide	Sigma-Aldrich	1313-13-9
Zinc acetate dihydrate	Sigma-Aldrich	5970-45-6
1,8-Diazabicyclo[5.4.0]undec-7-en	Sigma-Aldrich	6674-22-2
n-Butyllithium solution	Sigma-Aldrich	109-72-8
2,3-Dichloro-5,6-dicyano-p-benzoquinone	Sigma-Aldrich	84-58-2
Triethylamine	Sigma-Aldrich	121-44-8
Copper(I) iodide	Sigma-Aldrich	7681-65-4
Tetrakis(triphenylphosphine)palladium(0)	TCI	14221-01-3
2-Ethylhexane-1-thiol	Sigma-Aldrich	7341-17-5
4,5-Dichlorophthalonitrile	TCI	139152-08-2
2-(4-Fluorophenyl)acetic acid	ABCR	405-50-5
3-Chloroperbenzoic acid	Sigma-Aldrich	937-14-4
tert-Butyllithium	Sigma-Aldrich	594-19-4

3.2 Chromatography

3.2.1 Thin layer chromatography

The reaction progress was monitored via thin layer chromatography. TLC silica gel plates from Merck (silica gel 60 F_{254} aluminum sheets $20 \cdot 20\,\text{cm}$) were utilized. For detection of the signals (spots) UV light with wavelength λ either 254 or 366 nm was used.

3.2.2 Flash column chromatography

Further purification of the products was done via flash column chromatography. Silica gel from Acros Organics (0.035 – 0.070 mm, 60 Å) or aluminum oxide 90 (neutral, Macherey-Nagel) was used. Depending on the separation problem amount of silica gel or aluminum oxide ranged between the 100 fold of the amount of product up to the 200 fold. Solvents for eluting of the

desired product were chosen by having a look to the R_f-value. This value ranged between 0.20 and 0.35. The used solvent mixtures are given in the experimental sections.

3.3 Photophysical measurements

3.3.1 Absorption

The absorption spectra were recorded on a VARIAN CARY 50 conc. UV-Vis spectrophotometer by Varian (Palo Alto, United States). A fast scan mode with baseline correction (blank sample of used solvent) was used for the measurements. Spectra were recorded either in chloroform or toluene. For these measurements Hellma 100-QS 10 mm precision cuvettes were used.

3.3.2 Emission and excitation spectra

Emission and excitation measurements were recorded on a Fluorolog®3 spetrofluorometer (by Horiba Scientific). This was equipped with a cooled R2658 photomultiplier (NIR sensitive, by Hamamazu). Hellma 100-QS 10 mm precision cuvettes with screw-caps were used. As software FluorEssence^{TM} was used.

3.4 Structural measurements

3.4.1 Nuclear Magnetic Resonance Spectroscopy (NMR)

^{1}H, APT and HH-COSY NMR were recorded on a Bruker AVANCE III instrument (300.36 MHz for ^{1}H-NMR and 75.53 MHz for ^{13}C-NMR) which was coupled to an autosampler. In all spectra the residual signal of the deuterated solvent (eg. $CDCl_3$, DMSO-d6) was used as an internal standard for the interpretation of the chemical shifts δ (in ppm, parts per million).
The coupling constant is indicated in Hz (hertz) and for signal multiplicities abbreviations are used: singlet (s), doublet (d), triplet (t), quartet (q), pentett (p), doublet of a doublet (dd), multiplet (m). For analysis of the data MestraNova NMR software was used.

3.4.2 High Resolution Mass Spectrometry (HR-MS)

The mass spectrometry measurements were performed with a Micromass TofSpec 2E (positive reflector) on a MALDI-TOF/TOF (Bruker Ultraflex Extreme). For external calibration a suitable mixture of poly(ethylenglycol)s (PEG) was used. For analysis of spectra MassLynx-Software V4.1 from Waters was used. This analysis was done by Prof. Dr. Saf's group at the Institute for Chemistry and Technology of Materials at Graz University of Technology.

4 Experimental

4.1 Carbazole based Phthalocyanine: Zn-Tbut-indole-Pc (6)

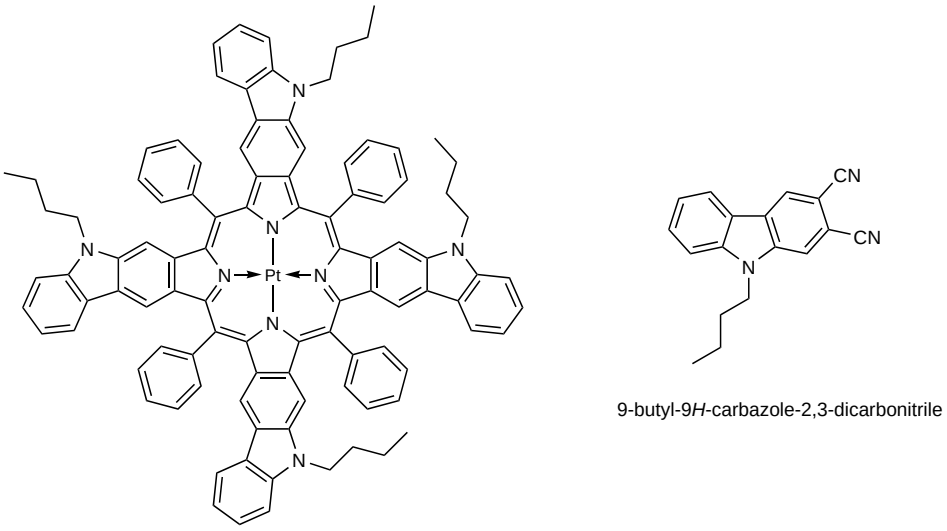

Figure 4.1: Chemical structure of desired Pt-Porphyrin (left) based on the carbazole precursor (right)

4.1.1 diethyl pyridazine-4,5-dicarboxylate (1)

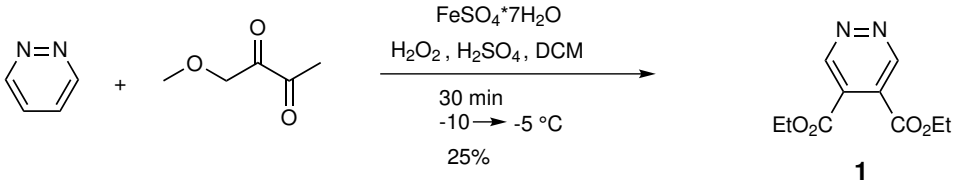

Figure 4.2: Synthesis of compound **1**

This synthesis was performed analogously to [116]
1.53 ml of 30% aqueous H_2O_2 (14.98 mmol, 3.00 eq) were added dropwise to stirring ethyl pyruvate (2.54 ml, 22.97 mmol, 4.60 eq) at -10 °C. This solution was then (after 15 min) added dropwise at -5 °C to a stirring mixture of pyridazine (400 mg, 4.99 mmol,1.00 eq), $Fe_2SO_4 \cdot 7\,H_2O$ (4.19 g, 15.00 mmol, 3.00 eq), concentrated H_2SO_4 (0.79 ml, 14.98 mmol, 3.00 eq), H_2O (8 ml) and DCM (15 ml). After 15 min stirring the reaction mixture was poured on ice and extracted

with DCM ($3 \cdot 15$ ml). The organic layer was washed with H_2O ($2 \cdot 20$ ml) and dried over Na_2SO_4. After removal of the solvent under reduced pressure the crude product was purified via flash column chromatography (silica-gel, cond. CH:DCM 10+1, DCM:EtOAc 10+1) to yield a yellow liquid (**1**).

Yield: 280 mg (25%), yellow liquid

TLC: R_f= 0.55 (silica-gel, DCM:EtOAc 5+1)

NMR spectra in the appendix 10.1 page 87:
^{1}H-NMR (300 MHz, Chloroform-d): δ 9.49 (s, 2H), 4.45 (q, J = 7.1 Hz, 4H), 1.40 (t, J = 7.1 Hz, 6H)

APT-NMR (76 MHz, Chloroform-d): δ 163.93, 149.32, 128.10, 63.17, 14.11

4.1.2 pyridazine-4,5-dicarboxamide (2)

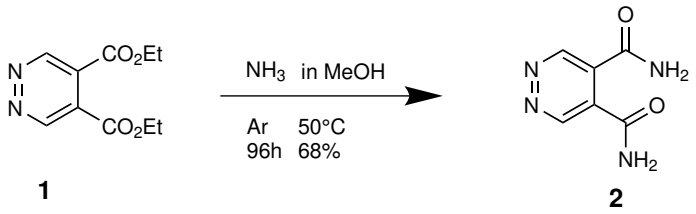

1 **2**

Figure 4.3: Synthesis of compound **2**

This synthesis was performed analogously to [116]
Compound **1** (1.00 g, 4.46 mmol, 1.00 eq) was added to a methanolic 7 N NH_3 solution (80 ml). The solution was stirred at 50 °C for 96 h. Precipitated product was washed with cold MeOH, yielding a white solid (**2**).

Yield: 488 mg (68%)

NMR spectra in the appendix 10.3 page 88:
^{1}H-NMR (300 MHz, DMSO-d6): δ 9.34 (s, 2H), 8.19 (s, 2H), 7.88 (s, 2H)

APT-NMR (76 MHz, DMSO-d6): δ 165.80, 149.25, 131.86

4.1.3 pyridazine-4,5-dicarbonitrile (3)

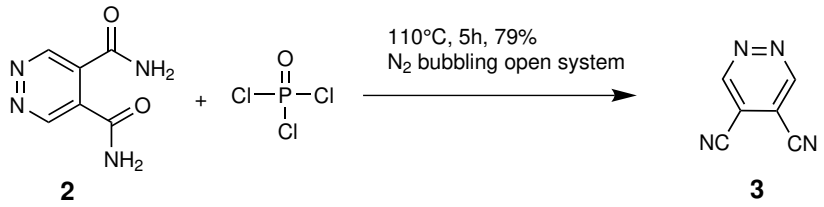

Figure 4.4: Synthesis of compound **3**

This synthesis was performed analogously to [116, 117]
Compound **2** (100 mg, 602 µmol, 1.00 eq) was added to 1.5ml (16.3 mmol, 27.0 eq) of $POCl_3$ in a Schlenk flask with reflux condenser, heated to 110 °C and stirred for 5 h (color change from cloudy colorless to green). To remove the in situ generated HCl N_2 was bubbled continuously through the solution during the reaction. The conversion of the reaction was controlled via TLC (silica-gel, DCM:EtOAc 5+1) and the excess of $POCl_3$ was quenched with saturated $NaHCO_3$ (20 ml). The product was extracted with DCM ($3 \cdot 100$ ml). The organic layer was dried over Na_2SO_4 and solvent removed under reduced pressure.

Yield: 62 mg (79%), yellow solid (**3**)

TLC: R_f= 0.72 (silica-gel, DCM:EtOAc 5+1)

NMR spectra in the appendix 10.5 page 89:
^{1}H-NMR (300 MHz, Chloroform-d): δ 9.63 (s, 2H)

APT-NMR (76 MHz, Chloroform-d): δ 150.38, 114.47, 111.55

4.1.4 1-butyl-1H-indole (4)

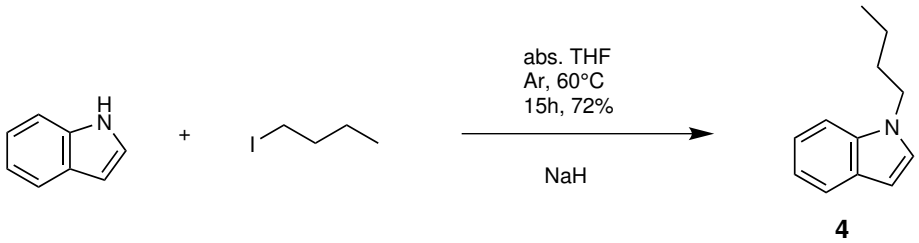

Figure 4.5: Synthesis of compound **4**

This synthesis was performed analogously to [118]
Indole (1.60 g, 13.7 mmol, 1.00 eq) was dissolved in 25 ml abs. THF in a Schlenk flask under Ar

atmosphere at RT. 765 mg (19.1 mmol, 1.40 eq) of a 60% NaH dispersion in mineral oil were added in portions (gas evolution, cloudy colorless solution). When no more gas evolution was observed 1-iodobutan (1.87 ml, 16.4 mmol, 1.20 eq) was added. The reaction was heated to 60°C and stirred for 15 h. After conversion control via TLC (silica-gel, CH:DCM 10+1) the excess of NaH was quenched with 100 ml H_2O. The product was extracted with EtOAc (4 · 400 ml) and dried over Na_2SO_4. After removal of the solvent under reduced pressure the yellow oil was further purified via flash column chromatography (silica-gel, cond. CH, CH:DCM 15+1) yielding a pale yellow oil (**4**).

Yield: 1.56 g (72%)

TLC: R_f= 0.40 (silica-gel, CH:DCM 10+1)

NMR spectra in the appendix 10.7 page 90:
^{1}H-NMR (300 MHz, Chloroform-d): δ 7.69 (d, J = 7.8 Hz, 1H), 7.41 (d, J = 8.1 Hz, 1H), 7.32 – 7.22 (m, 1H), 7.20 – 7.10 (m, 2H), 6.54 (d, J = 2.8 Hz, 1H), 4.17 (t, J = 7.1 Hz, 2H), 1.88 (p, J = 7.3 Hz, 2H), 1.40 (h, J = 7.4 Hz, 2H), 1.00 (t, J = 7.3 Hz, 3H)

APT-NMR (76 MHz, Chloroform-d): δ 127.91, 121.40, 121.05, 119.26, 109.50, 100.95, 46.25, 32.48, 20.34, 13.85

4.1.5 9-butyl-9H-carbazole-2,3-dicarbonitrile (5)

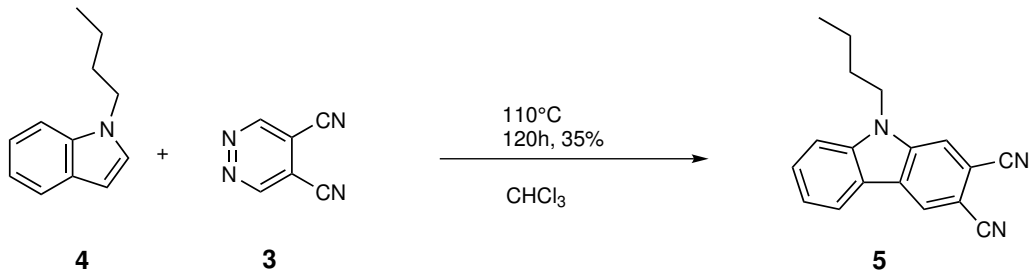

Figure 4.6: Synthesis of compound **5**

This synthesis was performed analogously to [119–121]
This reaction was performed in an Ace pressure tube. Compound **3** (25.1 mg, 193 µmol, 1.00 eq) and **4** (100 mg, 5773 µmol, 3.00 eq) were dissolved in 1.5 ml $CHCl_3$. The reaction was heated to 110 °C and stirred for 120 h. Conversion control was done by TLC (silica-gel, CH:EE 7+2). After removal of the solvent under reduced pressure the oil was purified via flash column chromatography (silica-gel, cond. CH, CH:EE 7+1), yielding a yellow solid (**5**).
Yield: 19 mg (35%)

TLC: R_f= 0.36 (silica-gel, CH:EE 7+1)

NMR spectra in the appendix 10.9 page 91:
^{1}H-NMR (300 MHz, Chloroform-d): δ 8.49 (s, 1H), 8.16 (d, J = 7.8 Hz, 1H), 7.81 (s, 1H), 7.66 (t, J = 7.5 Hz, 1H), 7.54 (d, J = 8.3 Hz, 1H), 7.41 (t, J = 7.4 Hz, 1H), 4.38 (t, J = 7.2 Hz, 2H), 1.95 – 1.81 (m, 2H), 1.42 (t, J = 7.4 Hz, 2H), 0.98 (t, J = 7.3 Hz, 3H)

APT-NMR (76 MHz, Chloroform-d): δ 140.57, 129.21, 126.46, 125.80, 121.69, 121.30, 117.27, 117.04, 114.59, 111.07, 110.14, 104.39, 43.75, 31.19, 20.66, 13.90

4.1.6 Zinc(II)-tetra(1-butyl-1H-indole)-phthalocyanine Zn-Tbut-indole-Pc (6)

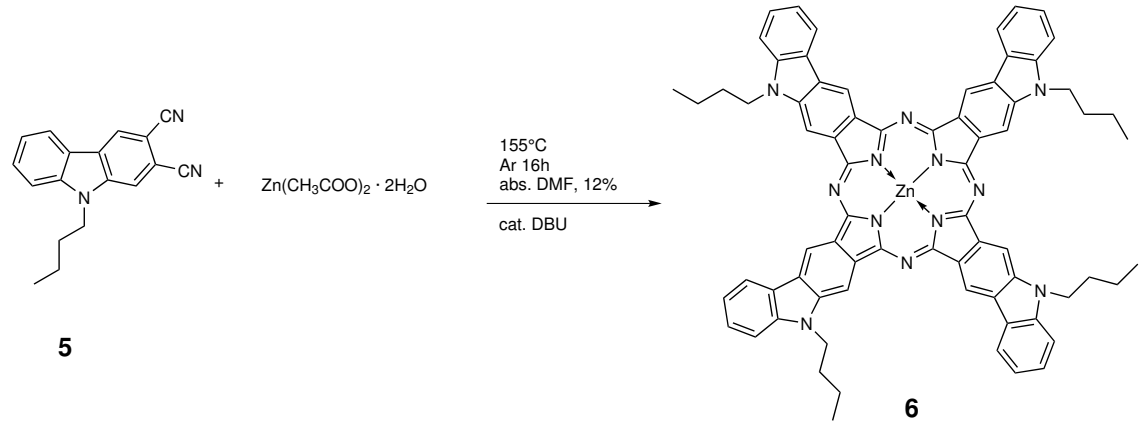

Figure 4.7: Synthesis of compound **6**

This synthesis was performed analogously to [122]
$Zn(CH_3COO)_2 \cdot H_2O$ (12.0 mg, 65.4 µmol, 2.50 eq) and compound **5** (53.6 mg, 196 µmol, 3.00 eq) were dissolved in a Schlenk flaks under Ar atmosphere in 2 ml abs. DMF (orange solution). After adding catalytic amounts of DBU (100 µl) a color change occurred (dark red solution). The reaction was heated to 155 °C and stirred for 16 h. The dark green solution was cooled to RT and precipitated into a 3+2 mixture of H_2O:MeOH. The green precipitate was separated by filtration an washed with cold MeOH (orange solution). The crude solid product was further purified via flash column chromatography (aluminum oxide, cond. CH, gradient elution starting from CH:EE 3+1 ending with EE:THF 5+1) yielding two fractions of solid green product (**6**).

Yield (fraction one): 5 mg (7%)
Yield (fraction two): 4 mg (5%)

MALDI-TOF (10.24, 10.25 page 100): $\frac{m}{z}$: [M^+]: calc. 1156.44, found: 1156.30 (F1), 1156.46 (F2)

λ_{max}(toluene): 333 nm (0.23) 663 nm (0.33), 742 nm (1.00)

4.2 Porphyrin Modification by Sonogashira coupling

4.2.1 Pt(II)-tetra(phenylacetylen)-tetra(tert-butyl)BP: Pt-TPhacetTtBuBP (7)

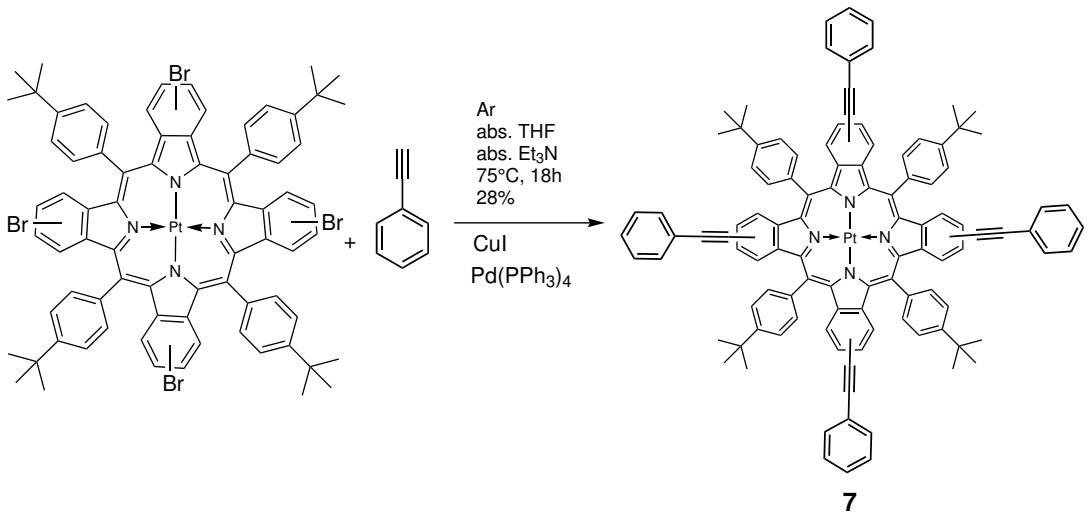

Figure 4.8: Synthesis of compound **7**

This synthesis was performed analogously to [123, 124]
Pt-TPTtBuBPBr (15.0 mg, 9.70 µmol, 1.00 eq) and catalytic CuI (0.20 eq) was dissolved in 1.5 ml abs. THF and 0.7 ml abs. Et_3N in a Schlenk flask under Ar atmosphere. To the green solution catalytic $Pd(PPh_3)_4$ (0.10 eq) and phenylacetylen (4.95 mg, 48.5 µmol, 5.00 eq) were added. The solution was stirred for 18 h at 75 °C. Conversion control of the reaction were done via TLC (silica-gel, CH:DCM 3+1). The green solution was first washed several times with 10% $CuSO_4$ to remove the excess of Et_3N (until the solution was clear). The product was extracted with DCM, the organic layer was dried over Na_2SO_4. The solvent was removed under reduced pressure. Further purification was conducted via flash column chromatography (silica-gel, cond. CH, CH:DCM 5+1) yielding different fractions of product. The product (**7**) containing fractions were determined via absorption spectra.

Yield: overall 2 mg (12%)

TLC: R_f= 0.50-0.70 (silica-gel, CH:DCM 5+1)

MALDI-TOF (10.26 page 102): $\frac{m}{z}$: [M^+]: calc. 1631.63, found: 1631.67

λ_{max}(toluene): 446 nm (1.00), 577 nm (0.08) 630 nm (0.63)

4.3 Porphyrin Modification by Friedel-Crafts reaction

4.3.1 Pt-TPTBPF-benzoyl-Cl (8)

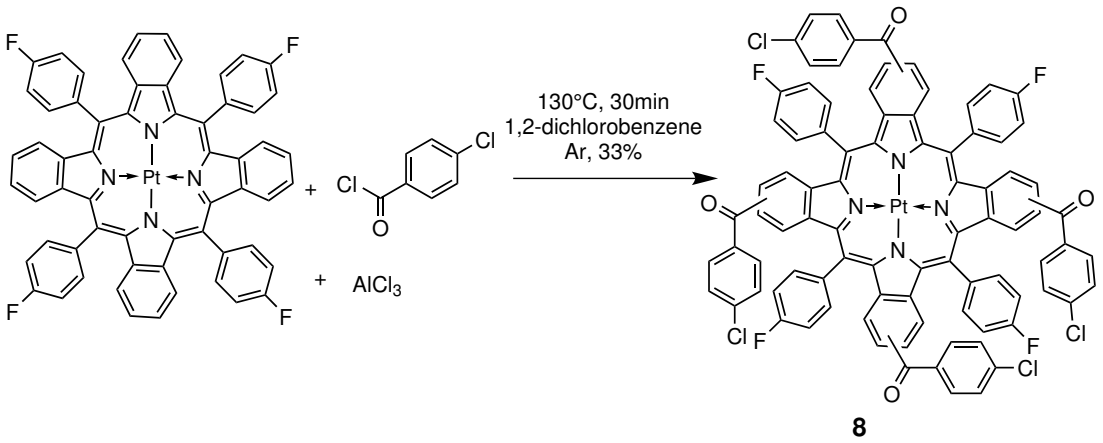

Figure 4.9: Synthesis of compound **8**

In a Schlenk flask Pt-TPTBPF (20.0 mg, 18.5 µmol, 1.00 eq) was dissolved in 1,2-dichlorobenzene (8 ml) under Ar atmosphere (green solution). 4-Chlorobenzoyl chloride (0.12 mL, 0.93 mmol, 50.0 eq) and $AlCl_3$ (40.0 mg, 0.30 mmol, 16.2 eq) were added to the solution. The reaction mixture was heated to 130 °C and stirred for 30 min. The reaction progress was monitored via absorption spectroscopy (solvent: $CHCl_3$, 50 µl of EtOH). After complete conversion the reaction mixture (green dark color) was cooled down to RT. In the work-up reaction mixture was treated with EtOH:H_2O (1+1, each 40 ml) and stirred for 10 minutes to neutralize the excess of $AlCl_3$. After addition of DCM, the organic layer was washed with dest. H_2O and dried over Na_2SO_4 and the solvent was removed under reduced pressure. Finally the crude product was purified via flash column chromatography (silica-gel, cond. toluene, DCM:Tol, 7+1), yielding a dark green solid (**8**).

Yield: 26.0 mg (33%)

TLC: R_f= 0.44 (silica-gel, DCM:Tol 4+1)

NMR spectra in the appendix 10.11 page 92:
^{1}H-NMR (300 MHz, Methylene Chloride-d2) δ 8.33 – 8.18 (m, 2H), 8.18 – 8.07 (m, 3H), 8.06 –

7.92 (m, 2H), 7.80 (dt, J = 13.5, 7.5 Hz, 4H), 7.66 (d, J = 7.4 Hz, 2H), 7.53 (dd, J = 11.8, 5.4 Hz, 16H), 7.44 – 7.32 (m, 5H), 7.31 – 7.19 (m, 2H), 7.19 – 7.02 (m, 4H)

λ_{max}(toluene), ε: 448
epsilon,nm (218,000), 579 nm (17,400), 631 nm (121,000)

MALDI-TOF (10.29 page 105): $\frac{m}{z}$: [M$^+$]: calc. 1634.17, found: 1634.17

4.3.2 Pd-TPTBPF-benzoyl-Cl (9)

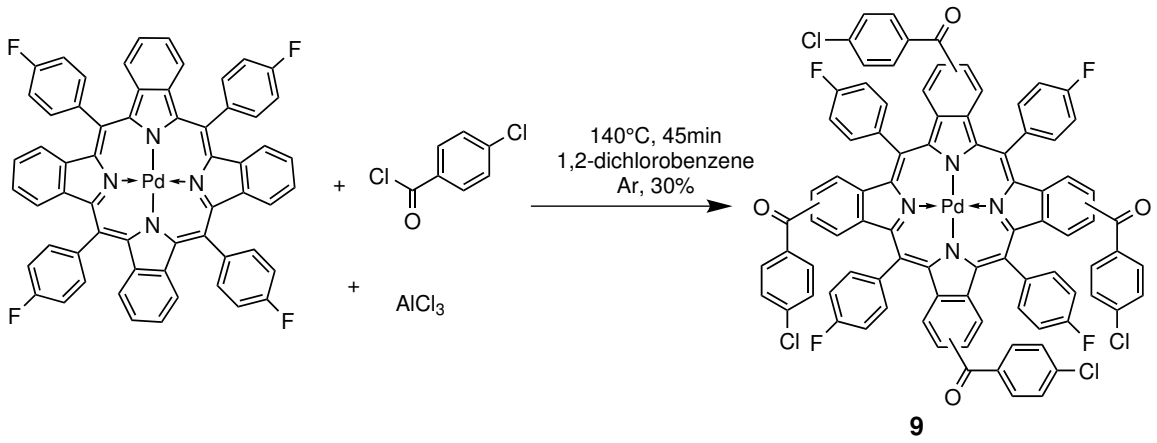

Figure 4.10: Synthesis of compound **9**

In a Schlenk flask Pd-TPTBPF (10.0 mg, 10.1 µmol, 1.00 eq) was dissolved in 1,2-dichlorobenzene (6 ml) under Ar atmosphere (green solution). 4-Chlorobenzoyl chloride (0.064 ml, 0.50 mmol, 50.0 eq) and $AlCl_3$ (30.0 mg, 0.23 mmol, 22.3 eq) were added to the solution. The reaction mixture was heated to 140 °C and stirred for 45 min. The reaction progress was monitored via absorption spectroscopy (solvent: $CHCl_3$, 50 µl of EtOH). After complete conversion the reaction mixture (green dark color) was cooled down to RT. In the work-up reaction mixture was treated with EtOH:H_2O (1+1, each 20 ml) and stirred for 10 minutes to neutralize the excess of $AlCl_3$. After addition of DCM, the organic layer was washed with dest. H_2O, dried over Na_2SO_4 and the solvent was removed under reduced pressure. Finally the crude product was purified via flash column chromatography (silica-gel, cond. toluene, DCM:Tol, 7+1), yielding a dark green solid (**9**).

Yield: 30%

TLC: R_f= 0.52 (silica-gel, DCM:Tol 4+1)

NMR spectra in the appendix 10.13 page 93:

^{1}H-NMR (300 MHz, Methylene Chloride-d2) δ 8.25 (dq, J = 9.6, 4.7 Hz, 2H), 8.18 – 8.07 (m, 3H), 7.98 (dt, J = 10.7, 5.4 Hz, 2H), 7.80 (dt, J = 14.0, 7.7 Hz, 4H), 7.72 – 7.61 (m, 2H), 7.60 – 7.43 (m, 16H), 7.38 (t, J = 6.8 Hz, 5H), 7.32 – 7.23 (m, 2H), 7.21 – 7.13 (m, 2H), 7.09 (dq, J = 8.3, 5.4, 4.5 Hz, 2H)

λ_{max}(toluene), ε: 461 nm (282,300), 595 nm (15,800), 647 nm (107,400)

MALDI-TOF (10.30 page 106 f.): $\frac{m}{z}$: [M$^+$]: calc. 1544.11, found: 1543.96

4.4 Highly soluble Porphyrin and Phthalocyanine dyes for J-aggregates

4.4.1 target compounds: Pt – TBPFbEHS$_2$ and Zn – bEHS$_2$ – Pc

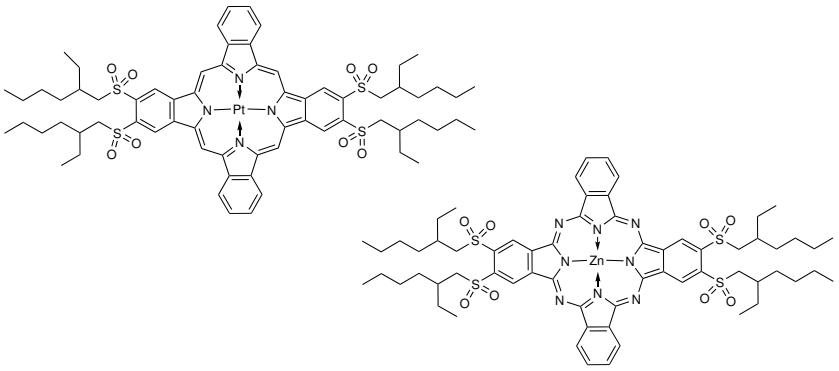

Figure 4.11: Target compounds for formation of J-aggregates: Pt – TBPbEHS$_2$ (left) and Zn – bEHS$_2$ – Pc (right)

4.4.2 4,5-bis((2-ethylhexyl)thio)phthalonitrile: bEHTPn (10)

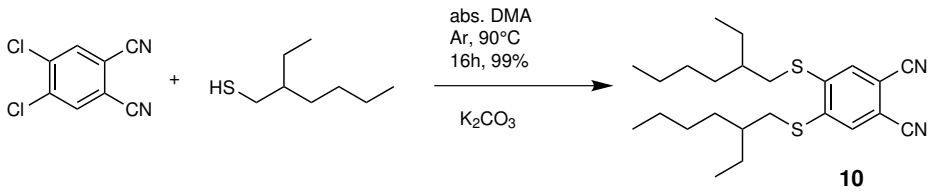

Figure 4.12: Synthesis of compound **10**

This synthesis was performed analogously to [125]
4,5-Dichlorophthalonitrile (1.20 g, 6.09 mmol, 1.00 eq) was first dissolved in 14 ml abs. DMA in a round bottom flask under Ar atmosphere. K_2CO_3 (2.40 g, 17.4 mmol, 2.85 eq) was homogenized with a ceramic pestle in a motar and then added to the solution and stirred for 10 min (color

change to red). 2-Ethylhexane-1-thiol (2.33 ml, 13.4 mmol, 2.20 eq) was added and the reaction mixture was heated to 90 °C and stirred for 16 h. The reaction progress was monitored via TLC (silica-gel, CH:EE, 3+1). The dark red solution was cooled to RT and poured onto an ice bath (100 ml H_2O). The product was extracted with DCM (3 · 150 ml), the organic layer was dried over Na_2SO_4. The solvent was removed under reduced pressure yielding a red-brown solid **10**.

Yield: 2.53 g (99%)

TLC: R_f= 0.80 (silica-gel, CH:EE, 3+1)

NMR spectra in the appendix 10.15 page 94:
^{1}H-NMR (300 MHz, Chloroform-d): δ 7.41 (s, 2H), 2.97 (d, J = 6.1 Hz, 4H), 1.71 (dt, J = 12.3, 6.1 Hz, 2H), 1.51 (m, J = 13.4, 6.8 Hz, 8H), 1.38 – 1.26 (m, 8H), 0.94 (t, J = 6.7 Hz, 12H)

APT-NMR (76 MHz, Chloroform-d): δ 144.96, 128.28, 115.85, 111.06, 38.60, 37.34, 32.71, 28.89, 25.96, 23.03, 14.18, 10.90

4.4.3 4,5-bis((2-ethylhexyl)sulfonyl)phthalonitrile: bEHSPn (11)

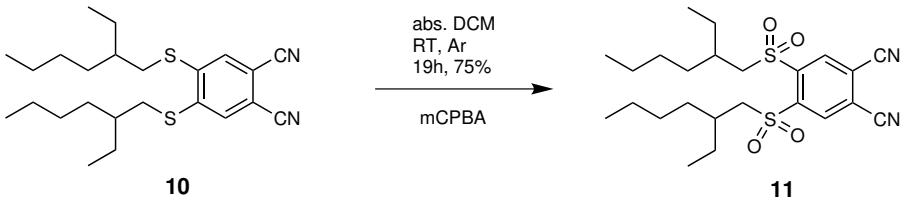

10 **11**

Figure 4.13: Synthesis of compound **11**

This synthesis was performed analogously to [125]
Compound **10** (200 mg, 480 µmol, 1.00 eq) was dissolved in 5 ml abs. DCM in a Schlenk flask under Ar atmosphere. mCPBA (533 mg, 3.09 mmol, 6.44 eq, 77% pure) was added with a plastic spatula in portions to the stirring solution (color change red to orange). The solution was stirred at RT for 19 h (color change orange to yellow) and the reaction progress was monitored via TLC (silica-gel, CH:EE, 3+1). The reaction mixture was then quenched with aq. $NaHCO_3$ (20 ml) solution. The product was extracted with Et_2O (3 · 100 ml), the organic layer was dried over Na_2SO_4. The solvent was removed under reduced pressure. Finally the crude product was purified via flash column chromatography (silica-gel, cond. CH, CH:EE, 5+1) yielding a yellow oil (**11**).

Yield: 173 mg (75%)

TLC: R_f= 0.70 (silica-gel, CH:EE, 3+1)

NMR spectra in the appendix 10.17 page 95:
^{1}H-NMR (300 MHz, Chloroform-d): δ 8.69 (s, 2H), 3.57 (d, J = 5.6 Hz, 4H), 2.24 – 2.09 (m, 2H), 1.49 (dt, J = 27.0, 8.1 Hz, 8H), 1.27 (d, J = 6.9 Hz, 8H), 0.89 (t, J = 7.1 Hz, 12H)

APT-NMR (76 MHz, Chloroform-d): δ 145.36, 137.21, 121.21, 113.22, 60.91, 34.67, 32.59, 28.15, 25.98, 22.80, 14.10, 10.22

4.4.4 zinc(II)-di(4,5-bis((2-ethylhexyl)thio)-phthalocyanine: Zn−bEHT$_2$−Pc (12)

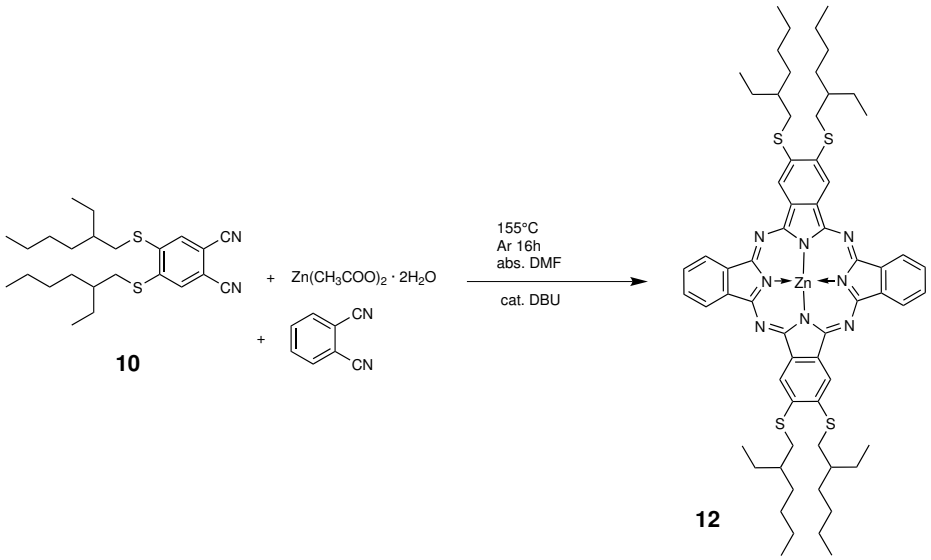

Figure 4.14: Synthesis of compound **12**; different isomers and substitutions are possible

This synthesis was performed analogously to [122]
$Zn(CH_3COO)_2 \cdot H_2O$ (65.9 mg, 300 µmol, 5.00 eq) and compound **10** (50.0 mg, 120 µmol, 1.00 eq) and phthalonitrile (15.4 mg, 120 µmol, 1.00 eq) were dissolved in a Schlenk flaks under Ar atmosphere in 5 ml abs. DMF giving a red solution. After adding catalytic amounts of DBU (100 µl) a color change occurred (brown solution). The reaction was heated to 155 °C and stirred for 16 h. The reaction progress was monitored via TLC (silica-gel, CH:DCM, 3+1, 1% MeOH) and absorption spectroscopy (solvent: toluene). The dark green solution was cooled to RT and precipitated into a 3+1 mixture of H_2O:MeOH. The green precipitate was separated by filtration an washed with cold MeOH. The crude solid product was further purified via flash column chromatography (silica-gel, cond. CH, CH:DCM 3+1, 1% MeOH) yielding no pure fraction of the desired product (**12**).

Yield (F6-13): 17.0 mg (22%)

TLC: R_f on silica-gel could not be detected, too many different spots

$\lambda_{max}(CHCl_3)$: 344 nm (0.25), 627 nm (0.20), 696 nm (1.00)

4.5 Pt(II) complexes supported by tetradentate N_2O_2 chelates: Diphenyphenanthroline system

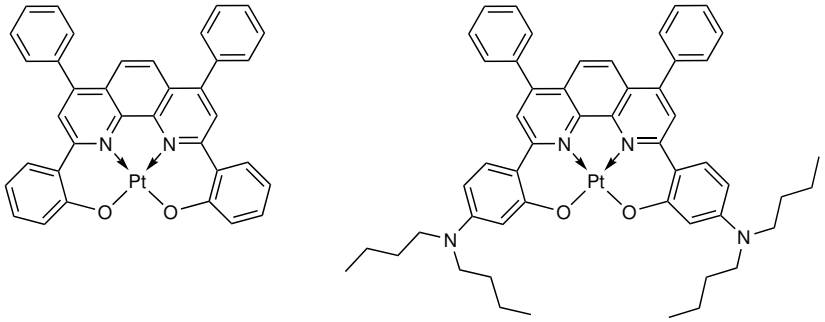

Figure 4.15: Published complex $Pt(Ph_2N_2O_2)$dpp [126] (left) and target complex $Pt(dBAN_2O_2)$dpp (right)

4.5.1 Attempted synthesis of Br-dbutMeOA (14)

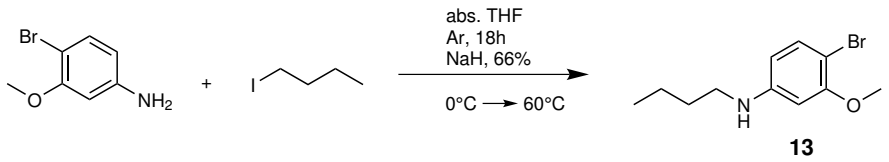

Figure 4.16: Synthesis of compound **13**

This synthesis was performed analogously to [118]
4-Bromo-3-methoxyaniline (100 mg, 495 µmol, 1.00 eq) was dissolved in 5 ml abs. THF in a Schlenk flask under Ar atmosphere. The solution was stirred at 0 °C and 60% NaH dispersion in mineral oil (50.0 mg, 1.24 mmol, 2.50 eq) was added in portions. The reaction mixture was stirred for 15 min. When no more gas evolution was observed 1-iodobutan (141 µl, 1.24 mmol, 2.50 eq) was added via a syringe to the brown solution. The reaction was heated carefully first to RT, then to 60 °C and stirred for 16 h. Reaction progress was monitored via TLC (silica-gel, CH:EE, 5+1). The reaction was poured into H_2O (20 ml) to neutralize the excess of NaH. The product was extracted with EtOAc ($3 \cdot 100$ ml), the organic layer was dried over Na_2SO_4. The solvent was removed under reduced pressure. Finally the crude product was purified via flash

column chromatography (silcia-gel, cond. CH, CH:EE, 7+1) yielding a yellow oil (**13**).

Yield: 85 mg (66%)

TLC: R_f= 0.47 (silica-gel, CH:EE, 5+1)

NMR spectra in the appendix 10.19 page 96:
^{1}H-NMR (300 MHz, Chloroform-d): δ 7.25 (d, J = 8.4 Hz, 1H), 6.15 (d, J = 2.2 Hz, 1H), 6.10 (dd, J = 8.5, 2.4 Hz, 1H), 3.84 (s, 3H), 3.66 (s, 1H), 3.08 (t, J = 7.0 Hz, 2H), 1.60 (dt, J = 14.1, 6.9 Hz, 2H), 1.42 (dq, J = 14.2, 7.1 Hz, 2H), 0.96 (t, J = 7.3 Hz, 3H)

APT-NMR (76 MHz, Chloroform-d): δ 156.58, 149.41, 133.40, 106.11, 98.11, 97.47, 56.12, 43.88, 31.68, 20.41, 14.03

4.5.2 4-bromo-N,N-dibutyl-3-methoxyaniline: Br-dbutMeOA (14)

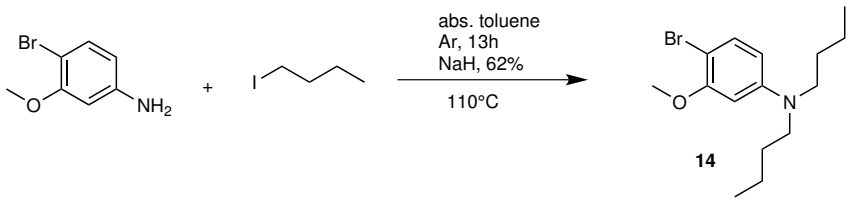

Figure 4.17: Synthesis of compound **14**

This synthesis was performed analogously to [118]
4-Bromo-3-methoxyaniline (1.00 g, 4.95 mmol, 1.00 eq) was dissolved in 15 ml abs. toluene in a Schlenk flask under Ar atmosphere. The solution was stirred at 0 °C and 60% NaH dispersion in mineral oil (500 mg, 12.4 mmol, 2.50 eq) was added in portions. The reaction mixture was stirred for 30 min. When no more gas evolution was observed 1-iodobutan (1.41 ml, 12.4 mmol, 2.50 eq) was added via a syringe to the brown solution. The reaction was heated carefully first to RT, then to 110 °C and stirred for 13 h (addition of another 2.00 eq of NaH and 1-iodobutan after 6 h). Reaction progress was monitored via TLC (silica-gel, CH:EE, 5+1). The reaction was poured into H_2O (50 ml) to neutralize the excess of NaH. The product was extracted with EtOAc (3 $\cdot$ 200 ml), the organic layer was dried over Na_2SO_4. The solvent was removed under reduced pressure. Finally the crude product was purified via flash column chromatography (silcia-gel, cond. CH, CH:EE, 15+1) yielding an orange oil (**14**).

Yield: 955 mg (62%)

TLC: R_f= 0.50 (silica-gel, CH:EE, 10+1)

NMR spectra in the appendix 10.21 page 97:
$_1$H-NMR (300 MHz, Chloroform-d): δ 7.39 – 7.22 (m, 1H), 6.25 – 6.12 (m, 2H), 3.84 (d, J = 21.9 Hz, 3H), 3.34 – 3.21 (m, 4H), 1.58 (p, J = 9.3, 8.2 Hz, 4H), 1.37 (dq, J = 14.6, 7.3 Hz, 4H), 0.97 (t, J = 7.2 Hz, 6H)

APT-NMR (76 MHz, Chloroform-d): δ 156.58, 149.07, 133.18, 105.84, 96.87, 56.10, 51.14, 29.47, 20.48, 14.13

4.5.3 4-lithium-N,N-dibutyl-3-methoxyaniline: Li-dbutMeOA (15)

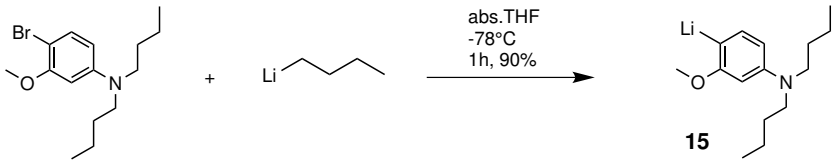

Figure 4.18: Synthesis of compound **15**

This synthesis was performed analogously to [127, 128]
Compound **14** (82.3 mg, 261 µmol, 1.00 eq) was dissolved in 1 ml abs. THF in a Schlenk flask under Ar atmosphere. The soltuion was cooled to -75 °C. n-Butyllithium solution (108 µl 270 µmol, 1.05 eq, 2.5 M in hexanes solution) was added drop-wise via a syringe (color change yellow to orange). The reaction mixture was stirred for 30 min. In the work-up NH_4Cl solution was added to the reaction mixture to quench the remaining lithium. The product (**15**) was extracted with DCM, the organic layer was dried over Na_2SO_4. To confirm the metal-halogen exchange the solution was measured via GC-MS.

Yield: estimated from the GC-MS spectra 90%

4.5.4 Attempted synthesis of Br-dbutMeOA via 3-(dibutylamino)phenol

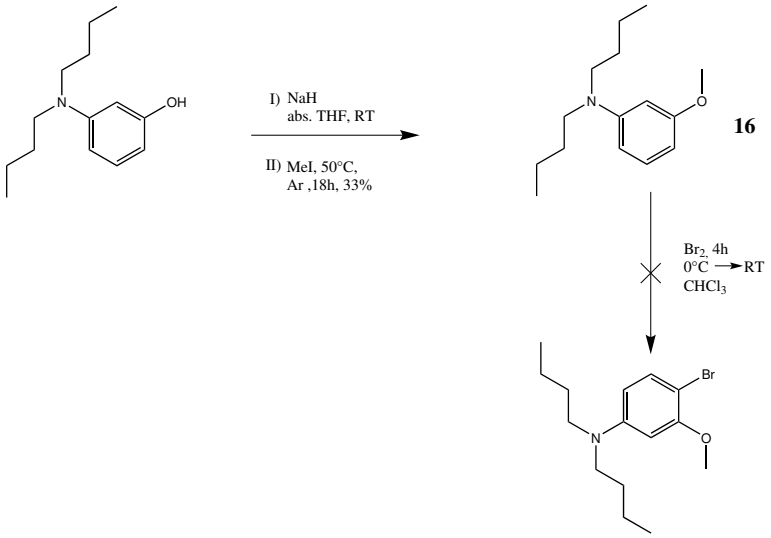

Figure 4.19: Estimated synthesis of compound **14**

This synthesis was performed analogously to [129]
3-(Dibutylamino)phenol (1.00 g, 4.52 mmol, 1.00 eq) was dissolved in 10 ml abs. THF in a Schlenk flask under Ar atmosphere. The solution was stirred at 0 °C and 60% NaH dispersion in mineral oil (198 mg, 4.97 mmol, 1.10 eq) was added in portions. The reaction mixture was stirred for 20 min. When no more gas evolution was observed iodomethane (310 µl, 4.97 mmol, 1.10 eq) was added via a syringe to the solution. The reaction was heated carefully first to RT, then to 50 °C and stirred for 18 h. Reaction progress was monitored via TLC (silica-gel, CH:EE, 5+1). The reaction mixture was poured into H_2O (250 ml) to neutralize the excess of NaH. The product was extracted with DCM ($3 \cdot 300$ ml), the organic layer was dried over Na_2SO_4. The solvent was removed under reduced pressure. Finally the crude product was purified twice via flash column chromatography (silcia-gel, cond. CH, CH:EE, 7+1 (first), CH:EE, 12+1 (second)) yielding a brown oil (**16**).

Yield: 350 mg (33%)

TLC: R_f= 0.65 (silica-gel, CH:EE, 10+1)

NMR spectra in the appendix 10.23 page 98:
^{1}H-NMR (300 MHz, Chloroform-d): δ 7.13 (t, J = 8.2 Hz, 1H), 6.30 (d, J = 9.2 Hz, 1H), 6.23 (d, J = 6.5 Hz, 2H), 3.81 (s, 3H), 3.31 – 3.22 (t, 4H), 1.59 (p, J = 7.5 Hz, 4H), 1.45 – 1.30 (m, 4H), 0.97 (t, J = 7.3 Hz, 6H)

For the bromination reaction N,N-Dibutyl-3-methoxyaniline (100 mg, 425 µmol, 1.00 eq) was dissolved in 2 ml $CHCl_3$ in a round bottom flask. Via a dropping funnel 2 ml of a Br_2 solution (637 µmol, 1.50 eq) in $CHCl_3$ were added drop-wise to the stirring solution at 0 °C. The reaction mixture was heated to RT and stirred for 4 h. Reaction progress was monitored via TLC (silica-gel, CH:EE, 10+1). For neutralizing the excess of Br_2 3% aq. $Na_2S_2O_3 \cdot 5\,H_2O$ was added to the red solution (color change to grey, green). The organic layer was washed with H_2O ($3 \cdot 100$ ml) and the solvent was removed under reduced pressure. Finally the crude product was purified via flash column chromatography (silica-gel, cond, CH, CH:EE, 10+1) yielding a red-brown liquid. After taking NMR measurements one can see that the red-brown liquid is not the desired product.

5 Results and Discussion

In the following all experiments will be discussed and the photophysical properties of the dyes will be shown.

5.1 Synthetic considerations

The synthetic experiments for each reaction will be discussed in this section. The aim of this thesis was to synthesize new phthalocyanine and porphyrin based dyes with red shifted absorption. First, a new phthalocyanine dye based on a carbazole precursor (see figure 5.1 compound **5**) was synthesized. Second, existing porphyrin dyes (e.g. Pt-TPTBPF or Pt-TPTtBuBPBr) should be modified via Friedel-Crafts acylation reaction. Here two new dyes were synthesized. Next, Pt-TPTtBuBPBr (see figure 5.4 on page 49) was modified by Sonogashira coupling. Also synthesis of a new porphyrin dye based on a thiadiazole (TDA, see figure 5.9 on page 54) was attempted. This reaction was not successful. Moreover two other experiments were conducted.Synthesis of highly soluble porphyrin and phthalocyanine dyes was attempted which was expected to form J-aggregates (see figure 5.11 on page 55). On the other hand an existing system based on Pt(II) complexes supported by tetradentate N_2O_2-chelates (see figure 5.13 on page 57, [126]) was attempted to be modified to achieve longer wavelengths and improve brightness.

5.1.1 Carbazole based Phthalocyanine: compound 6

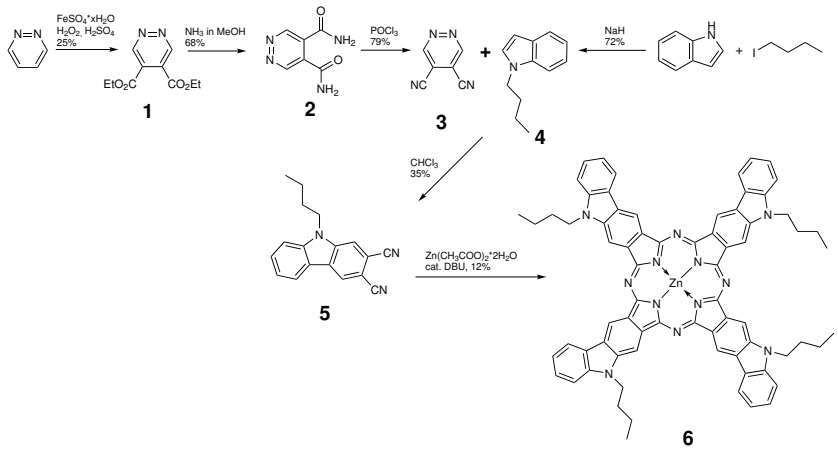

Figure 5.1: Overview of the route of synthesis for compound **6**

The synthetic pathway for the synthesis of compound **6** is shown in figure 5.1. For the synthesis of the carbazole precursor **5** several reaction steps were necessary, whereby some appeared to be challenging. The according literature is given in the experimental part at each reaction separately.

Pyridazine is the starting material. Compound **1** is the corresponding dicarboxylate which is then modified to amide **2**. These steps worked without a problem and with similar yields according to the literature [116]. Corresponding to the fact that compound **2** precipitates, no further work-up was needed and the product could be isolated as a white solid. On the contrary, the synthesis of **3** was challenging. Here several reaction conditions (see figure 5.2) had to be tested before the desired product could be synthesized within a reaction of $POCl_3$ in an open system (see 4.4 on page 32). Within these reactions in situ generated acid decreases the pH value of the solution drastically. Therefore the formed product is destroyed. To solve this problem the synthesis had to be conducted in an open system and not in a closed Schlenk flask. Additionally, one has to bubble N_2 through the solution to remove the formed acid immediately. With this modification of the synthetic procedure the desired product **3** could be synthesized in sufficient yield. The exact experimental procedures for each reaction shown in the figure below can be found in the appendix (see section 10.5.1 on page 109).

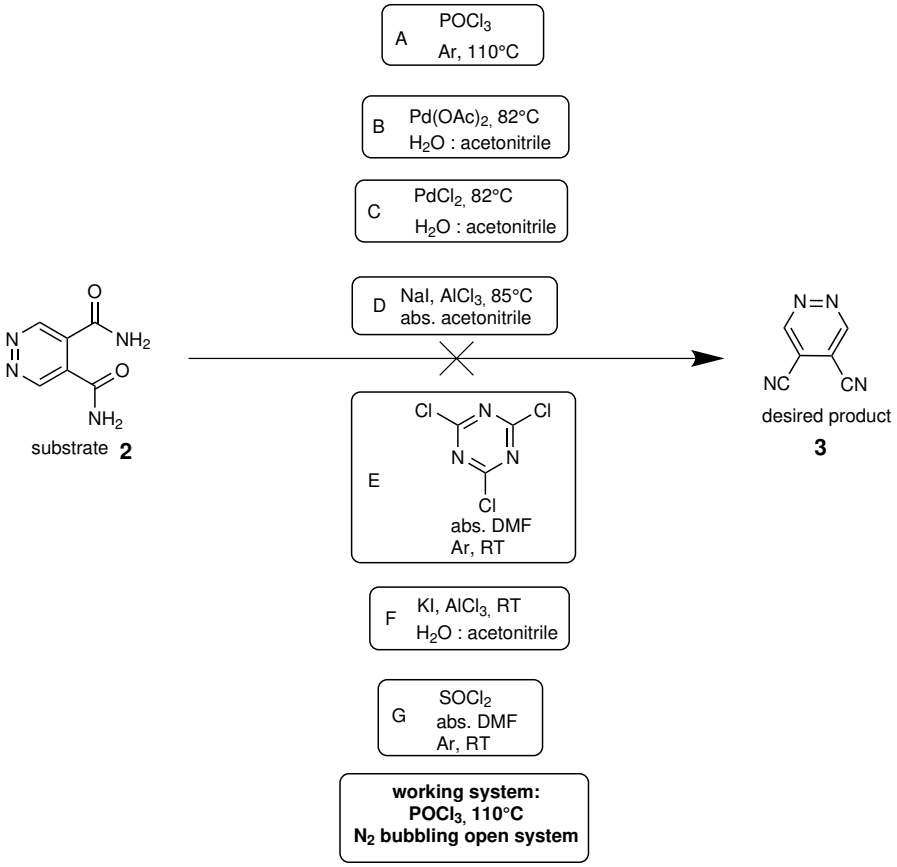

Figure 5.2: Screening of different synthetic routes for the synthesis of compound **3**

Besides these reactions also another synthetic route was investigated [130]. In figure 5.3 the direct reaction from **1** into compound **3** is shown. This reaction did not lead to the desired product. The ^{1}H-NMR did mainly show the educt so the reaction did not take place at all.

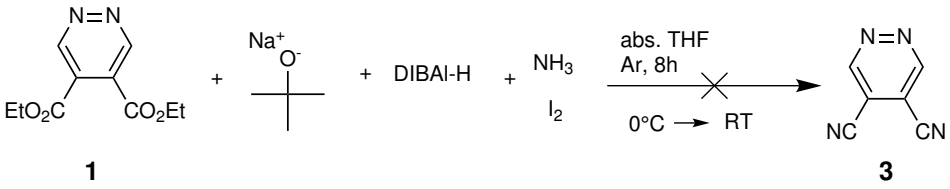

Figure 5.3: Attempted synthesis of compound **3** via direct conversion of compound **1**

For the second building block of compound **5** indole was alkylated with a butyl group by a straight forward synthesis according to literature [118] (see figure 5.1). To synthesize **5** the compounds **3** and **4** had to react under harsh conditions [119–121]. For this reaction an Ace pressure tube was needed. The problem with this reaction was not only its low yield but also the solvent ($CHCl_3$) attacking the sealing of the pressure tube. One had to find the right reaction time which was limited by the following two factors. It should be long enough for good yields but short enough that the solvent did not destroy the sealing. A better system for this reaction may be an autoclave or the usage of a Teflon based sealing.

Also the synthesis of compound **6** was challenging because the choice of the solvent was here very crucial. Finally the recation could be successfully performed by using abs. DMF as solvent, catalytic amounts of DBU, zinc acetate, Ar atmosphere and 16 h reaction time. After purification via flash column chromatography the desired green Zn-complex **6** could be isolated in two fractions with significantly different R_f values. After interpretation of the corresponding MS spectra which were identical (see appendix 10.4.1 on page 100) it could be conducted that these two spectra show two different isomers of compound **6**. Reaction 4.1.6 was not only conducted in the working system with abs. DMF but also in abs. N-methyl-2-pyrrolidone (200 °C), abs. N,N-dimehtylacetamide (165 °C) and abs. diphenyl ether (200 °C). None of these other solvents nor reaction conditions led to the desired product **6**. One approach was performed under the same reaction conditions as in reaction 4.1.6 not in a Schlenk flask but in an Ace pressure tube (same tube as used in reaction 4.1.5) at 180 °C. This reaction did only lead to traces of the desired product which could not be isolated.

5.1.2 Porphyrin Modification by Sonogashira coupling

For the modification of existing porphyrin dyes by Sonogashira coupling or under Friedel-Crafts reaction conditions Pt-TPTtBuBPBr and Pt-TPTBPF were used. These two dyes can be obtained in high yields via convenient template synthesis.

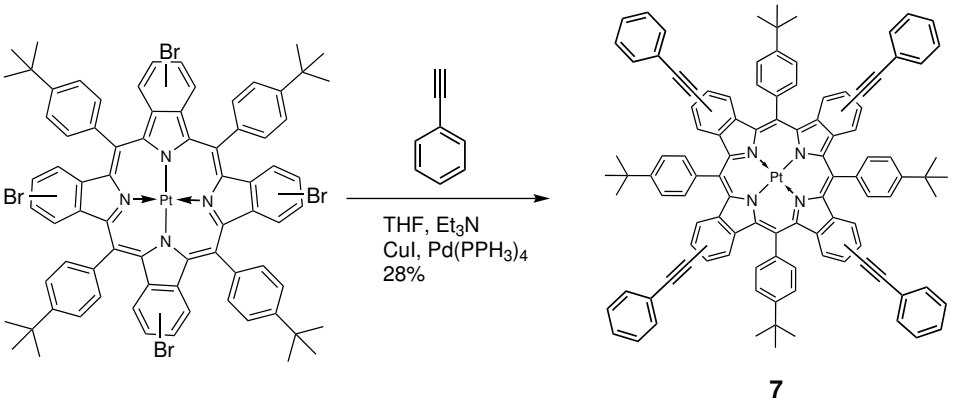

Figure 5.4: Synthesis of compound **7** under Sonogashira conditions

Phenylacetylene was coupled at the β position to Pt-TPTtBuBPBr by Sonogashira coupling (see figure 5.4) [123, 124]. The aim of this reaction was to introduce alkine substituents at the β positions by replacing the Br atoms. We wanted to investigate whether the substitution of the Br atoms by phenylacetylene results in a significant change in the spectral properties or if this hardly affects the π-system of the dye. The reaction could be successfully performed by using abs. THF, abs. Et_3N, Ar atmosphere, $Pd(PPh_3)_4$ and CuI the two catalysts and a reaction time of 18 h at 75 °C. After work-up and purification via flash column chromatography two different fractions with a tetra- and two three-substituted products (see MS spectra in the appendix 10.4.2 on page 102) could be isolated as green solid (compound **7**). One three-substituted product had a remaining Br atom the other one had no substitution at this position. Due to the challenging purification no pure fraction of the different products could be isolated.

5.1.3 Porphyrin Modification by Friedel-Crafts reaction

4-Chlorobenzoyl-chloride was coupled under Friedel-Crafts conditions at the β positions to M(II)-TPTBPF (see figure 5.5). As central metal ion platinum(II) or palladium(II) were used to achieve the desired products (**8, 9**). The aim of this synthetic modification was to investigate the impact of the new substituents on the π-system resulting in a bathochromic shift of the dye. These reactions are not time consuming (reaction time of 30-40 min) which allows a broad range of screenings in an appropriate time. The reaction could be successfully conducted by using abs. 1,2-dichlorobenzene, Ar atmosphere and $AlCl_3$ at 130 °C. After purification via flash column chromatography the green products **8** or **9** could be isolated as green solid (see MS spectra in the appendix 10.29 on page 105-107).

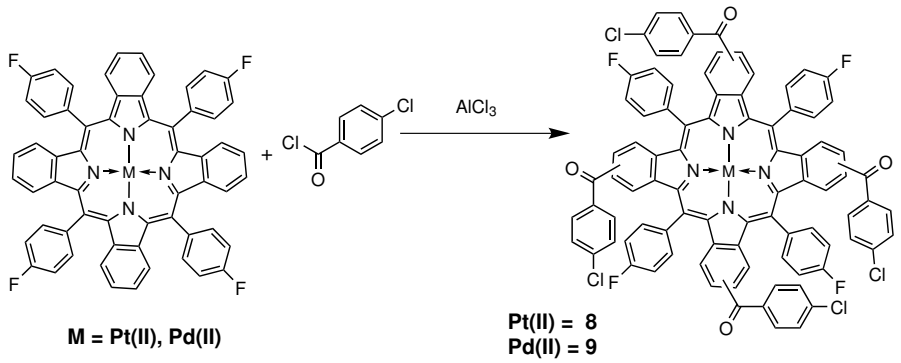

Figure 5.5: Synthesis of compounds **8** and **9** under Friedel-Crafts acylation conditions

After the success of the mentioned reactions above three other reagents were screened for the modification of Pt-TPTBPF by Friedel-Crafts acylation. For these screening reactions only the reagent was changed all other parameters stayed the same as in the reactions for **8** and **9**. The three used reagents for the screening were 2-(chloromethyl)benzoyl-chloride (see **a** in figure 5.6), α, α, $\acute{\alpha}$, $\acute{\alpha}$-tetrabromo-o-xylene (see **b** in figure 5.6) and 2-bromobenzoyl-chloride (see first reaction step in figure 5.7). The aim of the specific modification of the dye by using α, α, $\acute{\alpha}$, $\acute{\alpha}$-tetrabromo-o-xylene was to introduce Br atoms for further aromatization via dehalogenation. Additionally, the Br substituents give new opportunities of further functional modifications. Due to the fact that products formed in figure 5.5 are shifted bathochromically compared to their corresponding M-TPTBPF we wanted to investigate whether a further red shift could be achieved by introducing 2-(chloromethyl)benzoyl-chloride moieties. This substitution would lead to an even more rigid system of the dye due to further extension of the π-system.

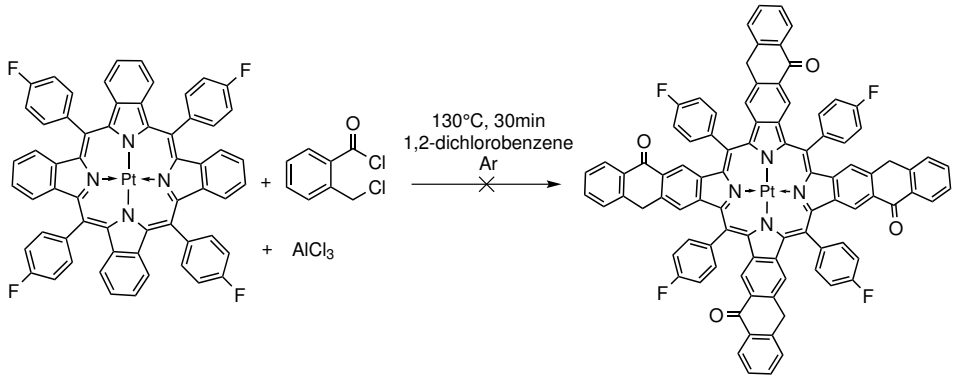

(a) Attempted synthesis of Pt-TPTBPF-naphthalen-1(4H)-one

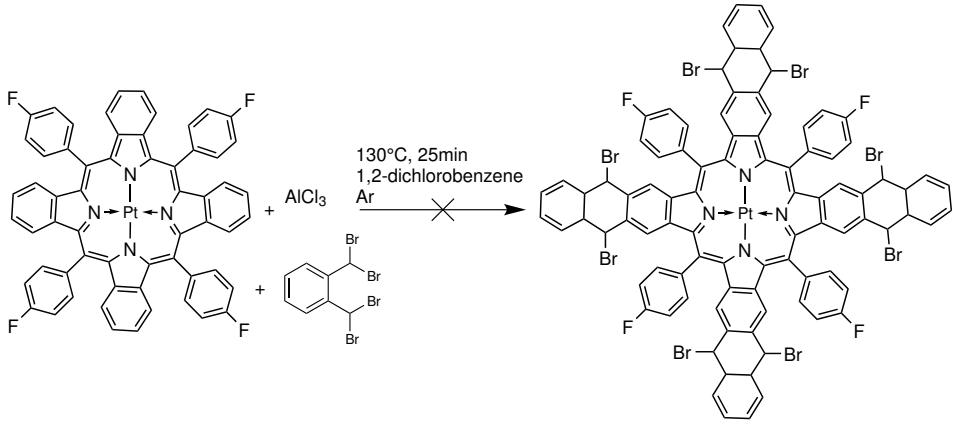

(b) Attempted synthesis of Pt-TPTBPF-DBr-naphthalene

Figure 5.6: Two reactions of the screening for modification of Pt-TPTBPF by Friedel-Crafts alkylation with different reagents

The progress of both reactions shown in figure 5.6 was monitored by absorption spectroscopy. After a significant change in the spectra the solution was quenched as described in the appendix (see section 10.5.2 on page 111). Whereas in reaction **a** a dark green solid could be isolated, this was not possible for reaction **b**. The absorption spectra after the work-up and purification showed the educt Pt-TPTBPF. A specific reason for this result could not be found yet but obviously the formed product gets degraded within the work-up procedure.

The next investigated experiment was the synthesis of Pt-TPTAPF (see figure 5.7). Therefore two reaction steps would be necessary. First, the addition of α, $\acute{\alpha}$-dibromo-o-xylene under Friedel-Crafts alkylation conditions and second, the oxidation of the ring system. This would lead to an extended and rigid π-system which would result in a bathochromical shift even more significant than for that observed for tetranaphthaporphyrin.

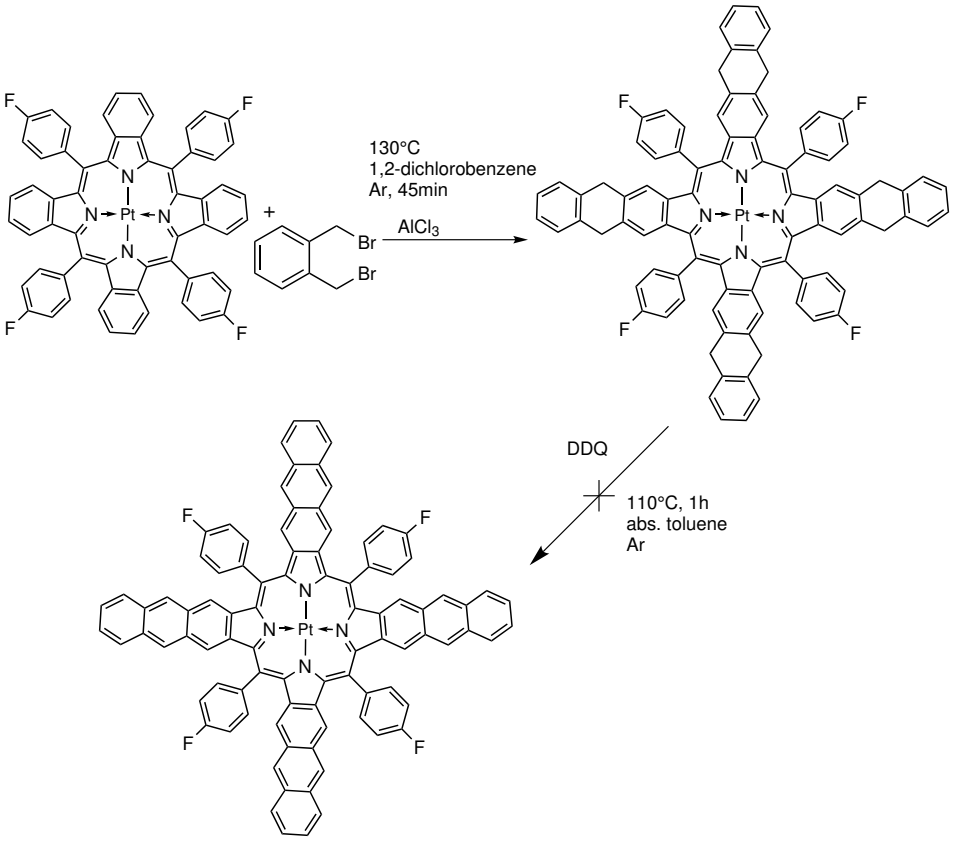

Figure 5.7: Attempted synthesis for Pt-TPTAPF under Friedel-Crafts alkylation conditions (first step) and oxidation with DDQ (second step)

The first reaction step was monitored via absorption spectroscopy and TLC. After the work-up a dark green solid could be isolated which was attempted to be oxidized in the second reaction step by DDQ (see experimental procedure in the appendix 10.5.2 on page 112). For the first reaction step a lower R_f value compared to the educt could be detected. Therefore it was assumed that the reaction did take place. Due to no significant change in the absorption spectra it was concluded that the oxidation reaction did not work. As mentioned above the oxidation of the ring system should lead to an rigid molecule with extended π-system.

As different dye for the modification via Friedel-Crafts acylation with 2-bromobenzoyl-chloride Pt-TPTtBuBPBr was used. A second reaction step with an alkyl amine should then result in a porphyrin dye with four attached acridone moieties (see figure 5.8). The aim of this synthesis was again to modify an existing porphyrin dye by introduction of aromatic substituents to achieve a bathochromic shift. The introduction of the acridone moieties would result in a more rigid complex which decreases the solubility but should also shift the absorption/emission spectra to longer wavelengths. To counteract this effect long alkyl chains at the nitrogen atoms were introduced, resulting in an increased solubility of this new compound.

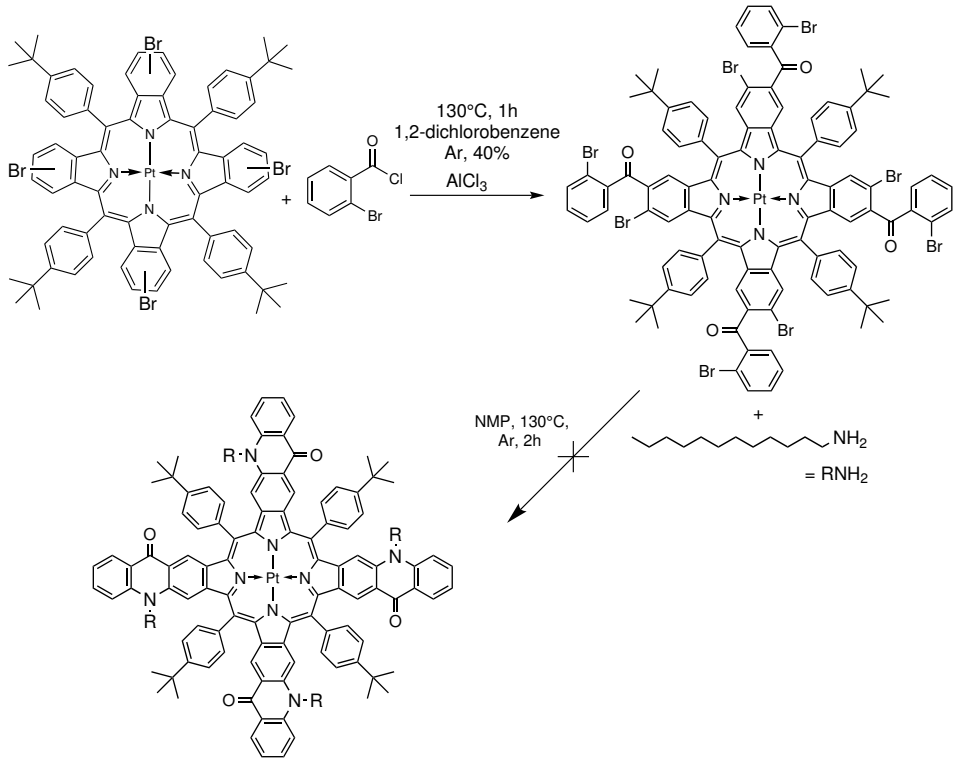

Figure 5.8: Attempted synthesis of Pt-TPTtBuBPBr-2-benzoyl-Br under Friedel-Crafts acylation conditions

For the first reaction step again the same reaction conditions were applied. 2-Bromobenzoyl chloride was used as reagent to couple to the porphyrin core. Conversion control was performed by using absorption spectroscopy and TLC. After work-up and flash column chromatography a dark green solid could be isolated (see experimental procedure in the appendix 10.5.2 on page 112) which was added to react with 1-dodecylamine leading to a new porphyrin dye with attached acridone moieties. The reaction progress was monitored via absorption spectroscopy and TLC. For the second step no product formation could be observed. Since no structural analysis were performed after the first reaction, one can not be sure which reaction step did not work properly.

5.1.4 New Porphyrin with thiadiazole as main building block

A new porphyrin dye based on a benzothiadiazole (BTD) as main building block was attempted and the electronic influence of such moieties on the porphyrin core unit investigated. Due to the fact that these are EWGs a red shift was expected. After the synthesis, this compound should be characterized and its photophysical properties compared to the corresponding Pt-TPTBPF. The first two reaction steps to achieve the precursor were performed by Matthias Schwar according to literature [131, 132]. Here starting material was 1,2-diamino-4,5-dibromobenzene which yielded after treatment with $SOCl_2$ the corresponding thiadiazole.

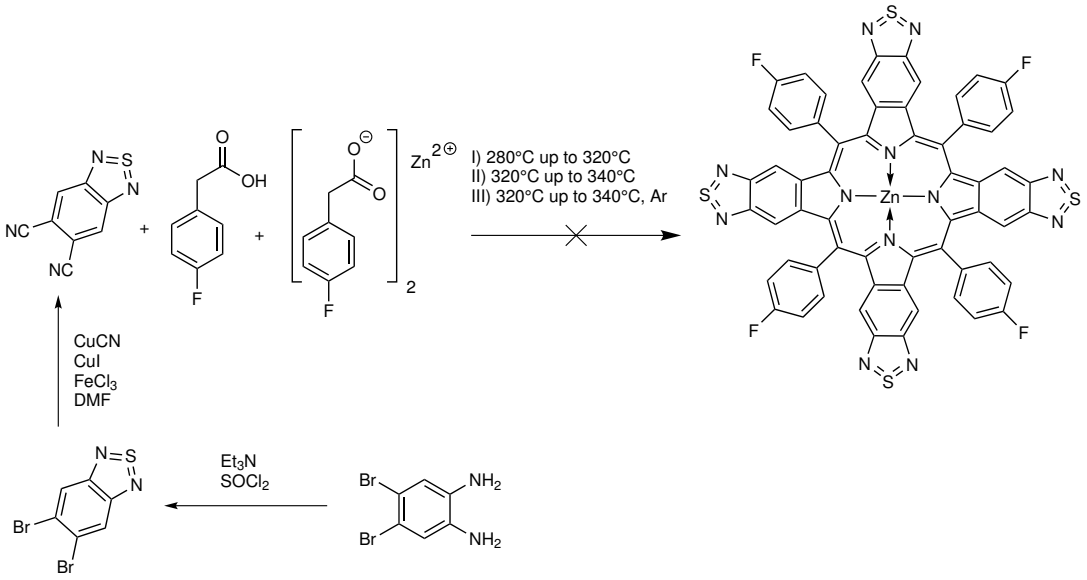

Figure 5.9: Attempted template synthesis of Pt-TPTBPF-TDA

The template method was used for the screening shown in figure 5.9. Due to the fact that the precursor was just available in small amounts a very small scale of a few milligrams for this synthesis was necessary. Therefore a pre-screening with a reference porphyrin dye was successfully conducted (5.10). For the screening for the new porphyrin dye different starting temperatures as well as different reaction times and atmospheres were investigated (see experimental procedure in the appendix 10.5.3 on page 113). In the monitoring of the reaction progress no specific porphyrin signals (Soret- and Q-band) could ne detected. Due to the fact, that the color of the reaction mixture changed to brown instead of green, it was assumed that this precursor is not suitable for the template method and degrades at higher temperatures.

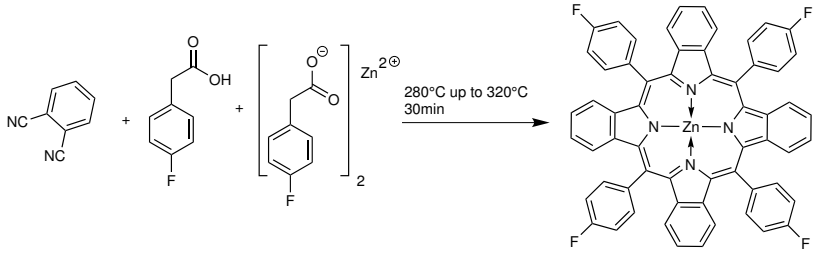

Figure 5.10: Synthesis of Pt-TPTBP as reference for this small template synthesis in a sealed 200 µl capillary

5.1.5 Highly soluble Porphyrin and Phthalocyanine dyes for J-aggregates

As mentioned in section 2.6 on page 23 f porphyrin and phthalocyanine dyes can be used for the formation of J-aggregates. The synthetic pathway for the synthesis of suitable complexes is shown in figure 5.11. For the synthesis of the precursor compounds **10** and **11** only one or two

synthetic steps were necessary. These reactions were performed according to literature [125] (see experimental procedure in section 4.12 on page 38 and 39). Since within the synthesis of porphyrins many different substitution patterns and also side products like aza-benzoporphyrins are formed, leading to a very challenging separation process. Therefore we decided to first investigate this phenomenon with phthalocyanines, due to their comparable behavior in forming J-aggregates like their corresponding porphyrins.

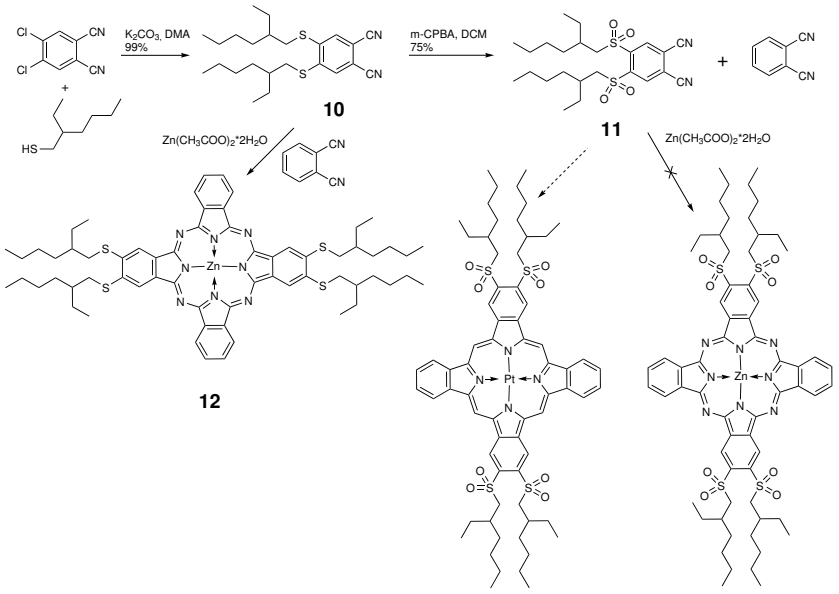

Figure 5.11: Synthetic route for the synthesis of compound **12** and other phthalocyanine or porphyrin dyes with compound **10** or **11** as main building block

Here 4,5-Dichlorophthalonitrile is the starting material. Compound **10** could be isolated after substitution of the chloride atoms by 2-ethylhexane-1-thiol groups. Oxidation of compound **10** by m-CPBA results in the formation of compound **11**. Both reactions worked without any problems. The synthesis of the phthalocyanine **12** was challenging. Even though the equivalents of the used building blocks can be adapted different substitution patterns were expected. Besides the in figure 5.11 shown 2/2 trans substitution also a cis configuration as well as 3/1 or 1/3 patterns are possible. This reaction could be performed by using abs. DMF, precursor **10**, zinc acetate, phthalonitrile, DBU as a catalyst, and Ar atmosphere at 155 °C for 16 h. Nevertheless the purification was very challenging and even after precipitation into a 3+1 mixture of H_2O:MeOH and several purification attempts with flash column chromatography no pure fraction of the product could be isolated (see experimental procedure section 4.14 on page 40).

Due to this very challenging reaction another attempt for the synthesis of a phthalocyanine dye with this type of precursor was performed (see figure 5.12). For this reaction the oxidized precursor **11** was used. Besides that, abs. DMF, zinc acetate, DBU as a catalyst and phthalonitrile under Ar atmosphere at 155 °C for 16 h were necessary. After conversion control

via absorption spectroscopy, the work-up and purification, a green solid could be isolated. However, the MS spectra did not show any signals which could be estimated as a phthalocyanine dye (see appendix 5.12 on page 108). The calculated exact mass of this disubstituted complex should be 1308.46, a monosubstituted complex should have an exact mass of 956.29 but non of these values could be observed in the MALDI-TOF spectra. Due to the fact that the main signal is located at 574.16 it is confirmed that no phthalocyanine dye with compound **11** as main building block was formed.

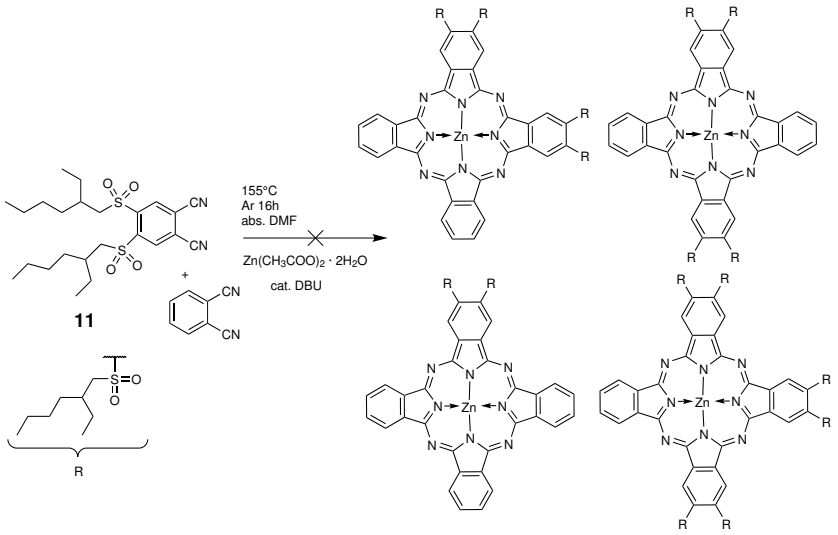

Figure 5.12: Attempted synthesis of Zn−bEHS$_2$−Pc; different isomers possible

5.1.6 Pt(II) complexes supported by tetradentate N_2O_2 chelates: Diphenyphenanthroline system

An overview of a completely different system for an oxygen sensitive Pt(II) complex is given in figure 5.13. This system is based on a tetradentate N_2O_2 chelate ligand. Thereby the ground structure is 4,7-diphenyl-1,10-phenanthroline, where at the α positions besides the nitrogen atoms N,N-dibutyl-3-methoxyaniline groups are attached. After deprotection of the methoxy groups Pt(II) should coordinate at the two oxygen and the two nitrogen atoms. This synthesis was inspired by the work of Lin et al. [126]. This group already published a similar system which is shown in figure 4.15 on page 41. The idea for the new synthesis was to modify their Pt($Ph_2N_2O_2$)dpp system by adding an electron donating substituent in the para position which results in a push-pull system. The according literature is given in the experimental part at each reaction step separately.

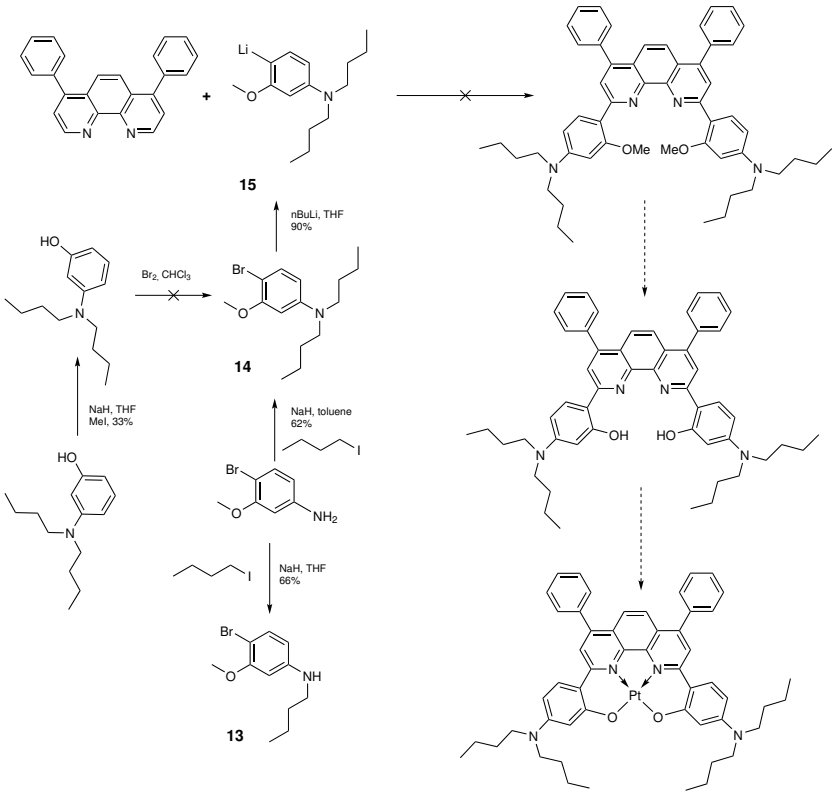

Figure 5.13: Theoretical synthetic overview for the synthesis of Pt(II) complexes with tetradentate N_2O_2 chelates

4-Bromo-3-methoxyaniline is the starting material. The first step was the di-alkylation by 1-iodobutane of this molecule leading to compound **14**. The mono substituted product **13** is also shown in figure 5.13. The alkyl chains should increase the solubility of the desired complex in the end. Although this reaction looks quiet easy it was challenging to get the di-substituted product. Different reaction conditions had to be investigated. When the reaction was conducted in abs. THF at 60 °C, only the mono-substituted product could be achieved. For the introduction of the second alkyl chain another solvent at harsher conditions was necessary. The successful synthesis of **14** could be achieved in sufficient yield by using abs. toluene as solvent at 110 °C. Besides this synthetic route for the desired building block **14** an alternative route was investigated (see figure 4.19 on page 44). Therefore 3-(dibutylamino)phenol was methylated and after specific bromination at the para position according to the nitrogen the reaction was expected to lead compound **14**. However only the methylation was successful. The bromination reaction could not be performed in a specific way. This was proven by NMR measurements. Compound **15** was *in situ* formed. Therefore different reagents and reaction conditions were conducted (see figure 5.14). First, the reaction was performed according to Lin et al. by using lithium metal in abs. Et_2O under reflux (**a** in figure 5.14). After 2 h the reaction was quenched with NH_4Cl and conversion control was performed by GC-MS. Here no product formation could be established.

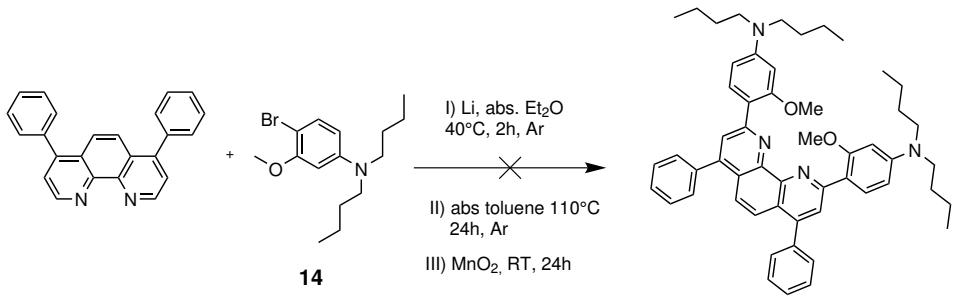

(a) $dBAN_2O_2$ –dpp: published method for bipyridyl system

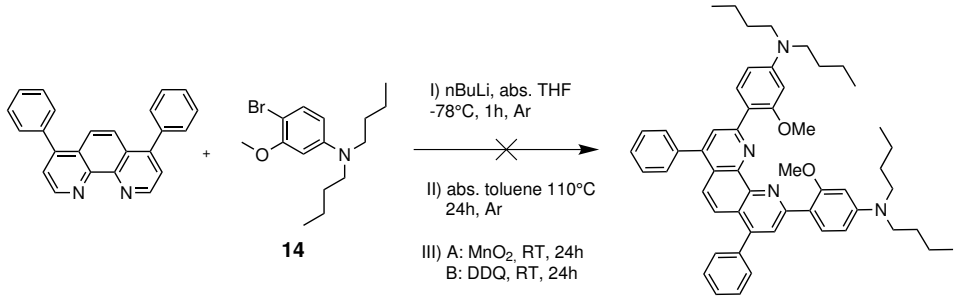

(b) $dBAN_2O_2$ –dpp: metal-halogen exchange with nBuLi

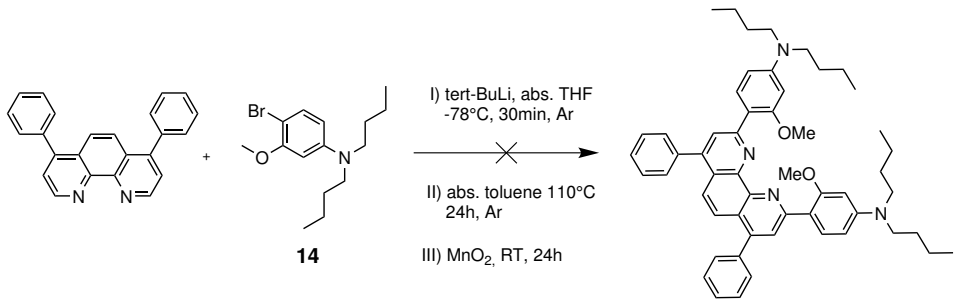

(c) $dBAN_2O_2$ –dpp: metal-halogen exchange with tert-BuLi

Figure 5.14: Different attempted synthesis for the reaction of **14** with 4,7-diphenyl-1,10-phenanthroline

Therefore another method for the metal-halogen exchange was investigated by using n-BuLi in abs. THF at -78 °C (**b** in figure 5.14). This reaction shows complete conversion after 1 h as visible from GC-MS analysis. Nevertheless the next reaction steps did not work. **15** was expected to react with 4,7-diphenyl-1,10-phenanthroline to form the desired ligand. The reaction conditions are given in figure 5.14. After the work-up, NMR measurements as well as HPLC-MS measurements were performed. None of these showed the desired product. The HPLC measurement, however showed traces of two other products. After the interpretation of the masses it was confirmed that these signals result from mono and di alkylated 4,7-diphenyl-1,10-phenanthroline species whereby the butyl chains instead of precursor **15** were substituted at the ring system. For the metal-halogen exchange 1.2 eq of n-BuLi were used, wherefore it was conducted that the unreacted n-BuLi may have reacted with 4,7-diphenyl-1,10-phenanthroline to

form these side products. In another attempt 2 eq of tert-BuLi were used for the metal-halogen exchange. Thereby the first equivalent reacted as desired to exchange the Br atom at the phenyl ring. The second equivalent was involved in the dehydrohalogenation of tert-BuBr leading to LiBr, isobutene and isobutane (two volatile compounds). Because of this, the equilibrium of the reaction is shifted towards the product side. However, this reaction did not show any product formation. The exact experimental procedures of these different attempts for the formation of the ligand molecule can be looked up in the appendix 10.5.5 on page 114f.

5.2 Dye characterization

For photophysical characterization of the synthesized dyes absorption and emission spectra were measured. All measurements were performed in solution (toluene). For compound **8** and **9** further photophysical properties were investigated by Peter Zach.

5.2.1 Photophysical properties

Compound 6

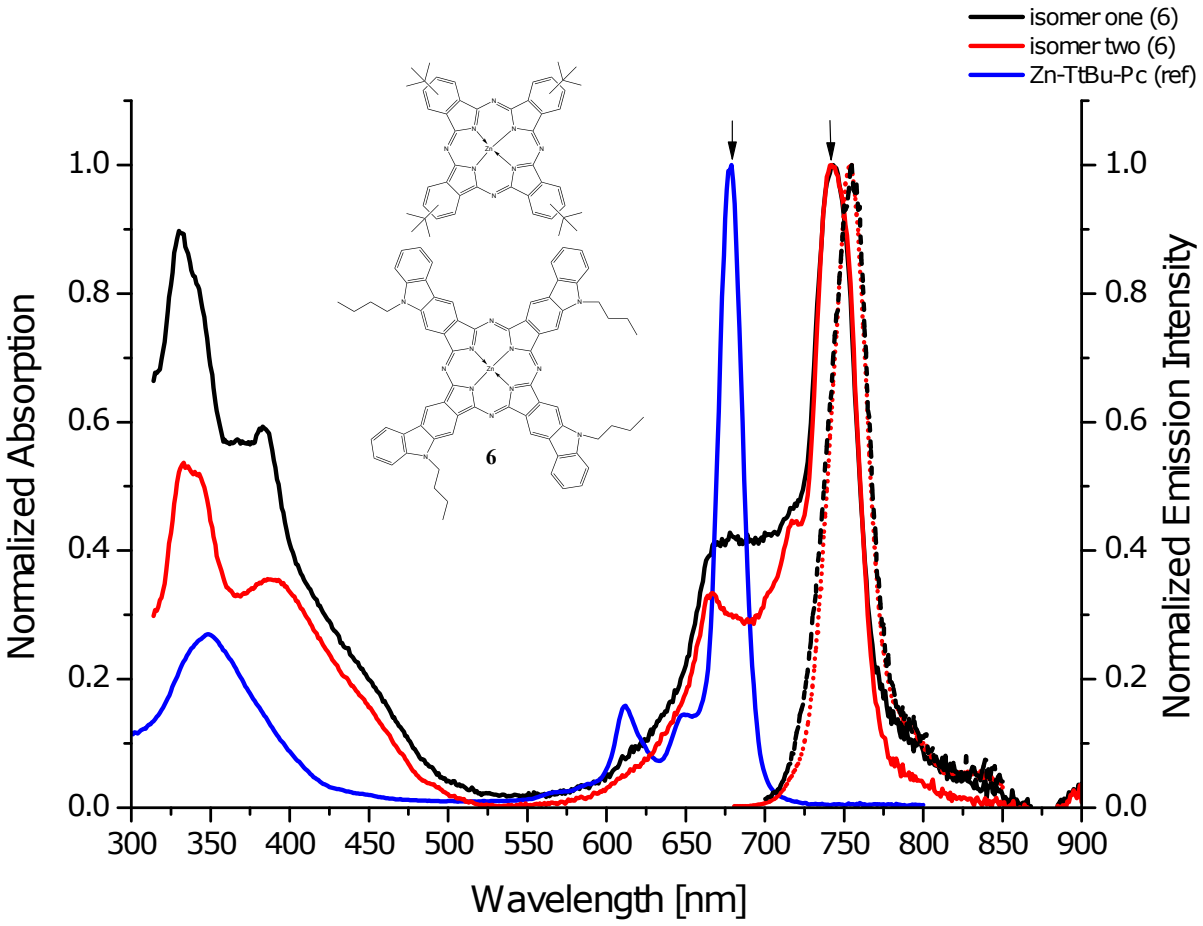

Figure 5.15: Absorption and emission spectra of different isomers of compound **6** compared to a reference dye in anoxic toluene

Aim of this experiment was the synthesis of a new porphyrin dye based on the carbazole precursor **5** with red shifted absorption spectrum. Unfortunately this could not be achieved due to the very challenging synthesis and thus very small amount of precursor, not sufficient for the template synthesis. Nevertheless compound **6**, a new phthalocyanine dye could be isolated. In figure 5.15 the absorption and emission spectra of two different isomers of compound **6** are

shown (red and black curves). The significant peaks of both fractions have the same shift in absorption as well as in the emission spectra. Just the intensities of the specific signals vary in their heights. Comparing absorption and emission spectra one can see that these dyes have a very small Stoke's shift which is typical for phthalocyanine dyes. The absorption maximum is located at 742 nm whereas the emission maximum is just shifted 11 nm so that the two spectra have a high overlap. The blue curve represents the absorption spectrum of the reference dye Zn-TtBu-Pc. Compared to this reference the absorption spectrum of the new dye **6** is bathochromically shifted by over 60 nm. According to this result it would be interesting to synthesize the corresponding porphyrin dye, which would be interesting in NIR sensing applications. For instance the absorption of such a Pt(II) porphyrin complex is expected to be at around 675 nm which would compete with Pt(II) complexes of tetranaphthaporphyrin.

Compound 7

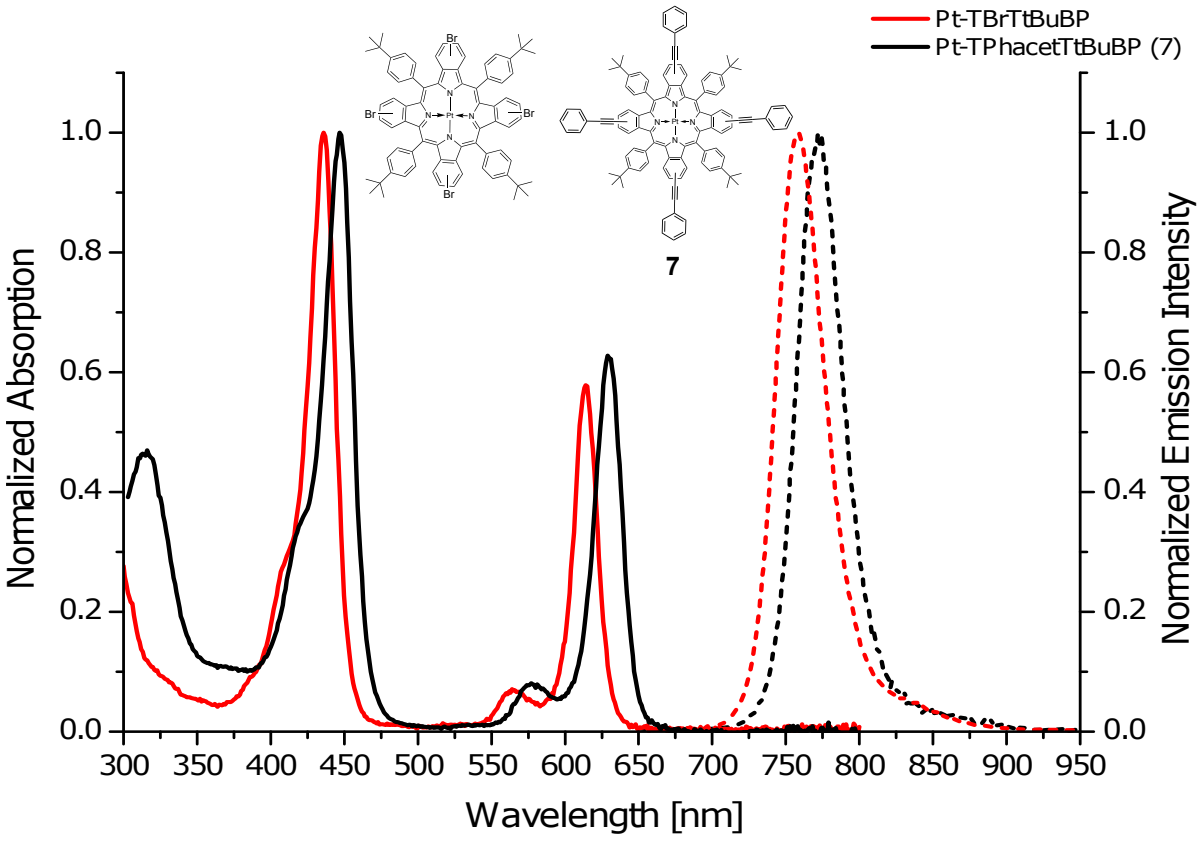

Figure 5.16: Absorption (pure) and emission (dotted) spectra of compound **7** compared to the substrate in anoxic toluene

The aim of this synthesis was to investigate the influence of substituting a Br atom by an aromatic alkine moiety at the β position of the porphyrin core on the spectral properties of

the dye. Figure 5.16 shows the absorption and emission spectra of the substrate (Pt-TPTBP, red curve) and compound **7** (black curve). Neither the absorption nor the emission maxima are significantly shifted bathochromically compared to the substrate. Therefore it is assumed that the substitution at the β position of the porphyrin dye only slightly affects the π-system. One reason for this could be that the angle of the orbitals does not fit so that the π-system cannot be further extended. Nevertheless, even this shift (10 nm) races the new Pt(II) complex compatible with the emission of 635 nm laser diode.

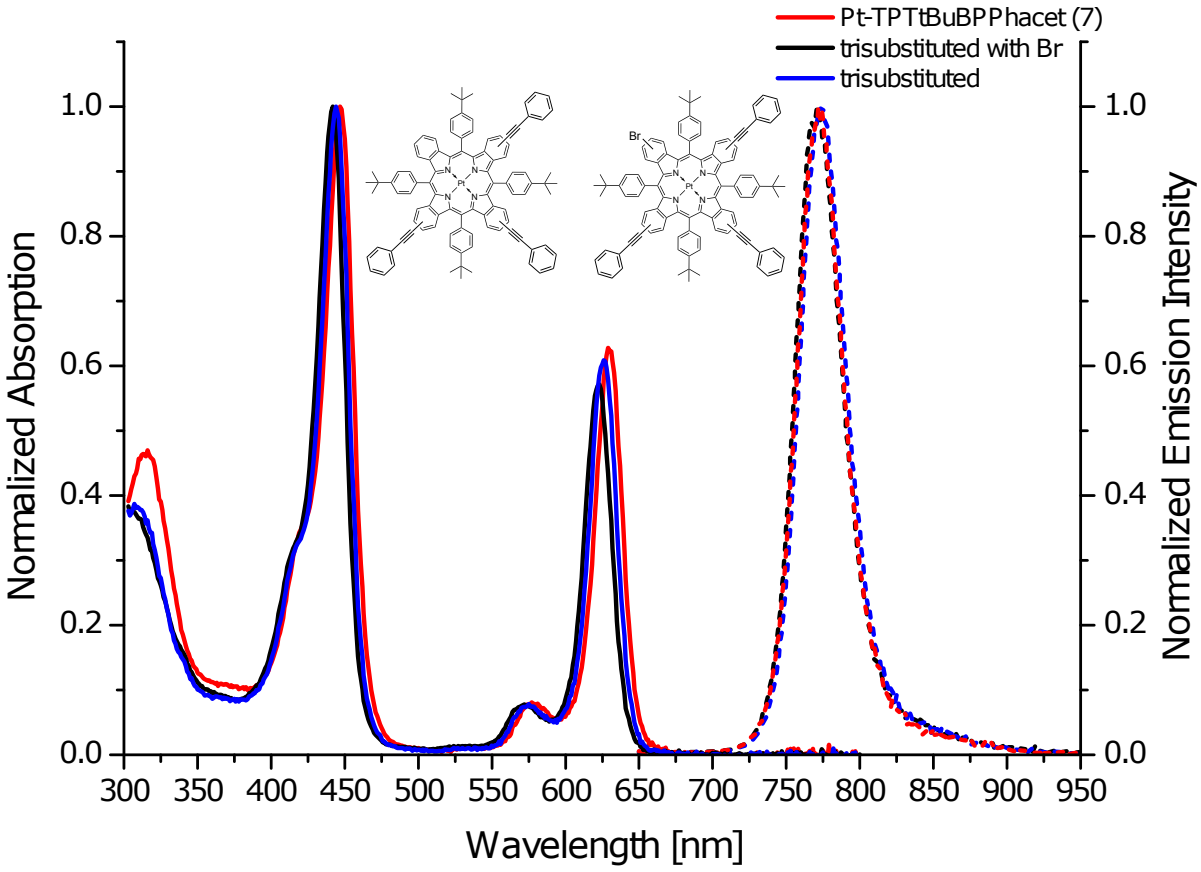

Figure 5.17: Absorption and emission spectra of different substituted products involved in the synthesis of compound **7** in anoxic toluene

In figure 5.17 the absorption and emission spectra of different substituted side products of this synthesis are shown (see **a**). According to the MS data (see appendix section 10.4.2 on page 102f) a trisubstituted product (blue curve) as well as a trisubstituted product with a remaining Br atom attached at the last β position (black curve) could be isolated. The proposed structures of these complexes are shown in **b** and **c** in figure 5.17. The curves show no significant change concerning their maxima compared to compound **7**. This result supports the theory that the π-system of the complex cannot be extended significantly by linkage of an aromatic group over an alkine moiety at the β position of a porphyrin dye.

Porphyrin Modification by Friedel-Crafts acylation

As mentioned above (see 5.1.3) different porphyrin dyes as well as different reagents were screened for this reaction type to investigate the influence of these substitutions at the β position of the porphyrin core on the photophysical properties of the dyes.

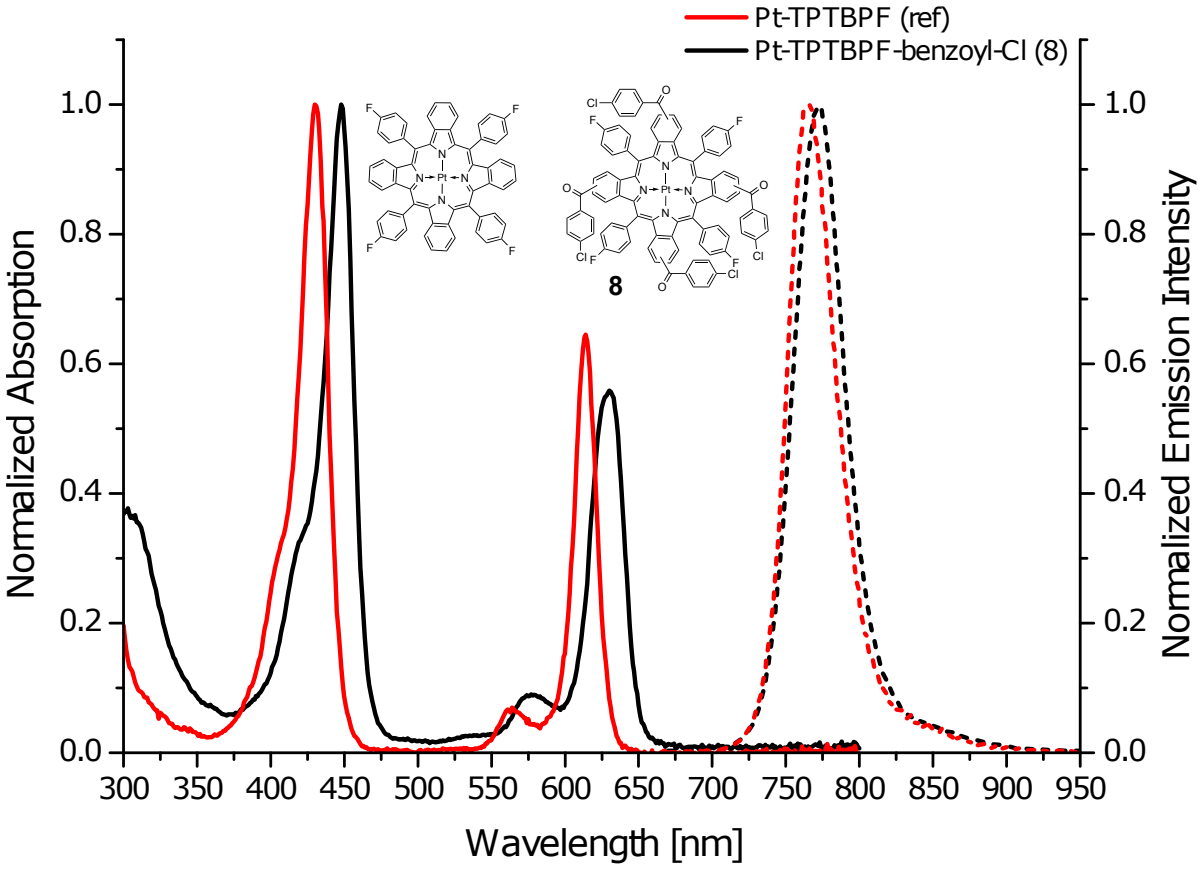

Figure 5.18: Absorption (pure) and emission (dotted) spectra of compound **8** compared to Pt-TPTBPF in anoxic toluene

Figure 5.18 shows the absorption and emission spectra of compound **8** (black curve) compared to the educt (Pt-TPTBPF, red curve). Here, one can see that the substitution of 4-chlorobenzoyl chloride at the β positions of the porphyrin core extended the π-system resulting in a bathochromic shift. Compared to the reference dye the Soret (430/449 nm) and Q-band (614/633) of the new dye are shifted by approximately 20 nn, whereas the emission maxima are just slightly red shifted (769/773 nm). Similar results could be achieved with the corresponding Pd(II) dye (see figure 5.19, black curve). Here, also the Soret (443/461 nm) as well as the Q-band (628/647 nm) were bathochromically shifted by approximately 20 nm compared to the substrate (Pd-TPTBPF, red curve). The emission spectra are almost identical (797/799 nm). A lower energy gap between the singlet and the triplet state of these new dyes compared to the educts could be an explanation for this behavior. **8** and **9** are now compatible with blue LEDs

and red laser diodes which makes them more attractive for new applications.

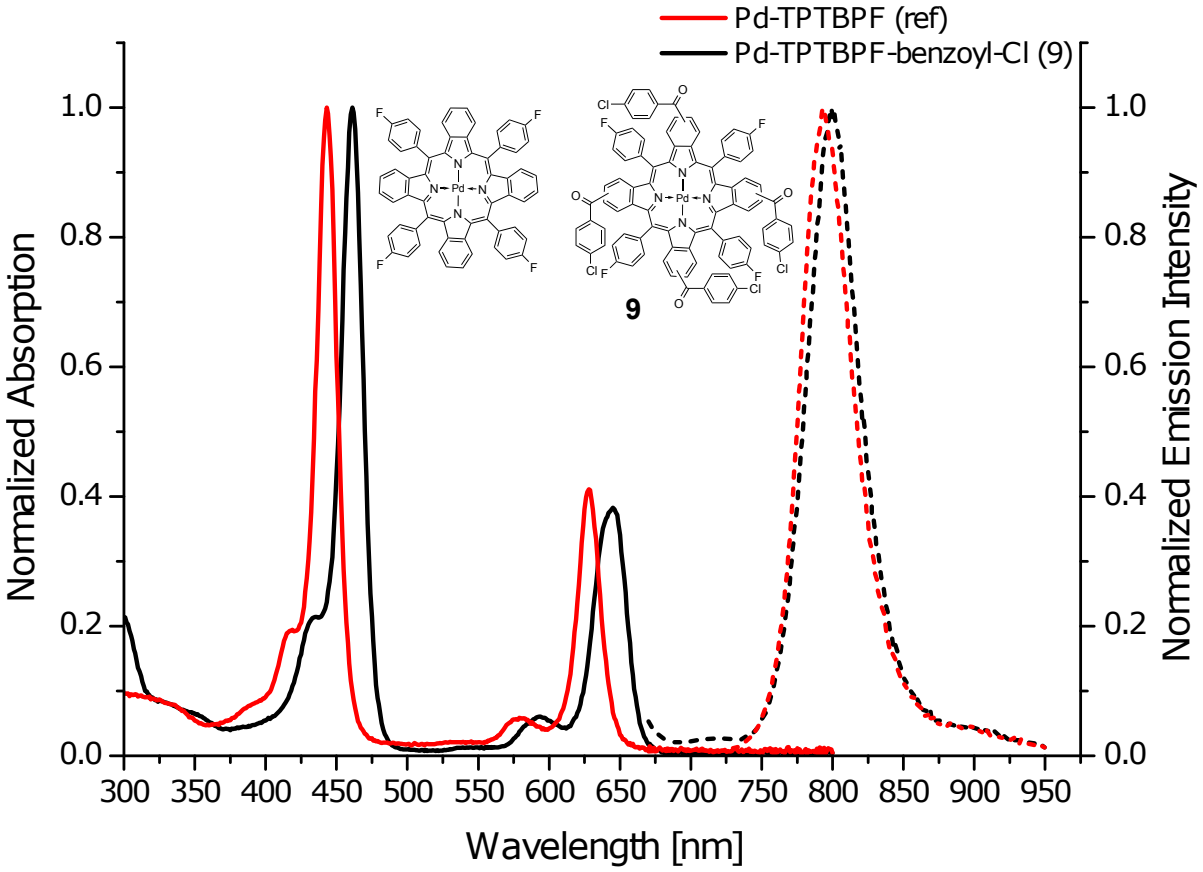

Figure 5.19: Absorption (pure) and emission (dotted) spectra of compound **9** compared to Pd-TPTBPF in anoxic toluene

For further dye characterization relative quantum yield and lifetime measurements in solution (toluene) were performed at RT for compound **8** and **9**. As reference dyes Pt- and Pd-TPTBP were used (see table 5.1). These results show that the new dyes have higher QY's and similar lifetimes compared to the corresponding reference dyes.

Table 5.1: Quantum yield and lifetime measurements of compound **8** and **9** in anoxic toluene at 23 °C compared to references [83]

Data	Compound 8	Pt-TPTBP	Compound 9	Pd-TPTBP
Excitation λ [nm]	619	619	633	633
QY [%]	70	51	31	21
τ [μ] in solution	47	47	313	289

Figure 5.20 shows the absorption spectrum of a fraction after purification via flash column chromatography of the attempted synthesis of Pt-TPTBPF-naphthalen-1(4H)-one (black curve)

compared to the substrate (Pt-TPTBPF). Here, one can see a bathochromical shift of the Soret and the Q-band. Nevertheless, this spectrum shows very broad bands, wherefore it is likely assumed that no pure product could be isolated. One explanation for this could be that the reagent and the porphyrin core unit just reacted at one position so that no ring closure occurred resulting in a free rotation of the new substituents. Also alkylation of meso-phenyl rings restricting their rotation and improving of the conjugation is possible. Furthermore various isomers would be formed if there was no ring closure at all four β positions.

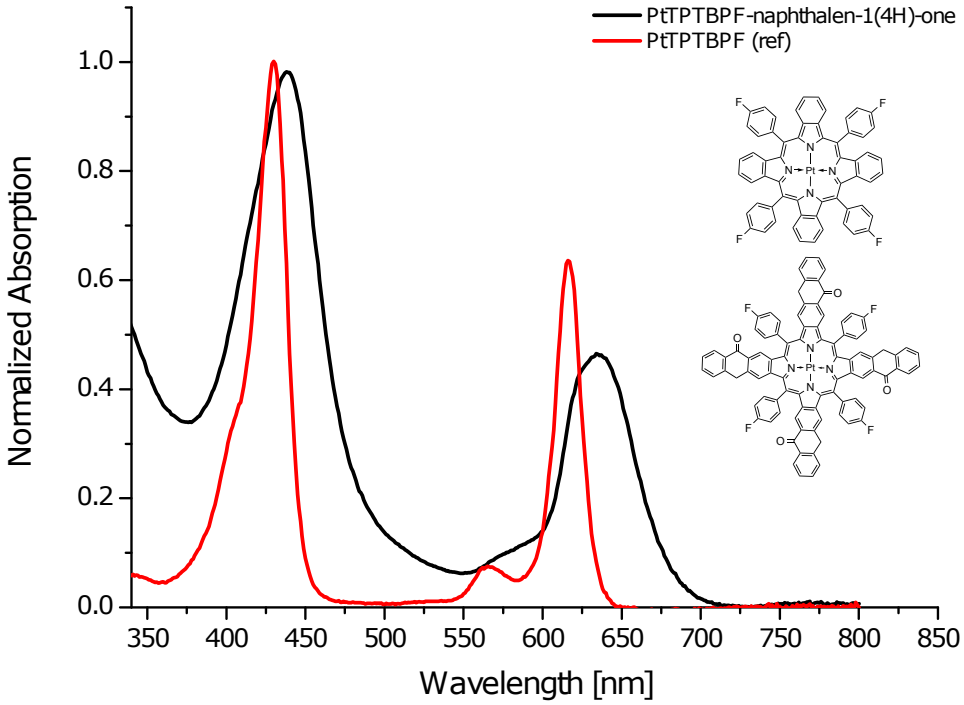

Figure 5.20: Absorption spectrum of product of attempted synthesis of Pt-TPTBPF-naphthalen-1(4H)-one and Pt-TPTBPF in toluene

Figure 5.21 shows the absorption spectrum of Pt-TPTtBuBPBr-2-benzoyl-Br (black curve) compared to the substrate (Pt-TPTtBuBPBr, red curve). The Soret and the Q-band of these two dyes just vary slightly. This result was expected due to the fact that the substitution by 2-bromobenzoyl-chloride at the β position did not create an extension of the π-system. A significant red shift was only expected after the second reaction step (see figure 5.8 on page 53) but as mentioned before this reaction could not be performed successfully. Nevertheless, the Q-band maximum is broader than the reference signal which indicates that this spectrum does not show a pure substance.

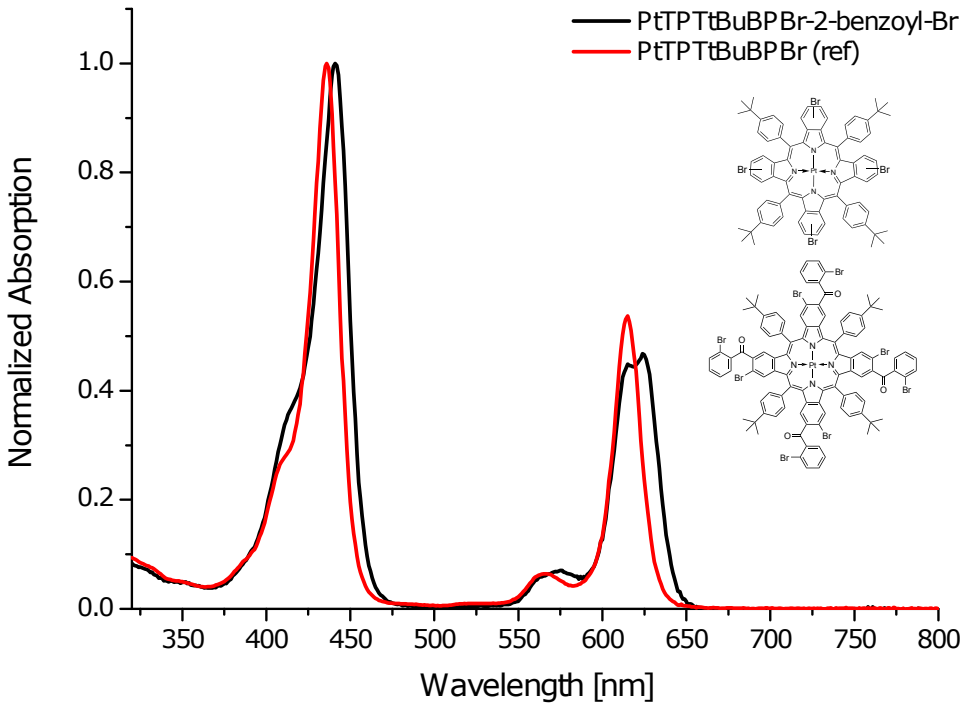

Figure 5.21: Absorption spectrum of product of attempted synthesis of PtTPTtBuBPBr-2-benzoyl-Br and Pt-TPTtBuBPBr in toulene

Compound 12

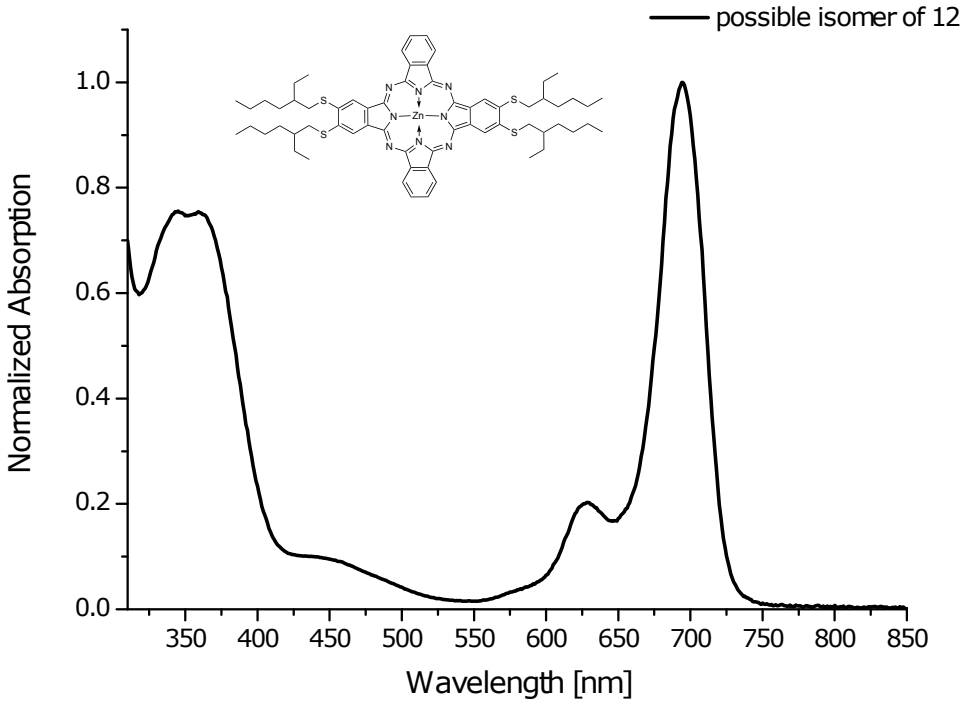

Figure 5.22: Absorption spectrum of a mixture of possible isomers of compound **12** in toluene

Figure 5.22 shows an absorption spectrum of a possible isomer or isomer mixture of compound **12**. The maxima of the significant peaks are located at around 344 nm, 627 nm and the Q-band at 696 nm. The shifts of these maxima are comparable to those of Zn-TtBu-Pc (see figure 5.15 on page 60). This result proofed that a phthalocyanine with compound **10** as building block is not shifted bathochromically. Here, just the formation of J-aggregates would lead to a sharp and significantly bathochromically shifted signal. Without being sure if the isolated product is pure, the formation of J-aggregates could not be performed.

6 Conclusion and Outlook

One aim of this thesis was the synthesis of new benzoporphyrin and phthalocyanine dyes with red shifted absorption and emission spectra. This was attempted via different strategies. First, the synthesis of a new Pt(II) porphyrin dye based on the carbazole precursor **5** was attempted. For this synthesis five reaction steps were necessary, whereby some appeared to be challenging and time consuming. However, very small amount of compound **5** were isolated and thus could not be used as precursor for the well established template synthesis for benzoporphyrin dyes. Hereby, a new phthalocyanine dye **6** could be synthesized. This dye showed a significant red shifted absorption maximum (742 nm) as well as emission maximum of ∼60 nm compared to Zn-TtBu-Pc (678 nm). The absorption maximum of the Q-band of a Pt(II) benzoporphyrin dye with this carbazole precursor as building block could therefore be expected to appear at ∼675 nm. Consequently, this complex would be interesting for biomedical applications due to the fact that at this part of the spectrum the autofluorescence of the biological tissue is minimized. Also this complex would be compatible with red laser diodes. Second, different modifications of the existing porphyrin dyes Pt/Pd-TPTBPF and Pt-TPTtBuBPBr were conducted. Compound **7** could be synthesized in a one step synthesis by Sonogashira coupling of Pt-TPTtBuBPBr with phenylacetylene. This complex shows a slightly bathochromically shifted absorption spectrum. Nevertheless, this shift allows the Pt(II) complex to be compatible with a red laser diode (635 nm). Pt/Pd-TPTBPF were modified in a one step synthesis by addition of 4-chlorobenzoyl chloride at the β position of the porphyrin core under Friedel-Crafts conditions. Compound **8** and **9** show a bathochromically shifted absorption spectrum by $\sim$ 20 nm. Additionally, quantum yield and lifetime measurements were performed. Compared to the corresponding Pt/Pd-TPTBP dyes, the new dyes show comparable lifetime and increased quantum yield. Further modifications of Pt/Pd-TPTBPF by e.g. formylation, Friedel-Crafts reaction with fluorinated species like 2,3,4,5,6-pentafluorobenzoyl chloride or even dimer coupling by using the specific acid chloride species are interesting possibilities in future.

Another aim of this thesis was the synthesis of highly soluble porphyrin and phthalocyanine dyes compatible for the formation of J-aggregates. A phthalocyanine, compound **12**, based on the unoxidized precursor **10** could be synthesized. Unfortunately, due to the very challenging purification, this complex could not be isolated as a pure substance. Therefore compound **10** was oxidized yielding **11**. Unfortunately, also the synthesis of a phthalocyanine dye with compound **11** as main building block could not be performed successfully which was proven by MALDI-TOF spectra.

The last aim of this thesis was the synthesis of a Pt(II) complex supported by tetradentate

N_2O_2 chelate ligands. Therefore an existing Pt($Ph_2N_2O_2$)dpp system [126] was modified by adding an electron donating substituent in the para position which should then result in a push-pull system. A suitable precursor with these properties is compound **14**. Also the metal-halogen exchange could be successfully conducted. However, no further reaction could be performed with this precursor. Changing reaction conditions as well as reactants for the metal-halogen exchange and further reaction steps did not result in a successful reaction for the synthesis of the desired modified chelate ligand.

7 References

1. Skoog, D. A., West, D. M. & Holler, F. J. *Fundamentals of analytical chemistry.* OCLC: 19670232. p. 344 (Saunders College, 1988).
2. US Patent, 2,913,386 (1959).
3. US Patent 3,709,663 (1973).
4. Freeman, T. M. & Seitz, W. R. Oxygen probe based on tetrakis(alkylamino)ethylene chemiluminescence. *Analytical Chemistry* **53,** 98–102 (Jan. 1, 1981).
5. Amao, Y. Probes and Polymers for Optical Sensing of Oxygen. *Microchimica Acta* **143,** 1–12 (Sept. 1, 2003).
6. Feng, Y., Cheng, J., Zhou, L., Zhou, X. & Xiang, H. Ratiometric optical oxygen sensing: a review in respect of material design. *The Analyst* **137,** 4885 (2012).
7. Brasuel, M. *et al.* in *Optical Biosensors* DOI: 10.1016/B978-044450974-1/50016-1, 497–536 (Elsevier, 2002).
8. Dmitriev, R. I. & Papkovsky, D. B. Optical probes and techniques for O2 measurement in live cells and tissue. *Cellular and Molecular Life Sciences* **69,** 2025–2039 (June 2012).
9. Leiner, M. J. P. Optical sensors for in vitro blood gas analysis. *Sensors and Actuators B: Chemical. Proceedings of the 2nd European Conference on Optical Chemical Sensors and Biosensors* **29,** 169–173 (1995).
10. Arain, S., John, G. T., Krause, C., Gerlach, J., Wolfbeis, O. S. & Klimant, I. Characterization of microtiterplates with integrated optical sensors for oxygen and pH, and their applications to enzyme activity screening, respirometry, and toxicological assays. *Sensors and Actuators B: Chemical. Special Issue - In honour of Professor Karl Cammann* **113,** 639–648 (Feb. 27, 2006).
11. Wang, X.-d. & Wolfbeis, O. S. Optical methods for sensing and imaging oxygen: materials, spectroscopies and applications. **43,** 3666–3761 (Apr. 22, 2014).
12. Quaranta, M., Borisov, S. M. & Klimant, I. Indicators for optical oxygen sensors. *Bioanalytical Reviews* **4,** 115–157 (Dec. 1, 2012).
13. Xiang, H., Cheng, J., Ma, X., Zhou, X. & Chruma, J. J. Near-infrared phosphorescence: materials and applications. **42,** 6128–6185 (June 21, 2013).
14. Carvalho, C. M. B., Brocksom, T. J. & Oliveira, K. T. d. Tetrabenzoporphyrins: synthetic developments and applications. **42,** 3302–3317 (Mar. 25, 2013).

15. Che, C.-M., Lo, V. K.-Y., Zhou, C.-Y. & Huang, J.-S. Selective functionalisation of saturated C–H bonds with metalloporphyrin catalysts. **40,** 1950–1975 (Mar. 21, 2011).

16. Rosenow, T., Walzer, K. & Leo, K. Near-infrared organic light emitting diodes based on heavy metal phthalocyanines. *Journal of Applied Physics* **103,** 043105 (Feb. 15, 2008).

17. Nalwa, H. S. Organic Materials for Third-Order Nonlinear Optics. *Advanced Materials* **5,** 341–358 (1993).

18. Nalwa, S. & Shirk, J. in *Phthalocyanines: properties and applications. Volume 4 Volume 4* (eds Leznoff, C. C. & Lever, A. B. P.) 4th ed. OCLC: 36886051 (VCH, New York, NY, 1996).

19. McKeown, N. B. *Phthalocyanine Materials: Synthesis, Structure and Function* Google-Books-ID: iuDhWDW4FbcC. 225 pp. (Cambridge University Press, July 13, 1998).

20. Hanabusa, K. & Shirai, H. in *Phthalocyanines:: properties and applications* (eds Leznoff, C. C. & Lever, A. B. P.) 2nd ed. OCLC: 632893504 (VCH, New York, NY, 1993).

21. Simon, J. & Bassoul, P. in *Phthalocyanines:: properties and applications* (eds Leznoff, C. C. & Lever, A. B. P.) 2nd ed. OCLC: 632893504 (VCH, New York, NY, 1993).

22. Rosenthal, I. Phthalocyanines as Photodynamic Sensitizers. *Photochemistry and Photobiology* **53,** 859–870 (June 1, 1991).

23. Rosenthal, I. & Ben-Hur, E. in *Phthalocyanines: properties and applications* (eds Leznoff, C. C. & Lever, A. B. P.) 1st ed. (VCH, New York, NY, 1989).

24. Valeur, B. & Berberan-Santos, M. N. *Molecular fluorescence: principles and applications* Second edition. OCLC: ocn775030634. 569 pp. (Wiley-VCH ; Wiley-VCH Verlag GmbH & Co. KGaA, Weinheim, Germany : [Chichester, England], 2012).

25. Wöhrle, D., Tausch, M. W. & Stohrer, W.-D. *Photochemie: Konzepte, Methoden, Experimente* (Wiley-VCH Verlag GmbH & Co. KGaA, Weinheim, FRG, Oct. 15, 1998).

26. Lakowicz, J. R. *Principles of fluorescence spectroscopy* 3. ed., corr. 4. print. OCLC: 700510097. 954 pp. (Springer, New York, NY, 2010).

27. Turro, N. J. *Modern molecular photochemistry* OCLC: 610827654. 628 pp. (Univ. Science Books, Sausalito, Calif, 1991).

28. Atkins, P. W. & De Paula, J. *Atkins' Physical chemistry* 9th ed. 972 pp. (Oxford University Press, Oxford ; New York, 2010).

29. Carraway, E. R., Demas, J. N. & DeGraff, B. A. Luminescence quenching mechanism for microheterogeneous systems. *Analytical Chemistry* **63,** 332–336 (Feb. 1, 1991).

30. Wolfbeis, O. S. Chemical sensors — survey and trends. *Fresenius' Journal of Analytical Chemistry* **337,** 522–527 (Jan. 1, 1990).

31. McDonagh, C., Burke, C. S. & MacCraith, B. D. Optical Chemical Sensors. *Chemical Reviews* **108,** 400–422 (Feb. 1, 2008).

32. Asakura, N. & Okura, I. in *Molecular Catalysts for Energy Conversion* (eds Okada, D. T. & Kaneko, P. D. M.) *Springer Series in Materials Science* 111. DOI: 10.1007/978-3-540-70758-5_12, 299–328 (Springer Berlin Heidelberg, 2009).

33. Mills, A. & Lepre, A. Controlling the Response Characteristics of Luminescent Porphyrin Plastic Film Sensors for Oxygen. *Analytical Chemistry* **69,** 4653–4659 (Nov. 1, 1997).

34. Mohr, G. J. in *Optical Chemical Sensors* (eds Baldini, F., Chester, A. N., Homola, J. & Martellucci, S.) *NATO Science Series II: Mathematics, Physics and Chemistry* 224. DOI: 10.1007/1-4020-4611-1_15, 297–321 (Springer Netherlands, 2006).

35. Yeh, T.-S., Chu, C.-S. & Lo, Y.-L. Highly sensitive optical fiber oxygen sensor using Pt(II) complex embedded in sol–gel matrices. *Sensors and Actuators B: Chemical* **119,** 701–707 (2006).

36. *Fiber optic chemical sensors and biosensors* (ed Wolfbeis, O. S.) (CRC Press, Boca Raton, 1991). 2 pp.

37. Nagai, K. & Nakagawa, T. Effects of aging on the gas permeability and solubility in poly(1-trimethylsilyl-1-propyne) membranes synthesized with various catalysts. *Journal of Membrane Science* **105,** 261–272 (Sept. 1995).

38. Pauly, S. in *The Wiley Database of Polymer Properties* (John Wiley & Sons, Inc., 2003).

39. Amao, Y., Miyashita, T. & Okura, I. Platinum tetrakis(pentafluorophenyl)porphyrin immobilized in polytrifluoroethylmethacrylate film as a photostable optical oxygen detection material. *Journal of Fluorine Chemistry* **107,** 101–106 (Jan. 2001).

40. *Polymer handbook, 4th edition* (eds Brandrup, J., Immergut, E. H. & Grulke, E. A.) 4th ed. OCLC: ocm56457312 (Wiley, New York ; Chichester, 2004). 2 pp.

41. DeRosa, M. C., Mosher, P. J., Yap, G. P. A., Focsaneanu, K.-S., Crutchley, R. J. & Evans, C. E. B. Synthesis, Characterization, and Evaluation of [Ir(ppy)2(vpy)Cl] as a Polymer-Bound Oxygen Sensor. *Inorganic Chemistry* **42,** 4864–4872 (Aug. 1, 2003).

42. Enko, B., Borisov, S. M., Regensburger, J., Bäumler, W., Gescheidt, G. & Klimant, I. Singlet Oxygen-Induced Photodegradation of the Polymers and Dyes in Optical Sensing Materials and the Effect of Stabilizers on These Processes. *The Journal of Physical Chemistry A* **117,** 8873–8882 (Sept. 12, 2013).

43. Lee, S.-K. & Okura, I. Photostable Optical Oxygen Sensing Material: PlatinumTetrakis(pentafluorophenyl)porphyrin Immobilized in Polystyrene. **34,** 185–188 (Jan. 1, 1997).

44. Roberts, L., Lines, R., Reddy, S. & Hay, J. Investigation of polyviologens as oxygen indicators in food packaging. *Sensors and Actuators B: Chemical* **152,** 63–67 (Feb. 20, 2011).

45. Erskine, R. W. & Field, B. O. in *Electrons in Oxygen- and Sulphur-Containing Ligands Structure and Bonding* 28. DOI: 10.1007/3-540-07753-7_1, 1–50 (Springer Berlin Heidelberg, 1976).

46. Peterson, J. I., Fitzgerald, R. V. & Buckhold, D. K. Fiber-optic probe for in vivo measurement of oxygen partial pressure. *Analytical Chemistry* **56,** 62–67 (Jan. 1984).

47. Klimant, I. & Wolfbeis, O. S. Oxygen-Sensitive Luminescent Materials Based on Silicone-Soluble Ruthenium Diimine Complexes. *Analytical Chemistry* **67,** 3160–3166 (Sept. 1, 1995).

48. Mills, A. & Thomas, M. Fluorescence-based Thin Plastic Film Ion-pair Sensors forOxygen. **122,** 63–68 (Jan. 1, 1997).

49. Tanaka, T. & Osuka, A. Conjugated porphyrin arrays: synthesis, properties and applications for functional materials. **44,** 943–969 (Feb. 10, 2015).

50. Drain, C. M., Varotto, A. & Radivojevic, I. Self-Organized Porphyrinic Materials. *Chemical Reviews* **109,** 1630–1658 (2009).

51. Wohrle, D. The colours of life. An introduction to the chemistry of porphyrins and related compounds. By L. R. Milgrom. *Advanced Materials* **9,** 1191–1192 (Jan. 1, 1997).

52. Lukyanets, E. A. Phthalocyanines as Photosensitizers in the Photodynamic Therapy of Cancer. *Journal of Porphyrins and Phthalocyanines* **03,** 424–432 (Aug. 1, 1999).

53. Bonnett, R. Photosensitizers of the porphyrin and phthalocyanine series for photodynamic therapy. **24,** 19–33 (Jan. 1, 1995).

54. Boyle, R. W. & Dolphin, D. Structure and Biodistribution Relationships of Photodynamic Sensitizers*. *Photochemistry and Photobiology* **64,** 469–485 (Sept. 1, 1996).

55. Finikova, O. S., Cheprakov, A. V., Beletskaya, I. P., Carroll, P. J. & Vinogradov, S. A. Novel Versatile Synthesis of Substituted Tetrabenzoporphyrins. *The Journal of Organic Chemistry* **69,** 522–535 (Jan. 1, 2004).

56. Guldi, D. M. Fullerene–porphyrin architectures; photosynthetic antenna and reaction center models. **31,** 22–36 (Mar. 6, 2002).

57. Walter, M. G., Rudine, A. B. & Wamser, C. C. Porphyrins and phthalocyanines in solar photovoltaic cells. *Journal of Porphyrins and Phthalocyanines* **14,** 759–792 (Sept. 1, 2010).

58. Murphy, A. R. & Fréchet, J. M. J. Organic Semiconducting Oligomers for Use in Thin Film Transistors. *Chemical Reviews* **107,** 1066–1096 (Apr. 1, 2007).

59. Sommer, J. R., Farley, R. T., Graham, K. R., Yang, Y., Reynolds, J. R., Xue, J. & Schanze, K. S. Efficient Near-Infrared Polymer and Organic Light-Emitting Diodes Based on Electrophosphorescence from (Tetraphenyltetranaphtho[2,3]porphyrin)platinum(II). *ACS Applied Materials & Interfaces* **1,** 274–278 (Feb. 25, 2009).

60. Yi, X., Wang, F., Qin, W., Yang, X. & Yuan, J. Near-infrared fluorescent probes in cancer imaging and therapy: an emerging field. *International Journal of Nanomedicine* **9,** 1347–1365 (Mar. 5, 2014).

61. Pervaiz, S. & Olivo, M. Art and Science of Photodynamic Therapy. *Clinical and Experimental Pharmacology and Physiology* **33,** 551–556 (2006).

62. Eastwood, D. & Gouterman, M. Porphyrins: XVIII. Luminescence of (Co), (Ni), Pd, Pt complexes. *Journal of Molecular Spectroscopy* **35,** 359–375 (Sept. 1970).

63. Evans, R. C., Douglas, P. & Winscom, C. J. Coordination complexes exhibiting room-temperature phosphorescence: Evaluation of their suitability as triplet emitters in organic light emitting diodes. *Coordination Chemistry Reviews* **250,** 2093–2126 (Aug. 2006).

64. Papkovsky, D. B., Ponomarev, G. V., Trettnak, W. & O'Leary, P. Phosphorescent Complexes of Porphyrin Ketones: Optical Properties and Application to Oxygen Sensing. *Analytical Chemistry* **67,** 4112–4117 (Nov. 1, 1995).

65. Koren, K., Borisov, S. M., Saf, R. & Klimant, I. Strongly Phosphorescent Iridium(III)-Porphyrins New Oxygen Indicators with Tuneable Photophysical Properties and Functionalities. *European Journal of Inorganic Chemistry* **2011,** 1531–1534 (Apr. 1, 2011).

66. Rogers, J. E., Nguyen, K. A., Hufnagle, D. C., McLean, D. G., Su, W., Gossett, K. M., Burke, A. R., Vinogradov, S. A., Pachter, R. & Fleitz, P. A. Observation and Interpretation of Annulated Porphyrins: Studies on the Photophysical Properties of meso-Tetraphenylmetalloporphyrins. *The Journal of Physical Chemistry A* **107,** 11331–11339 (2003).

67. Borisov, S. M., Nuss, G. & Klimant, I. Red Light-Excitable Oxygen Sensing Materials Based on Platinum(II) and Palladium(II) Benzoporphyrins. *Analytical Chemistry* **80,** 9435–9442 (2008).

68. Diev, V. V., Schlenker, C. W., Hanson, K., Zhong, Q., Zimmerman, J. D., Forrest, S. R. & Thompson, M. E. Porphyrins Fused with Unactivated Polycyclic Aromatic Hydrocarbons. *The Journal of Organic Chemistry* **77,** 143–159 (Jan. 6, 2012).

69. Borisov, S. M., Nuss, G., Haas, W., Saf, R., Schmuck, M. & Klimant, I. New NIR-emitting complexes of platinum(II) and palladium(II) with fluorinated benzoporphyrins. *Journal of Photochemistry and Photobiology A: Chemistry* **201,** 128–135 (Jan. 25, 2009).

70. Khalil, G. *et al.* Synthesis and spectroscopic characterization of Ni, Zn, Pd and Pt tetra(pentafluorophenyl)porpholactone with comparisons to Mg, Zn, Y, Pd and Pt metal complexes of tetra(pentafluorophenyl)porphine. *Journal of Porphyrins and Phthalocyanines* **06,** 135–145 (Feb. 1, 2002).

71. Finikova, O. S., Cheprakov, A. V. & Vinogradov, S. A. Synthesis and Luminescence of Soluble meso-Unsubstituted Tetrabenzo- and Tetranaphtho[2,3]porphyrins. *The Journal of Organic Chemistry* **70,** 9562–9572 (Nov. 1, 2005).

72. Montforts, F.-P., Gerlach, B. & Hoeper, F. Discovery and Synthesis of Less Common Natural Hydroporphyrins. *Chemical Reviews* **94,** 327–347 (Mar. 1994).

73. Anderson, H. L., Wylie, A. P. & Prout, K. meso-Tetraalkynylporphyrins, 1607–1612 (Jan. 1, 1998).

74. Lash, T. D. Modification of the porphyrin chromophore by ring fusion: identifying trends due to annelation of the porphyrin nucleus. *Journal of Porphyrins and Phthalocyanines* **5,** 267–288 (2001).

75. Lewtak, J. P. & Gryko, D. T. Synthesis of pi-extended porphyrins via intramolecular oxidative coupling. **48,** 10069–10086 (Sept. 17, 2012).

76. Screen, T. E. O., Blake, I. M., Rees, L. H., Clegg, W., Borwick, S. J. & Anderson, H. L. Making conjugated connections to porphyrins: a comparison of alkyne, alkene, imine and azo links, 320–329 (Jan. 23, 2002).

77. Rozhkov, V. V., Khajehpour, M. & Vinogradov, S. A. Luminescent Zn and Pd Tetranaphthaloporphyrins. *Inorganic Chemistry* **42,** 4253–4255 (July 1, 2003).

78. Borek, C. *et al.* Highly Efficient, Near-Infrared Electrophosphorescence from a Pt–Metalloporphyrin Complex. *Angewandte Chemie* **119,** 1127–1130 (Feb. 5, 2007).

79. Qian, G. & Wang, Z. Y. Near-Infrared Organic Compounds and Emerging Applications. *Chemistry – An Asian Journal* **5,** 1006–1029 (2010).

80. Lu, W., Mi, B.-X., Chan, M. C. W., Hui, Z., Che, C.-M., Zhu, N. & Lee, S.-T. Light-Emitting Tridentate Cyclometalated Platinum(II) Complexes Containing sigma-Alkynyl Auxiliaries: Tuning of Photo- and Electrophosphorescence. *Journal of the American Chemical Society* **126,** 4958–4971 (Apr. 1, 2004).

81. Helberger, J. H., von Rebay, A. & Hevér., D. B. Über die Einwirkung von Metallen auf o-Cyanacetophenon sowie auf 3-Methylphtalimidin; Synthese des Tetrabenzoporphins. III. Mitteilung zur Kenntnis der Benzoporphine. *Justus Liebigs Annalen der Chemie* **533,** 197–215 (Jan. 1, 1938).

82. Barrett, P. A., Linstead, R. P., Rundall, F. G. & Tuey, G. a. P. 197. Phthalocyanines and related compounds. Part XIX. Tetrabenzporphin, tetrabenzmonazaporphin and their metallic derivatives, 1079–1092 (Jan. 1, 1940).

83. Borisov, S. M., Papkovsky, D. B., Ponomarev, G. V., DeToma, A. S., Saf, R. & Klimant, I. Photophysical properties of the new phosphorescent platinum(II) and palladium(II) complexes of benzoporphyrins and chlorins. *Journal of Photochemistry and Photobiology A: Chemistry* **206,** 87–92 (July 5, 2009).

84. Niedermair, F., Borisov, S. M., Zenkl, G., Hofmann, O. T., Weber, H., Saf, R. & Klimant, I. Tunable Phosphorescent NIR Oxygen Indicators Based on Mixed Benzo- and Naphthoporphyrin Complexes. *Inorganic Chemistry* **49,** 9333–9342 (2010).

85. Yuan, A., Wu, J., Tang, X., Zhao, L., Xu, F. & Hu, Y. Application of near-infrared dyes for tumor imaging, photothermal, and photodynamic therapies. *Journal of Pharmaceutical Sciences* **102,** 6–28 (Jan. 1, 2013).

86. Borisov, S. M., Zenkl, G. & Klimant, I. Phosphorescent Platinum(II) and Palladium(II) Complexes with Azatetrabenzoporphyrins—New Red Laser Diode-Compatible Indicators for Optical Oxygen Sensing. *ACS Applied Materials & Interfaces* **2,** 366–374 (Feb. 24, 2010).

87. Lebedev, A. Y., Cheprakov, A. V., Sakadžić, S., Boas, D. A., Wilson, D. F. & Vinogradov, S. A. Dendritic Phosphorescent Probes for Oxygen Imaging in Biological Systems. *ACS Applied Materials & Interfaces* **1,** 1292–1304 (June 24, 2009).

88. Clark, H. A. *et al.* Subcellular optochemical nanobiosensors: probes encapsulated by biologically localised embedding (PEBBLEs). *Sensors and Actuators B: Chemical* **51,** 12–16 (Aug. 31, 1998).

89. Lee, Y.-E. K., Kopelman, R. & Smith, R. Nanoparticle PEBBLE sensors in live cells and in vivo. *Annual review of analytical chemistry (Palo Alto, Calif.)* **2,** 57–76 (July 1, 2009).

90. Borisov, S. M. & Klimant, I. Efficient metallation in diphenylether A convenient route to luminescent platinum(II) complexes. *Dyes and Pigments* **83,** 312–316 (2009).

91. Qi, M.-H. & Liu, G.-F. Synthesis and properties of transition metal benzoporphyrin compound liquid crystals. **13,** 2479–2484 (Sept. 23, 2003).

92. Yamashita, K. Effects of expansion of the pi-electron system on photocurrent quantum yields for porphyrin photocells: magnesium and zinc tetrabenzoporphyrin sensitizers. *Chemistry Letters* **11,** 1085–1088 (July 5, 1982).

93. Vincett, P. Phosphorescence and Fluorescence of Phthalocyanines. *The Journal of Chemical Physics* **55,** 4131–4140 (1971).

94. Nacht, B., Larndorfer, C., Sax, S., Borisov, S. M., Hajnsek, M., Sinner, F., List-Kratochvil, E. J. W. & Klimant, I. Integrated catheter system for continuous glucose measurement and simultaneous insulin infusion. *Biosensors and Bioelectronics* **64,** 102–110 (Feb. 15, 2015).

95. Huang, L., Park, C., Fleetham, T. & Li, J. Platinum (II) azatetrabenzoporphyrins for near-infrared organic light emitting diodes. *Applied Physics Letters* **109,** 233302 (2016).

96. Kirstein, S. & Daehne, S. J-aggregates of amphiphilic cyanine dyes: Self-organization of artificial light harvesting complexes. *International Journal of Photoenergy* **2006,** e20363 (Jan. 16, 2007).

97. Losytskyy, M. Y. & Yashchuk, V. M. in *Advanced Fluorescence Reporters in Chemistry and Biology II* (ed Demchenko, A. P.) *Springer Series on Fluorescence* 9. DOI: 10.1007/978-3-642-04701-5_4, 135–157 (Springer Berlin Heidelberg, 2010).

98. Würthner, F., Kaiser, T. E. & Saha-Möller, C. R. J-Aggregates: From Serendipitous Discovery to Supramolecular Engineering of Functional Dye Materials. *Angewandte Chemie International Edition* **50,** 3376–3410 (Apr. 4, 2011).

99. Knoester, J. Modeling the optical properties of excitons in linear and tubular J-aggregates. *International Journal of Photoenergy* **2006,** e61364 (Jan. 9, 2007).

100. Obara, Y., Saitoh, K., Oda, M. & Tani, T. Room-Temperature Fluorescence Lifetime of Pseudoisocyanine (PIC) J Excitons with Various Aggregate Morphologies in Relation to Microcavity Polariton Formation. *International Journal of Molecular Sciences* **13,** 5851–5865 (May 15, 2012).

101. Birkan, B., Gülen, D. & Özçelik, S. Controlled Formation of the Two-Dimensional TTBC J-Aggregates in an Aqueous Solution. *The Journal of Physical Chemistry B* **110,** 10805–10813 (June 1, 2006).

102. Sorokin, A. V., Filimonova, I. I., Grynyov, R. S., Guralchuk, G. Y., Yefimova, S. L. & Malyukin, Y. V. Control of Exciton Migration Efficiency in Disordered J-Aggregates. *The Journal of Physical Chemistry C* **114,** 1299–1305 (Jan. 21, 2010).

103. Andrade, S. M. & Costa, S. M. B. Spectroscopic Studies on the Interaction of a Water Soluble Porphyrin and Two Drug Carrier Proteins. *Biophysical Journal* **82,** 1607–1619 (2002).

104. Struganova, I. A., Hazell, M., Gaitor, J., McNally-Carr, D. & Zivanovic, S. Influence of Inorganic Salts and Bases on the J-Band in the Absorption Spectra of Water Solutions of 1,1‘-Diethyl-2,2‘-cyanine Iodide. *The Journal of Physical Chemistry A* **107,** 2650–2656 (Apr. 1, 2003).

105. Passier, R., Ritchie, J. P., Toro, C., Diaz, C., Masunov, A. E., Belfield, K. D. & Hernandez, F. E. Thermally controlled preferential molecular aggregation state in a thiacarbocyanine dye. *The Journal of Chemical Physics* **133,** 134508 (Oct. 7, 2010).

106. Dimitriev, O. P., Dimitriyeva, A. P., Tolmachev, A. I. & Kurdyukov, V. V. Solvent-Induced Organization of Squaraine Dyes in Solution Capillary Layers and Adsorbed Films. *The Journal of Physical Chemistry B* **109,** 4561–4567 (2005).

107. Slavnova, T. D., Chibisov, A. K. & Görner, H. Kinetics of Salt-Induced J-aggregation of Cyanine Dyes. *The Journal of Physical Chemistry A* **109,** 4758–4765 (June 1, 2005).

108. V. Berlepsch, H. & Böttcher, C. Supramolecular Structure of TTBC J-Aggregates in Solution and on Surface. *Langmuir* **29,** 4948–4958 (Apr. 23, 2013).

109. Li, X., Zhang, L. & Mu, J. Formation of new types of porphyrin H- and J-aggregates. *Colloids and Surfaces A: Physicochemical and Engineering Aspects. Engineering Particle Technology* **311,** 187–190 (2007).

110. Sonogashira, K., Tohda, Y. & Hagihara, N. A convenient synthesis of acetylenes: catalytic substitutions of acetylenic hydrogen with bromoalkenes, iodoarenes and bromopyridines. *Tetrahedron Letters* **16,** 4467–4470 (Jan. 1, 1975).

111. Dieck, H. A. & Heck, F. R. Palladium catalyzed synthesis of aryl, heterocyclic and vinylic acetylene derivatives. *Journal of Organometallic Chemistry* **93,** 259–263 (July 8, 1975).

112. LeCours, S. M., DiMagno, S. G. & Therien, M. J. Exceptional Electronic Modulation of Porphyrins through meso-Arylethynyl Groups. Electronic Spectroscopy, Electronic Structure, and Electrochemistry of [5,15-Bis[(aryl)ethynyl]- 10,20-diphenyl-porphinato]zinc(II) Complexes. X-ray Crystal Structures of [5,15-Bis[(4‘-fluorophenyl)ethynyl]- 10,20-diphenylporphinato]zinc(II) and 5,15-Bis[(4‘-methoxyphenyl)ethynyl]-10,20-diphenylporphyrin. *Journal of the American Chemical Society* **118,** 11854–11864 (Jan. 1, 1996).

113. Shultz, D. A., Gwaltney, K. P. & Lee, H. A Modified Procedure for Sonogashira Couplings: Synthesis and Characterization of a Bisporphyrin, 1,1-Bis[zinc(II) 5‘-ethynyl-10‘,15‘,20‘-trimesitylporphyrinyl]methylenecyclohexane. *The Journal of Organic Chemistry* **63,** 4034–4038 (June 1, 1998).

114. Friedel, C. & Crafts, J. M. Organic chemistry A New General Synthetical Method of Producing Hydrocarbons. **32,** 725–791 (Jan. 1, 1877).

115. Sartori, G. & Maggi, R. Use of Solid Catalysts in Friedel-Crafts Acylation Reactions. *Chemical Reviews* **106,** 1077–1104 (Mar. 2006).

116. Ruggiero, A., Fuchter, M. J., Kokas, O. J., Negru, M., White, A. J., Haycock, P. R., Hoffman, B. M. & Barrett, A. G. A ‘push–pull’ tropylium-fused aminoporphyrazine. *Tetrahedron* **65,** 9690–9693 (Nov. 2009).

117. Rickborn, B. & Jensen, F. R. alpha-Carbon Isomerization in Amide Dehydrations1. *The Journal of Organic Chemistry* **27,** 4608–4610 (1962).

118. Colley, H. E. *et al.* An Orally Bioavailable, Indole-3-glyoxylamide Based Series of Tubulin Polymerization Inhibitors Showing Tumor Growth Inhibition in a Mouse Xenograft Model of Head and Neck Cancer. *Journal of Medicinal Chemistry* **58,** 9309–9333 (Dec. 10, 2015).

119. Nesi, R., Giomi, D., Turchi, S. & Falai, A. 4,5-Dicyanopyridazine: a 1,2-diazine superheterodiene for [4 + 2] cycloaddition reactions. *Journal of the Chemical Society, Chemical Communications,* 2201 (1995).

120. Turchi, S., Nesi, R. & Giomi, D. Reactions of 4,5-dicyanopyridazine with alkynes and enamines: A new straightforward complementary route to 4-mono- and 4,5-disubstituted phthalonitriles. *Tetrahedron* **54,** 1809–1816 (Feb. 1998).

121. Giomi, D. & Cecchi, M. Study on direct benzoannelations of pyrrole and indole systems by domino reactions with 4,5-dicyanopyridazine. *Tetrahedron* **58,** 8067–8071 (Sept. 2002).

122. Karaoğlan, G. K., Gümrükçü, G., Koca, A., Gül, A. & Avcıata, U. Synthesis and characterization of novel soluble phthalocyanines with fused conjugated unsaturated groups. *Dyes and Pigments* **90,** 11–20 (July 2011).

123. Hancock, J. M., Gifford, A. P., Zhu, Y., Lou, Y. & Jenekhe, S. A. n-Type Conjugated Oligoquinoline and Oligoquinoxaline with Triphenylamine Endgroups: Efficient Ambipolar Light Emitters for Device Applications. *Chemistry of Materials* **18,** 4924–4932 (2006).

124. Hur†, J. A., Bae, S. Y., Kim, K. H., Lee, T. W., Cho, M. J. & Choi, D. H. Semiconducting 2,6,9,10-Tetrakis(phenylethynyl)anthracene Derivatives: Effect of Substitution Positions on Molecular Energies. *Organic Letters* **13,** 1948–1951 (Apr. 15, 2011).

125. Ragoussi, M.-E., Katsukis, G., Roth, A., Malig, J., de la Torre, G., Guldi, D. M. & Torres, T. Electron-Donating Behavior of Few-Layer Graphene in Covalent Ensembles with Electron-Accepting Phthalocyanines. *Journal of the American Chemical Society* **136,** 4593–4598 (2014).

126. Lin, Y.-Y., Chan, S.-C., Chan, M. C. W., Hou, Y.-J., Zhu, N., Che, C.-M., Liu, Y. & Wang, Y. Structural, Photophysical, and Electrophosphorescent Properties of Platinum(II) Complexes Supported by Tetradentate N2O2 Chelates. *Chemistry - A European Journal* **9,** 1263–1272 (Mar. 17, 2003).

127. Guinot, S. G. R., Hepworth, J. D. & Wainwright, M. The effects of cyclic terminal groups in di- and tri-arylmethane dyes. Part 2.1 Steric and electronic effects in derivatives of Victoria Blue. *Journal of the Chemical Society, Perkin Transactions 2,* 297–304 (1998).

128. Murray, A., Foreman, W. W. & Langham, W. The Halogen-Metal Interconversion Reaction and Its Application to the Synthesis of Nicotinic Acid Labeled With Isotopic Carbon. *Science* **106,** 277–277 (Sept. 19, 1947).

129. Baldwin, A. W. & Robinson, R. 274. Attempts to find new antimalarials. Part VIII. Derivatives of 8-aminoalkylaminoquinoline, 1264–1267 (Jan. 1, 1934).

130. Suzuki, Y., Moriyama, K. & Togo, H. Facile transformation of esters to nitriles. *Tetrahedron* **67,** 7956–7962 (2011).

131. Ivanov, A. V., Kabanova, K. V., Breusova, M. O., Zhukov, I. V., Tomilova, L. G. & Zefirov, N. S. New phosphorus containing metal phthalocyanine complexes Synthesis and spectral and electrochemical studies. *Russian Chemical Bulletin* **57,** 1665–1670 (Aug. 1, 2008).

132. Burmester, C. & Faust, R. A Reliable Route to 1,2-Diamino-4,5-phthalodinitrile. *Synthesis* **2008,** 1179–1181 (Apr. 2008).

133. Maffioli, S. I., Marzorati, E. & Marazzi, A. Mild and Reversible Dehydration of Primary Amides with $PdCl_2$ in Aqueous Acetonitrile. *Organic Letters* **7,** 5237–5239 (Nov. 2005).

134. Konwar, D., Boruah, M., Sarmah, G. K., Bhattacharyya, N. K., Borthakur, N., Goswami, B. N. & Boruah, K. R. Aluminium chloride and sodium iodide (AlCl3-NaI): a versatile dehydrating agent. *Journal of Chemical Research* **2001,** 490–492 (Nov. 1, 2001).

135. Olah, G., Narang, S., Fung, A. & Balaram Gupta, B. Synthetic Methods and Reactions; 82 [1] . Cyanuric Chloride, a Mild Dehydrating Agent in the Preparation of Nitriles from Amides. *Synthesis* **1980,** 657–658 (1980).

136. Maetz, P. & Rodriguez, M. A simple preparation of N-protected chiral alpha-aminonitriles from N-protected alpha-amino acid amides. *Tetrahedron Letters* **38,** 4221–4222 (June 16, 1997).

137. Boruah, M. & Konwar, D. AlCl3 · 6H2O/KI/H2O/CH3CN: A New Alternate System for Dehydration of Oximes and Amides in Hydrated Media. *The Journal of Organic Chemistry* **67,** 7138–7139 (2002).

138. Siegl, W. O., Ferris, F. C. & Mucci, P. A. A convenient synthesis of 3- and 4-methylphthalonitrile. *The Journal of Organic Chemistry* **42,** 3442–3443 (Oct. 1977).

139. Oshiki, T. & Imamoto, T. The Reactions of Optically Pure Menthyloxymethylphenylphosphine-Borane with Organolithium Reagents. *Bulletin of the Chemical Society of Japan* **63,** 3719–3721 (Dec. 1990).

8 List of Figures

9 List of Tables

10 Appendix

10.1 Abbreviations

Table 10.1: List of used abbreviations

Abbreviation	Name
QY	Quantum yield
abs.	absoulte
av.	average
CAS	Chemical Abstracts Service
CH	Cyclohexane
DCM	Dichloromethane
EE	Etyhl acetate
DCB	1,2-Dichlorobenzene
NMP	N-Methyl-2-pyrrolidone
DMA	N,N-Dimethylacetamide
Et_2O	Diethylether
THF	Tetrahydrofuran
Tol	Toluene
t-BuLi	tert-Butyllithium
n-BuLi	n-Butyllithium
DMF	N,N-Dimethylformamide
MeOH	Methanol
HOMO	Highest occupied molecular orbital
LUMO	Lowest unoccupied molecular orbital
MO	Molecular orbital
NIR	Near-infrared
IC	Internal conversion
ISC	Intersystem crossing
HRMS	High Resolution Mass Spectrometry
K_{sv}	Stern-Volmer constant
MS	Molecular sieve
RT	Room temperature
TLC	Thin-layer chromatography
R_f	Retention factor
UV	Ultraviolet
TTA	Triplet-triplet annihilation
DBU	1,8-Diazabicyclo[5.4.0]undec-7-en
DDQ	2,3-Dichloro-5,6-dicyano-p-benzoquinone
Et_3N	Triethylamine
K_2CO_3	Pottasium carbonate
H_2SO_4	Sulfuric acid
$AlCl_3$	Aluminum chloride
Ar	Argon
N_2	Nitrogen
$Pd(PPh_3)_4$	Tetrakis(triphenylphosphine)palladium(0)

10.2 List of used solvents

Table 10.2: List of Solvents

Solvent	Supplier	CAS-Number
Tetrahydrofuran	Roth	109-99-9
Chloroform	VWR Chemicals	67-66-3
1,2-Dichlorobenzene	Sigma-Aldrich	95-50-1
Toluene	Sigma-Aldrich	108-88-3
N-Methyl-2-pyrrolidone	ABCR	872-50-4
N,N-Dimethylformamide	Sigma-Aldrich	68-12-2
Acetonitrile	Roth	75-05-8
Diethylether	VWR	60-29-7
N,N-Dimethylacetamide	Sigma-Aldrich	127-19-5
Dichloromethane	Fisher Scientific	75-09-2
1,2-Dicyanobenzene	Sigma-Aldrich	91-15-6
Novec 7200	3M	163702-06-5

10.3 NMR Data

10.3.1 compound 1

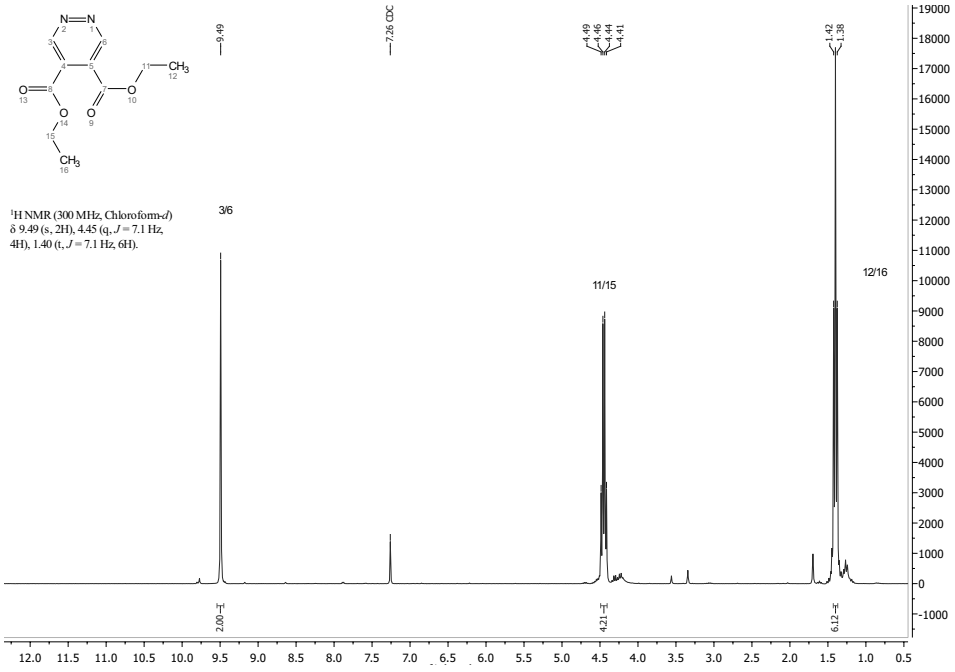

Figure 10.1: ^{1}H-NMR spectrum of compound **1**

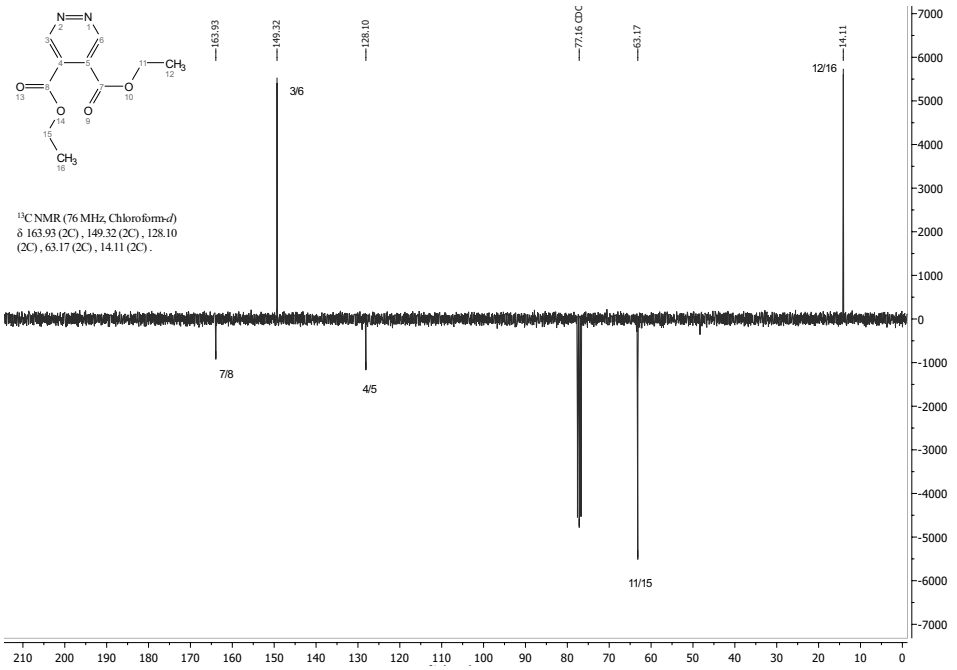

Figure 10.2: APT-NMR spectrum of compound **1**

10.3.2 compound 2

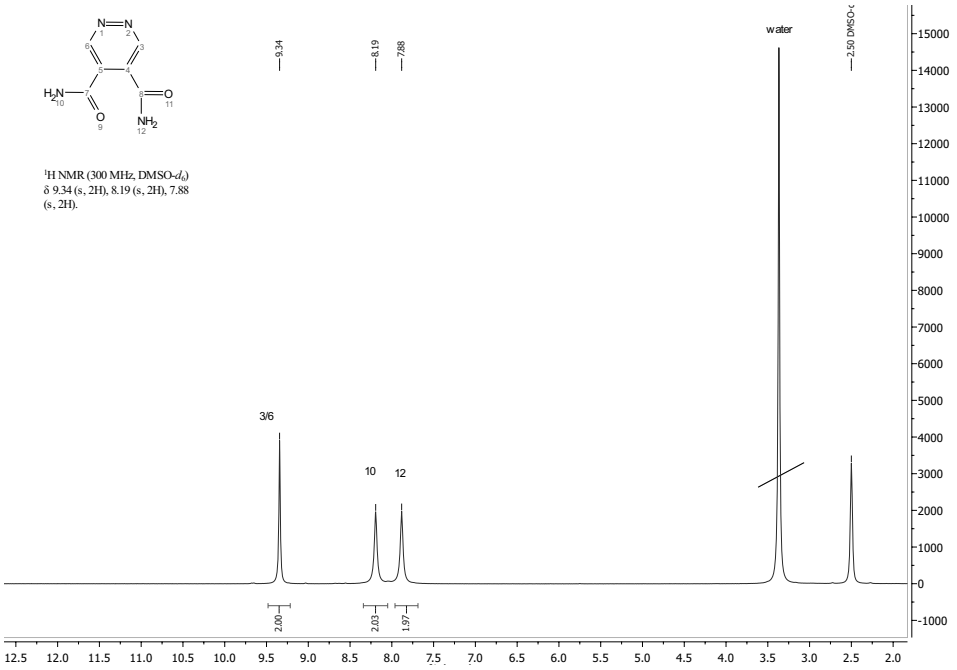

Figure 10.3: ^{1}H-NMR spectrum of compound **2**

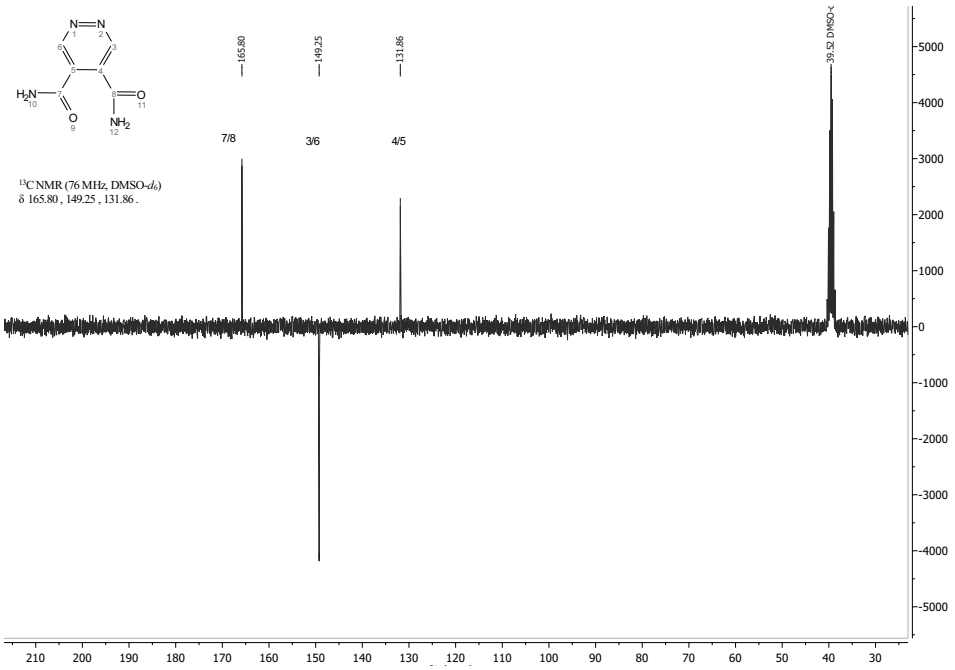

Figure 10.4: APT-NMR spectrum of compound **2**

10.3.3 compound 3

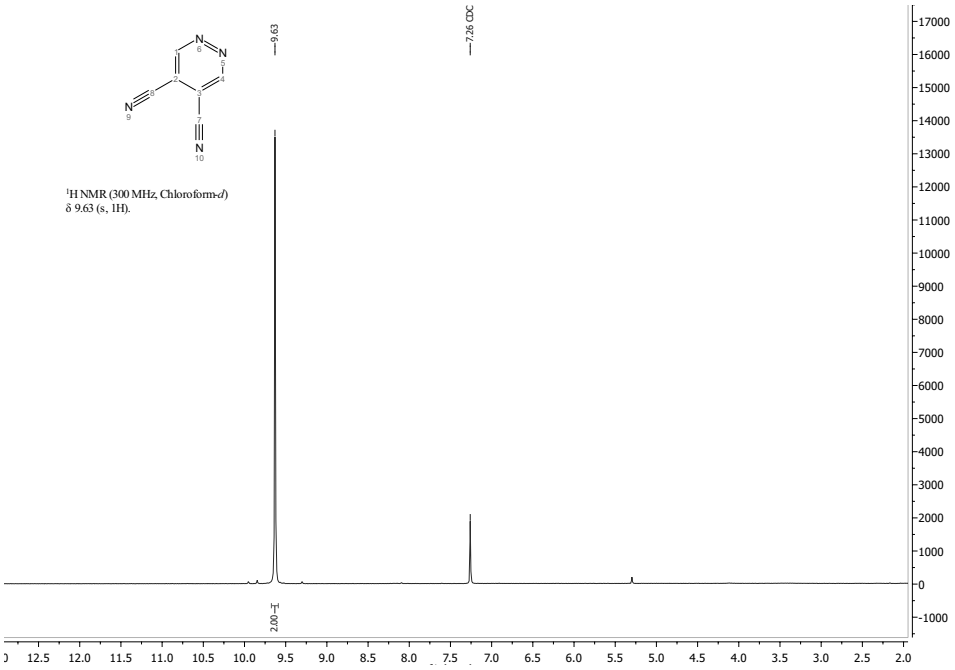

Figure 10.5: ^{1}H-NMR spectrum of compound **3**

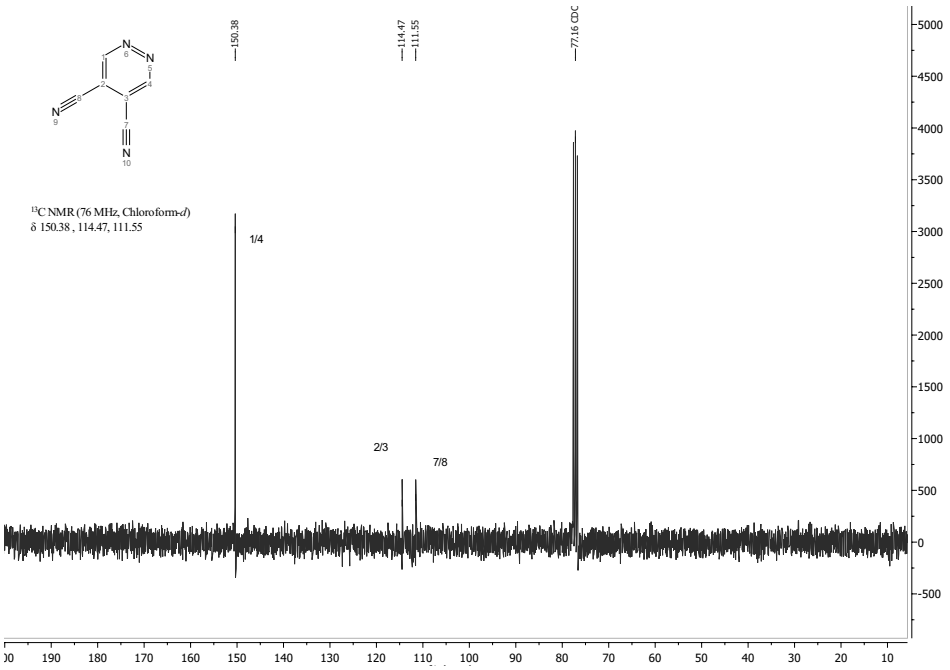

Figure 10.6: APT-NMR spectrum of compound **3**

10.3.4 compound 4

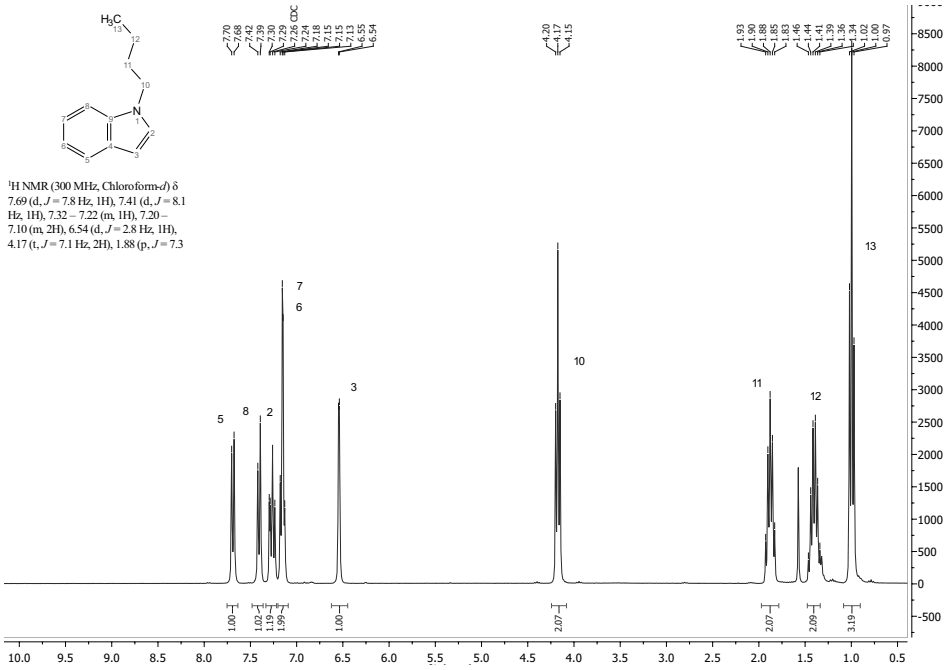

Figure 10.7: ^{1}H-NMR spectrum of compound **4**

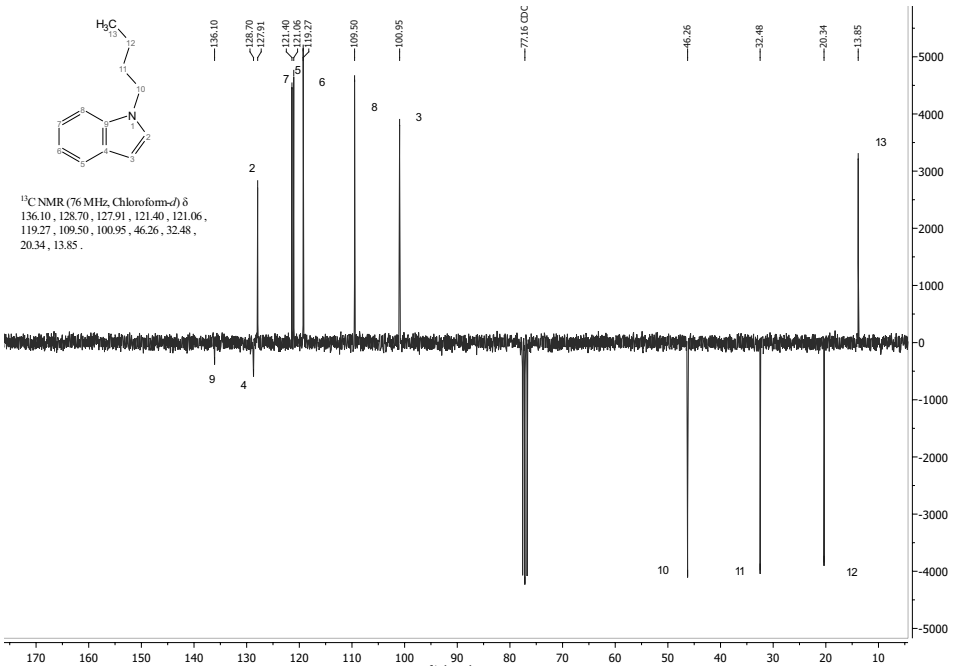

Figure 10.8: APT-NMR spectrum of compound **4**

10.3.5 compound 5

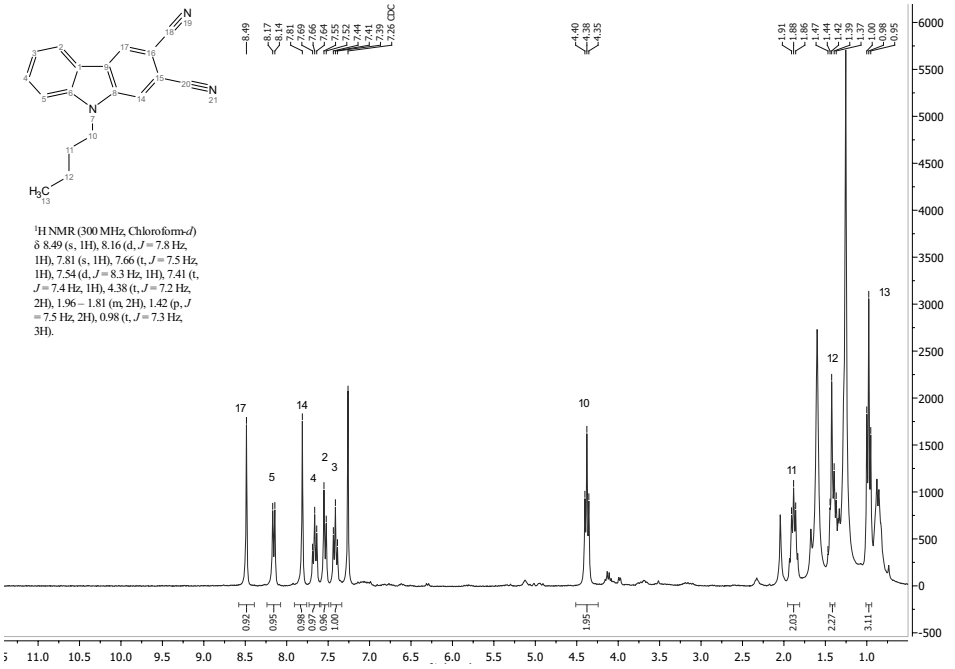

Figure 10.9: ^{1}H-NMR spectrum of compound **5**

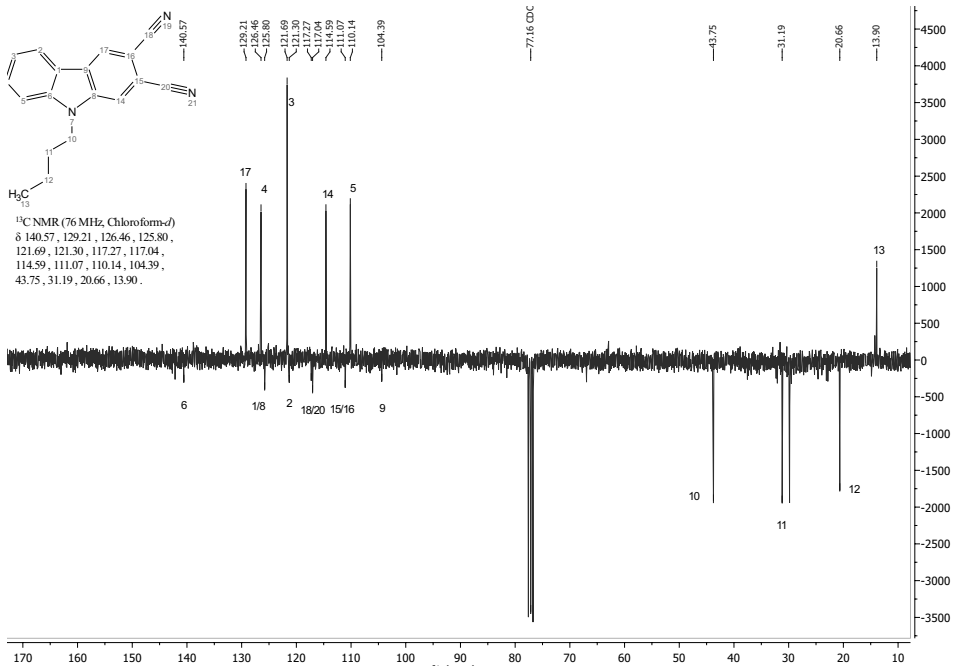

Figure 10.10: APT-NMR spectrum of compound **5**

10.3.6 compound 8

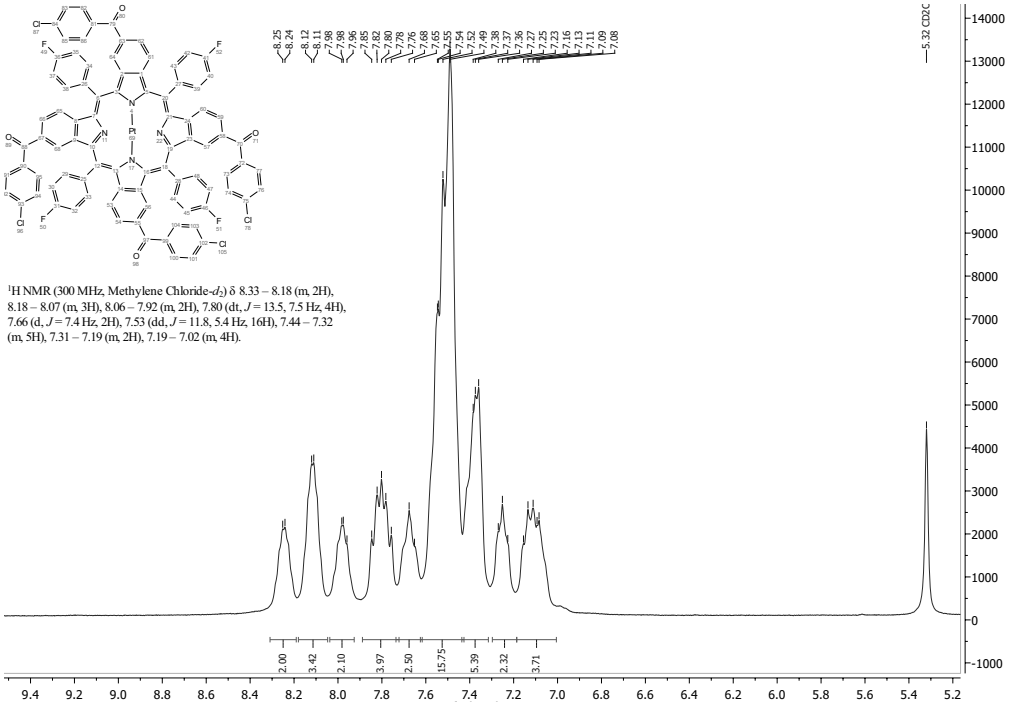

Figure 10.11: ^{1}H-NMR spectrum of compound **8**

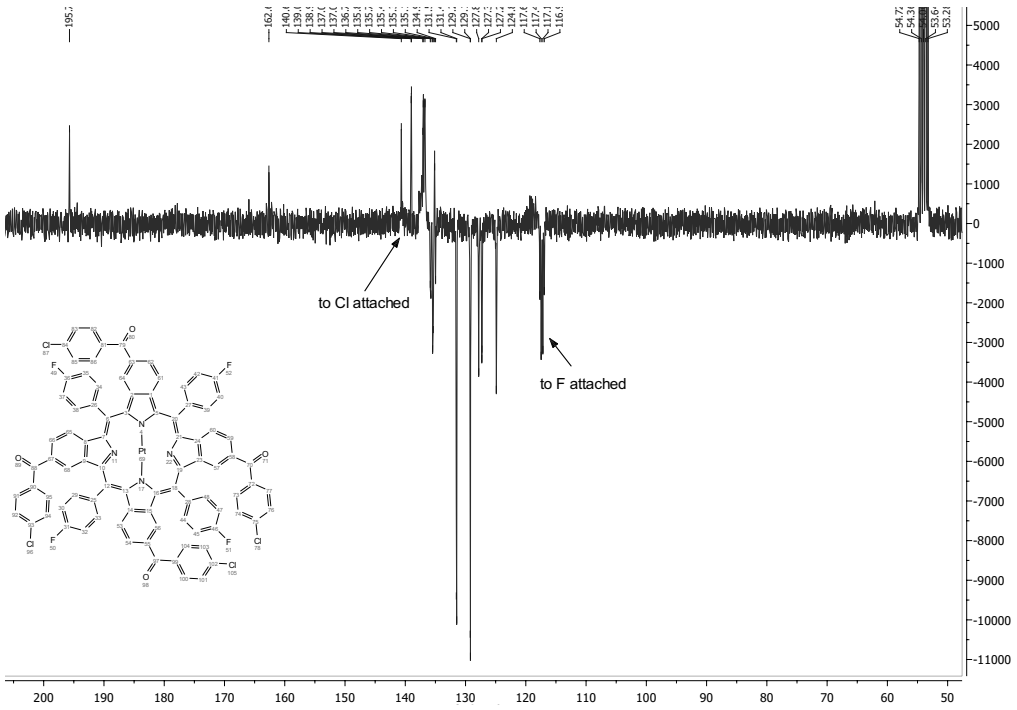

Figure 10.12: APT-NMR spectrum of compound **8**

10.3.7 compound 9

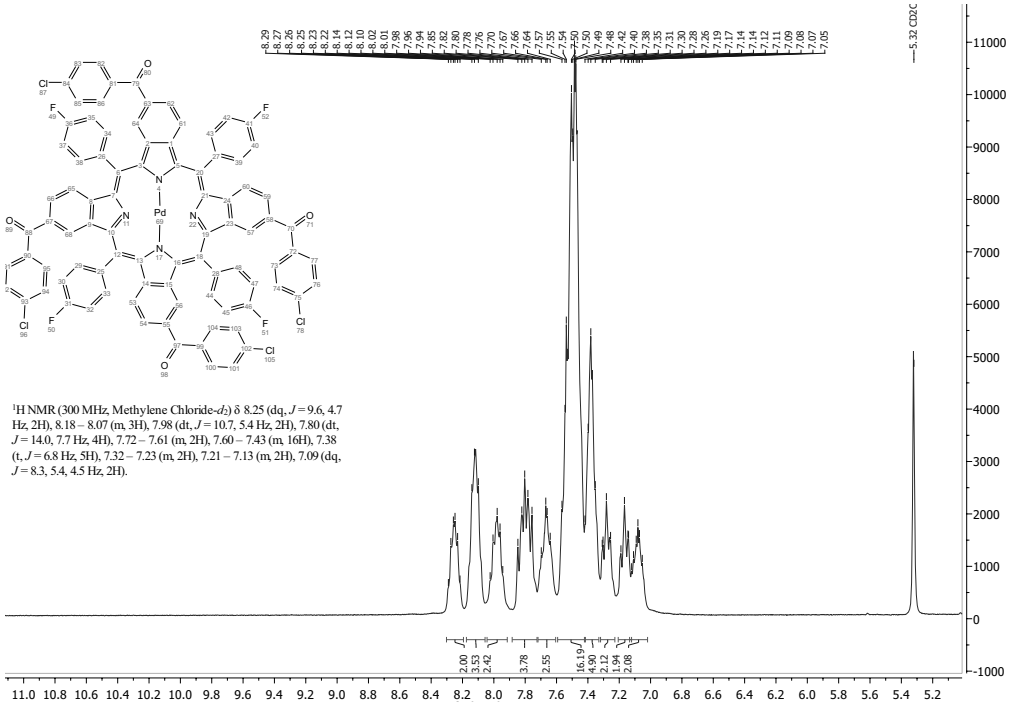

Figure 10.13: ^{1}H-NMR spectrum of compound **9**

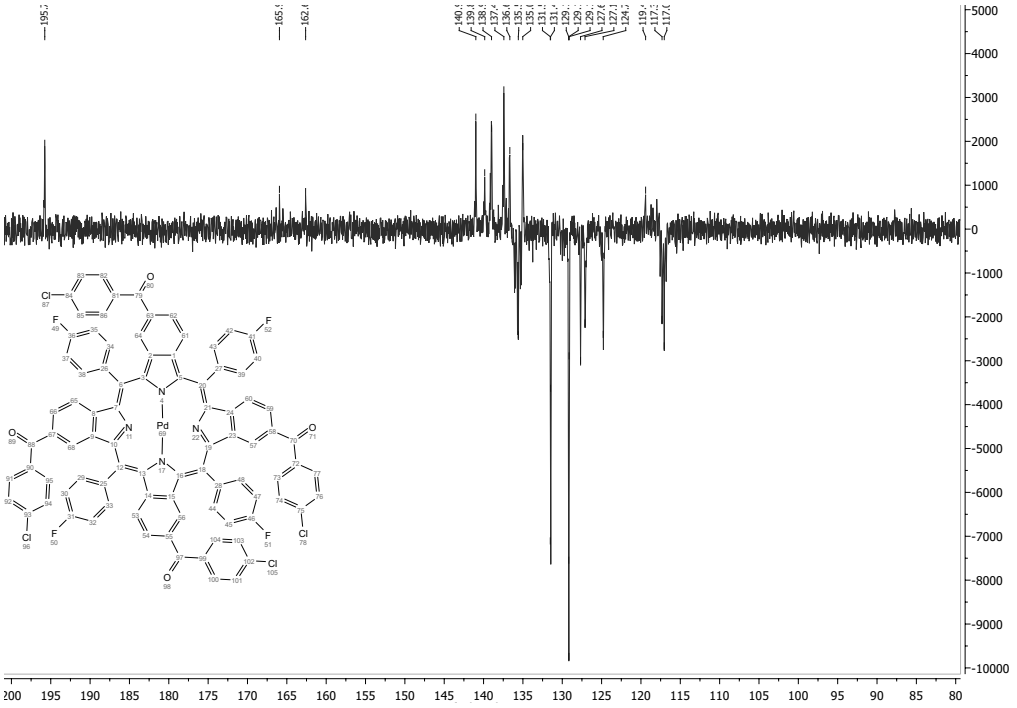

Figure 10.14: APT-NMR spectrum of compound **9**

10.3.8 compound 10

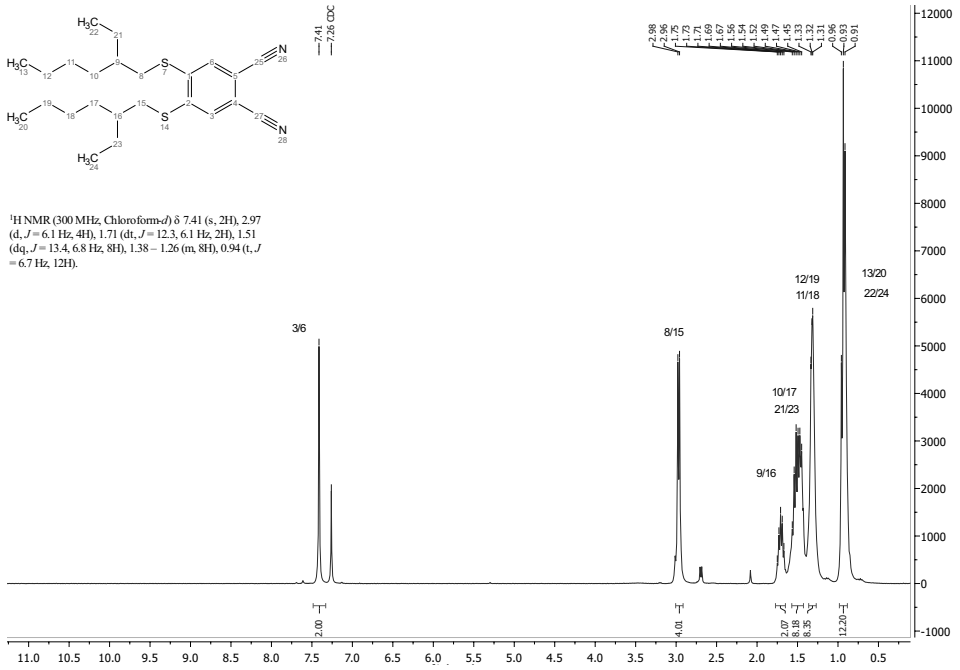

Figure 10.15: ^{1}H-NMR spectrum of compound **10**

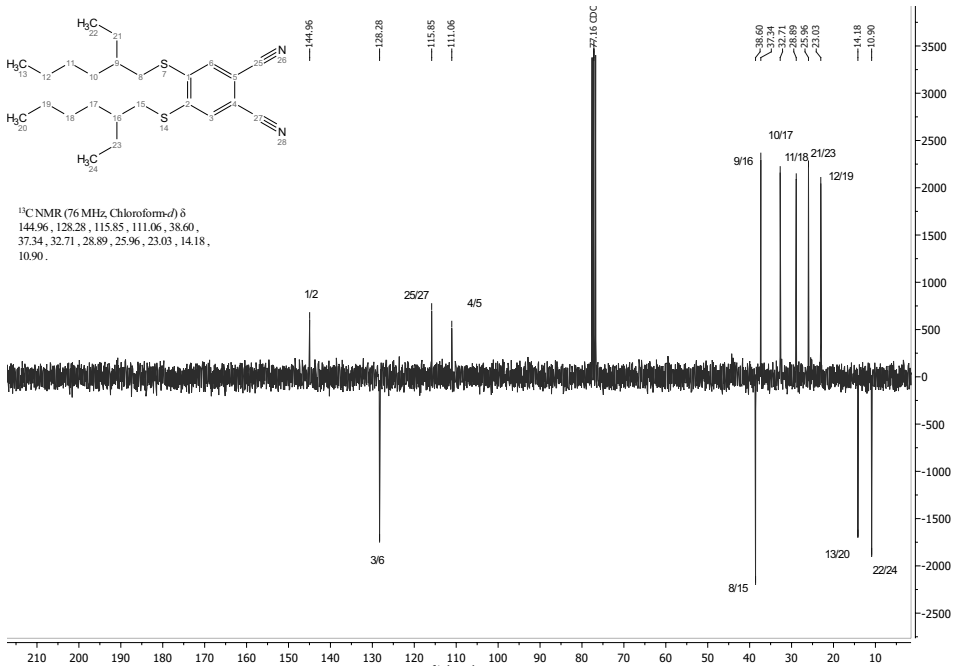

Figure 10.16: APT-NMR spectrum of compound **10**

10.3.9 compound 11

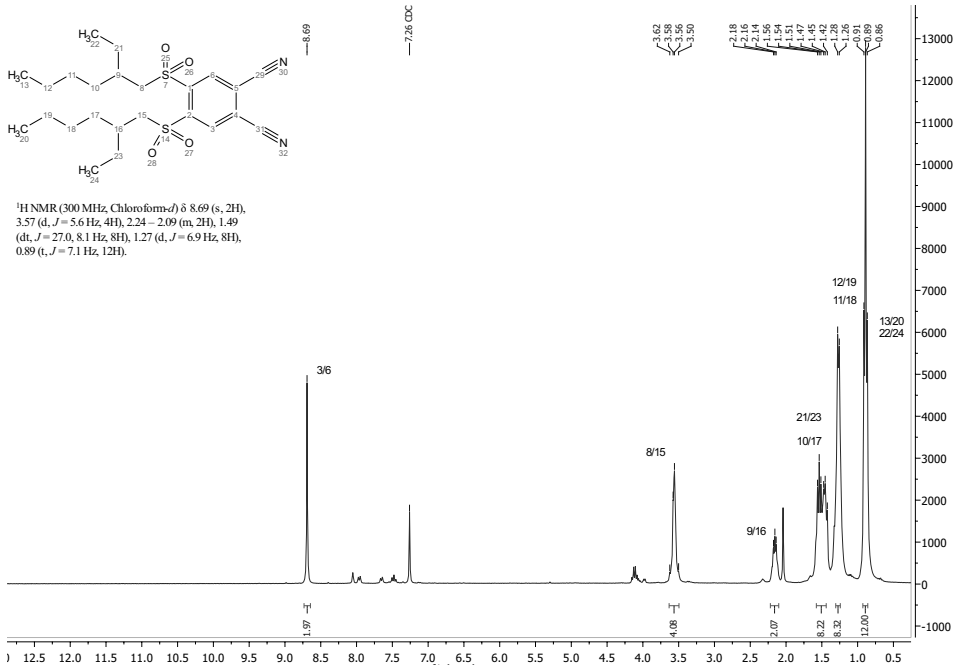

Figure 10.17: ^{1}H-NMR spectrum of compound **11**

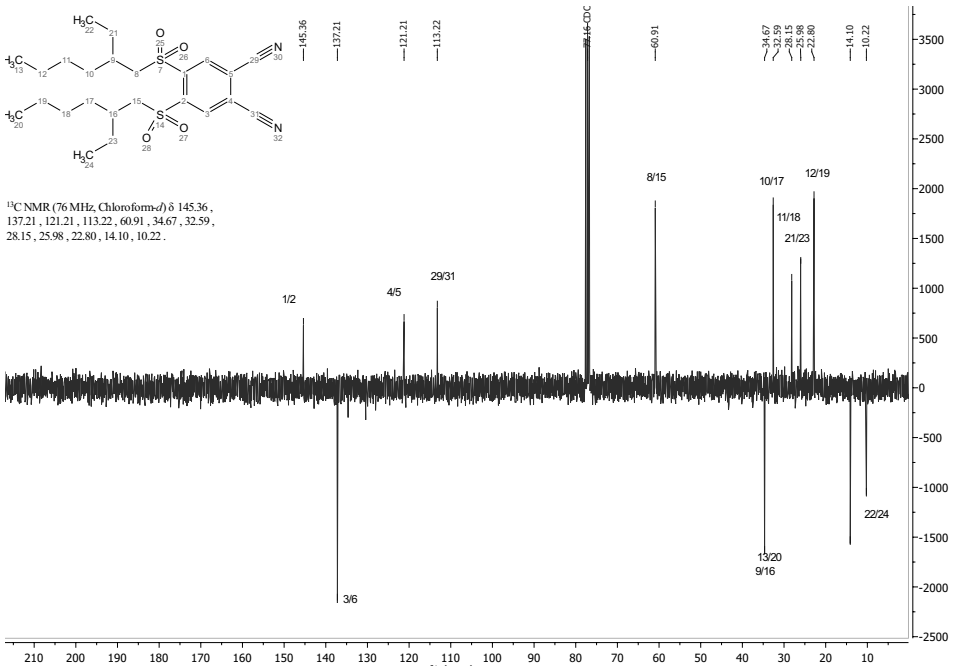

Figure 10.18: APT-NMR spectrum of compound **11**

10.3.10 compound 13

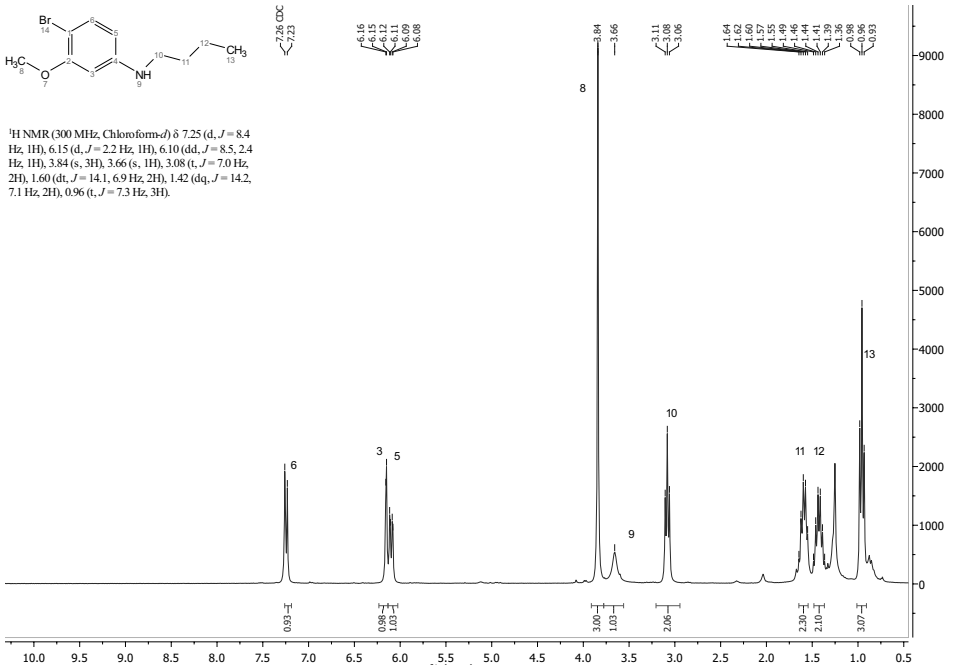

Figure 10.19: ^{1}H-NMR spectrum of compound **13**

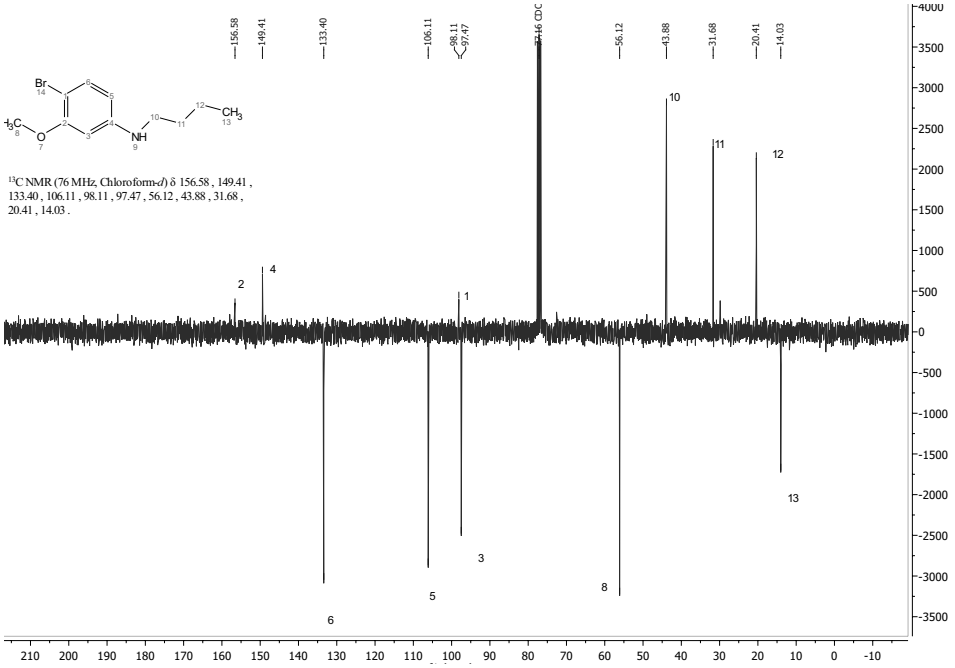

Figure 10.20: APT-NMR spectrum of compound **13**

10.3.11 compound 14

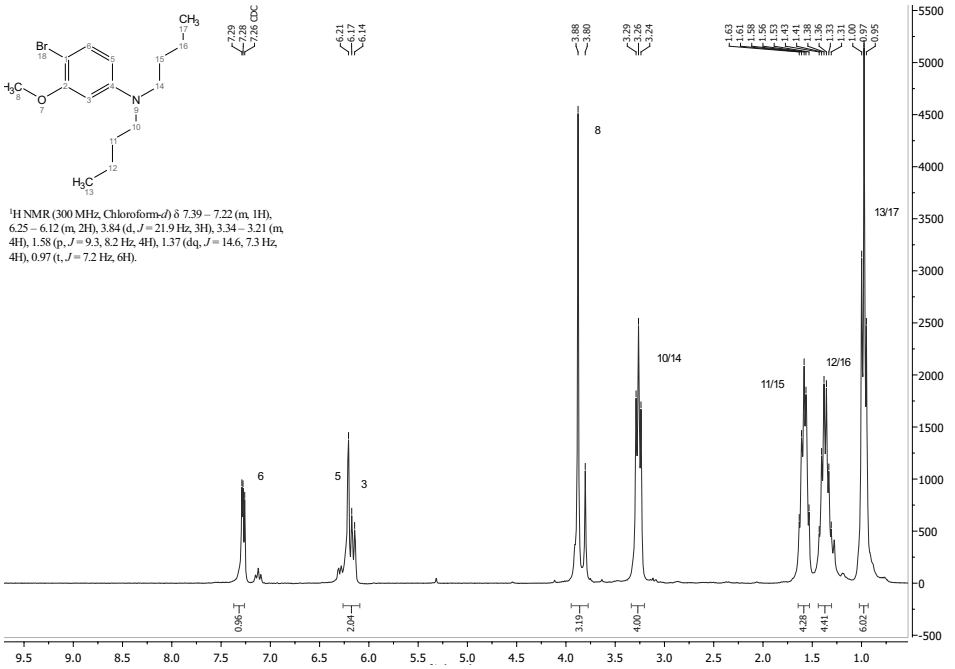

Figure 10.21: ^{1}H-NMR spectrum of compound **14**

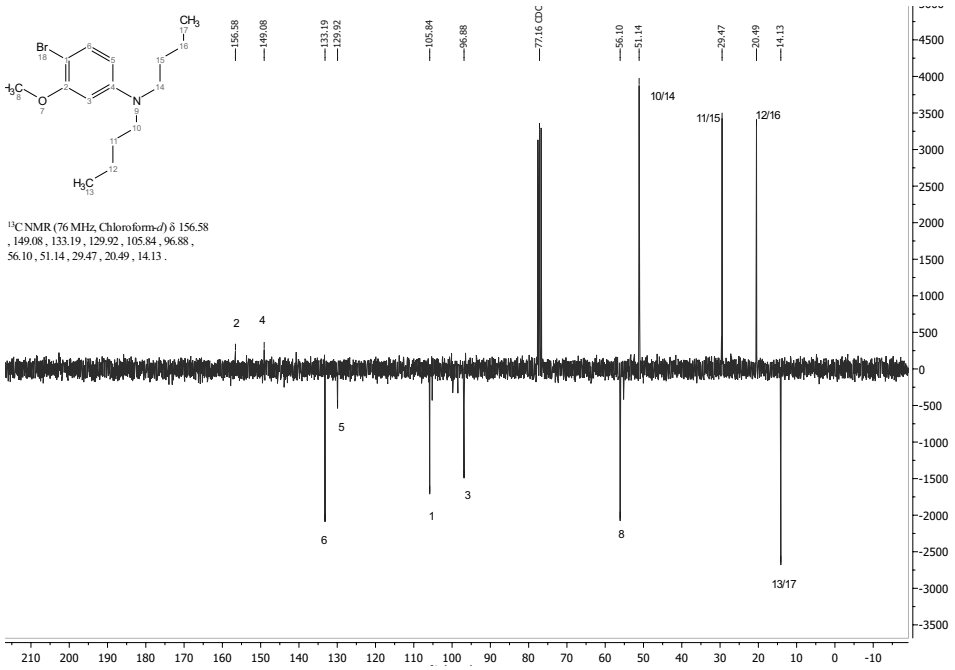

Figure 10.22: APT-NMR spectrum of compound **14**

10.3.12 compound 16

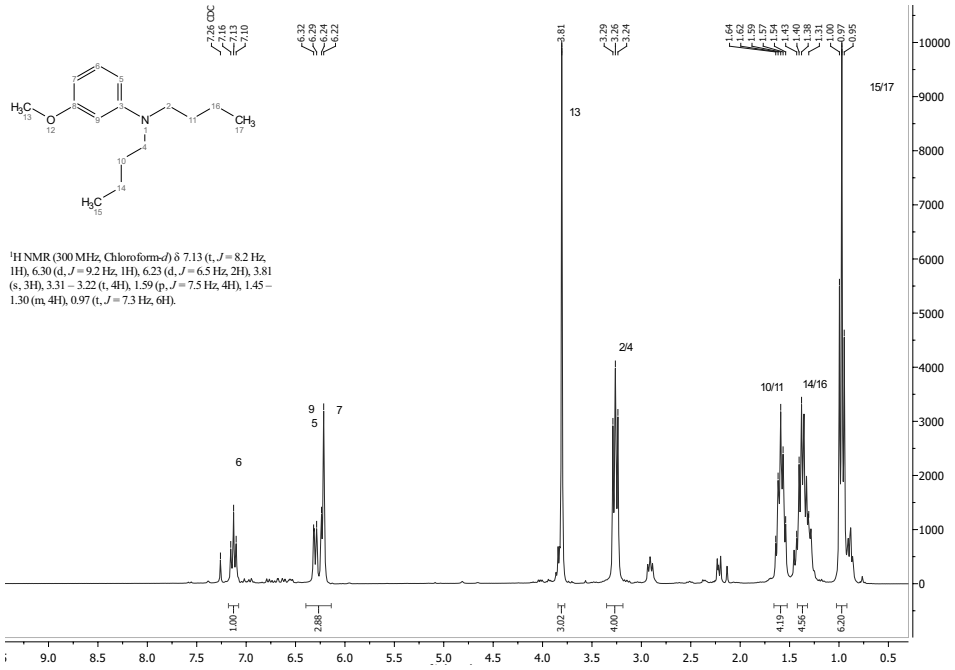

Figure 10.23: ^{1}H-NMR spectrum of compound **16**

10.4 MS Data

10.4.1 compound 6

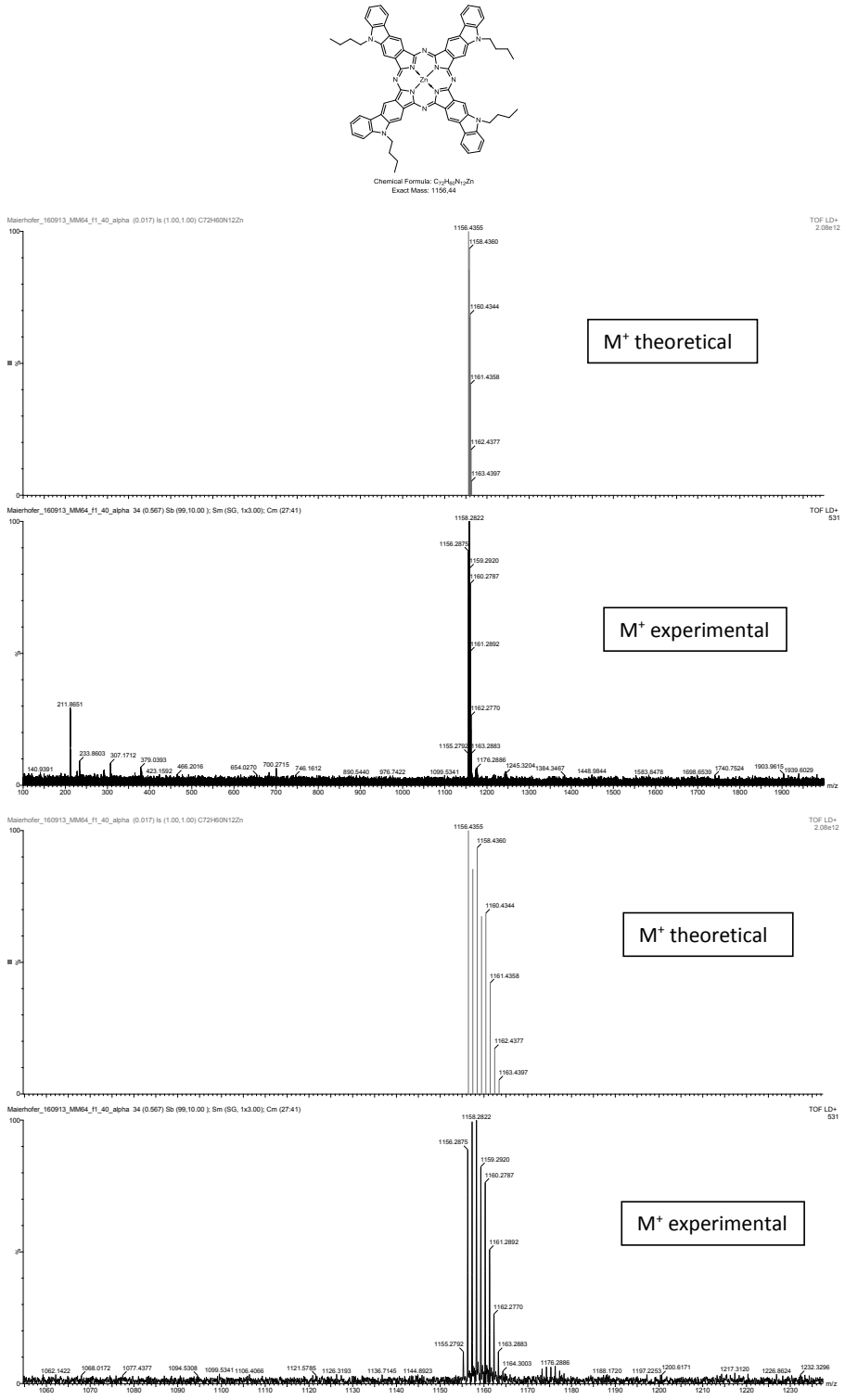

Figure 10.24: MALDI-TOF spectrum of compound **6** (fraction one, picture 2/4) in a alpha matrix with the corresponding isotope pattern (picture 1/3)

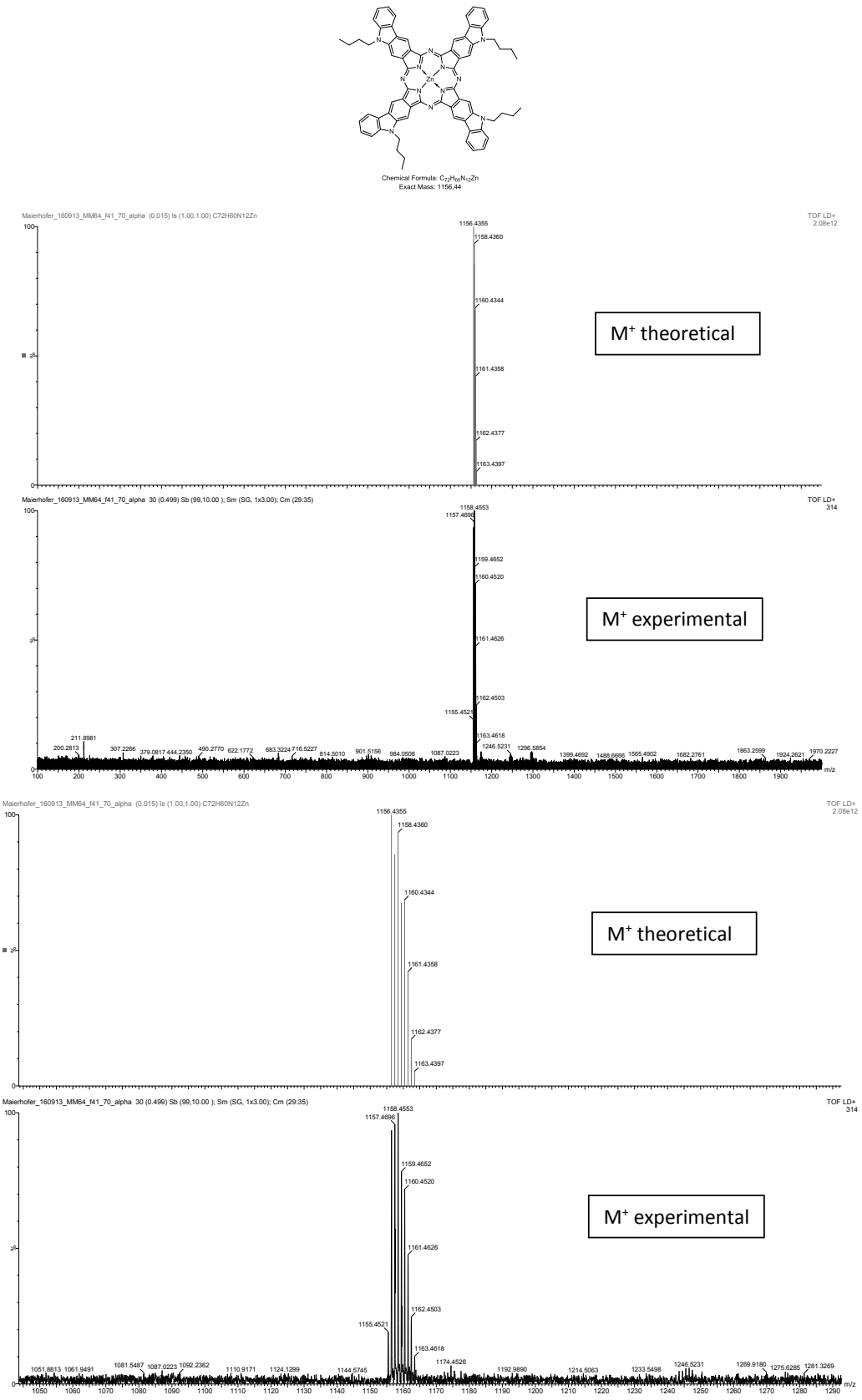

Figure 10.25: MALDI-TOF spectrum of compound **6** (fraction two, picture 2/4) in a alpha matrix with the corresponding isotope pattern (picture 1/3)

10.4.2 compound 7

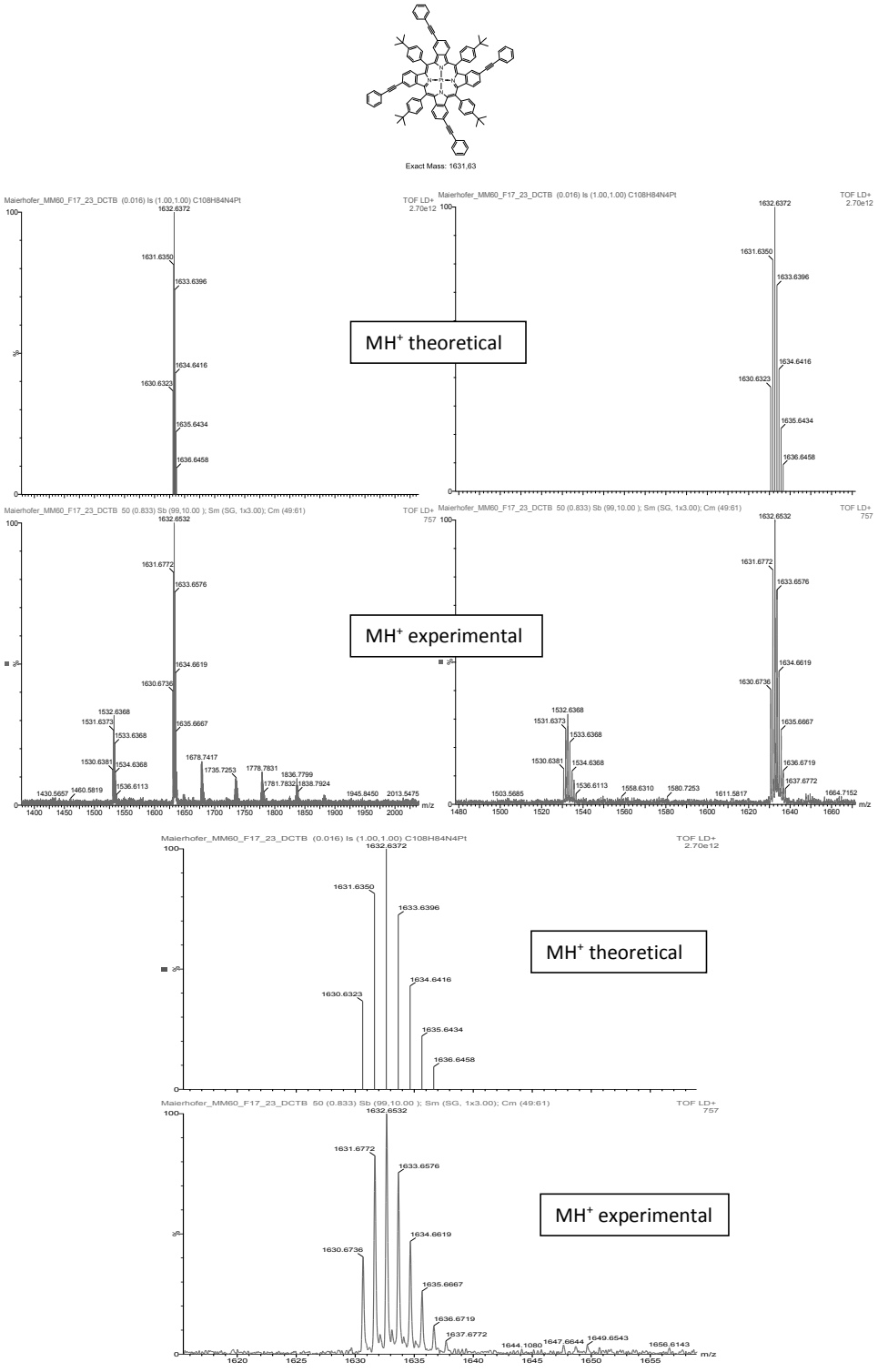

Figure 10.26: MALDI-TOF spectrum of compound **7** in a DCTB matrix with the corresponding isotope pattern (upper pictures)

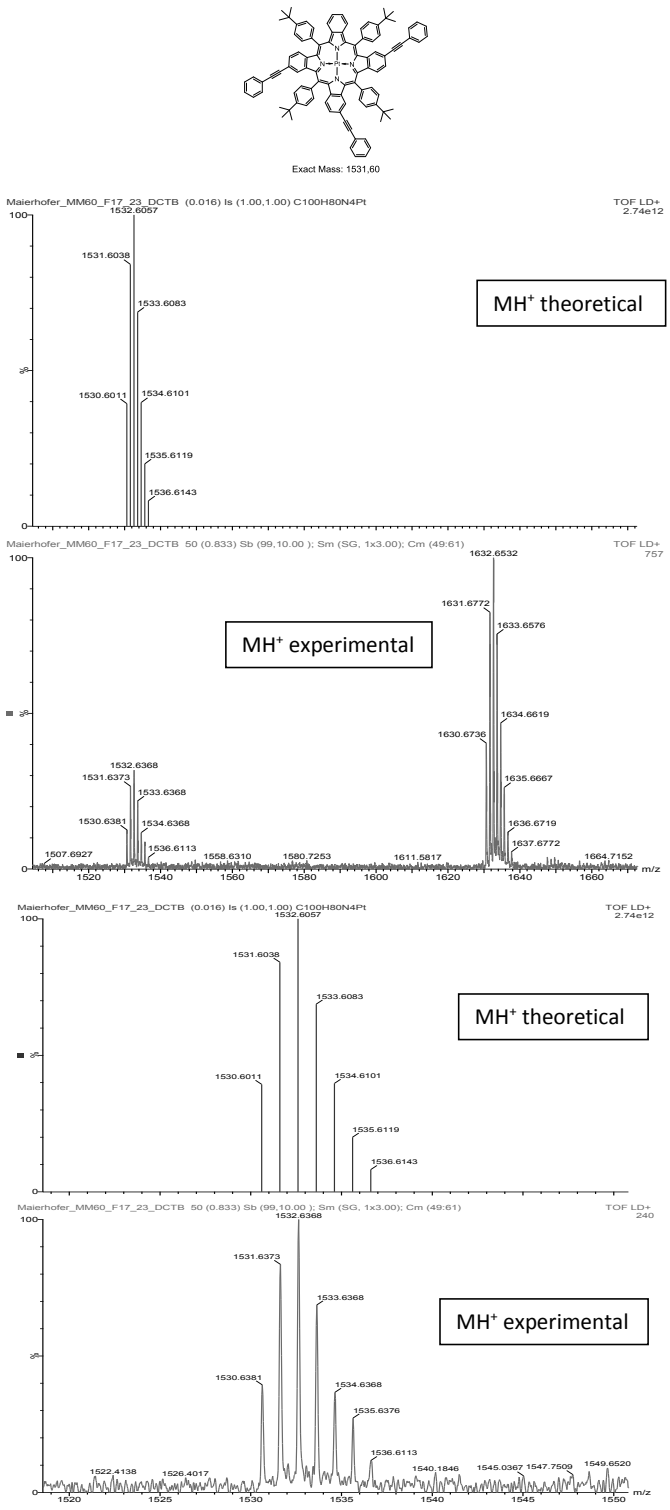

Figure 10.27: MALDI-TOF spectrum of Pt-triPhacetTtBuBP in a DCTB matrix with the corresponding isotope pattern (upper pictures)

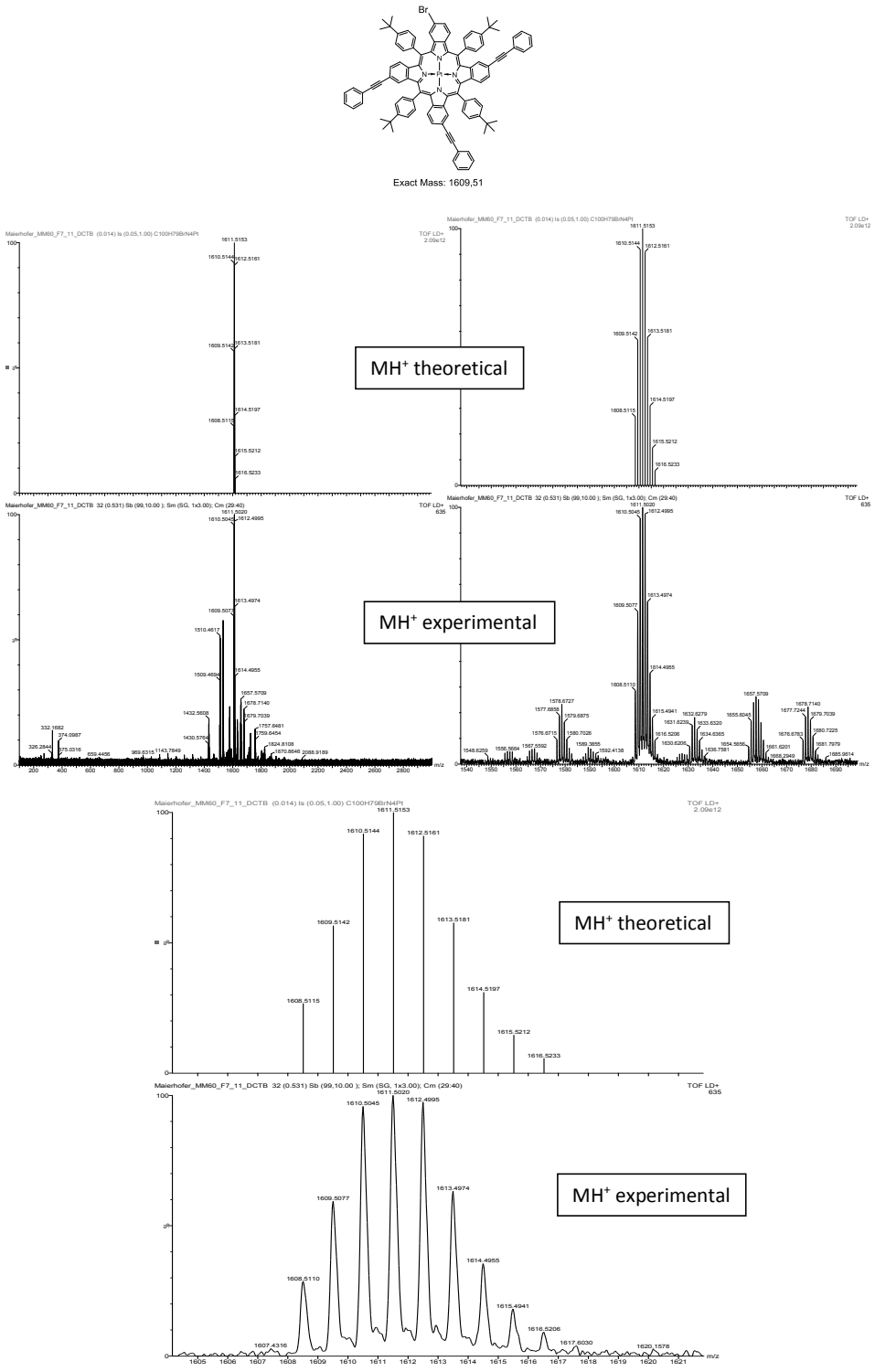

Figure 10.28: MALDI-TOF spectrum of Pt-BrtriPhacetTtBuBP in a DCTB matrix (picture 2/4) with the corresponding isotope pattern (picture 1/3)

10.4.3 compound 8

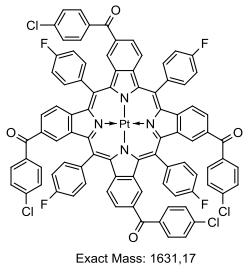

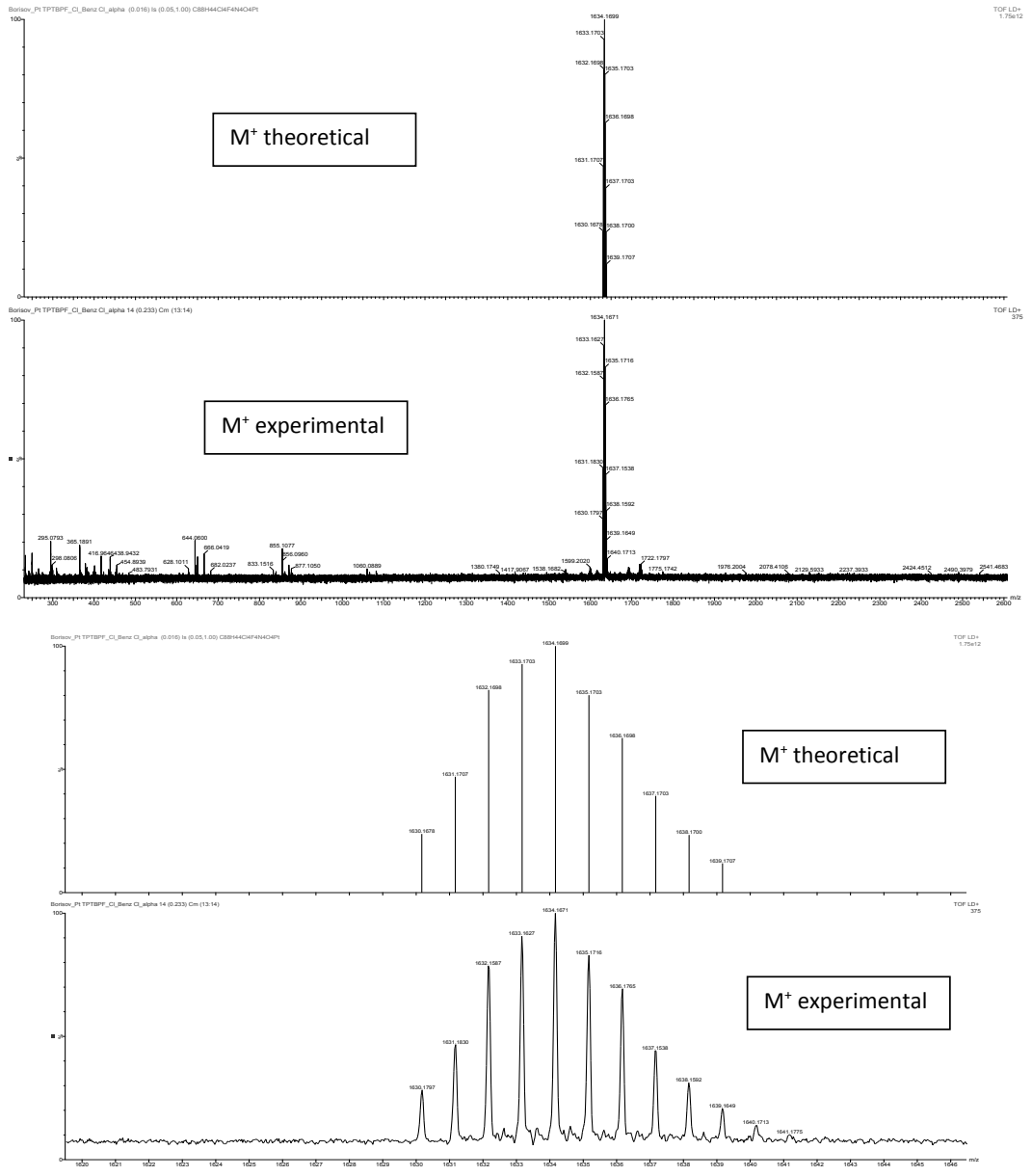

Figure 10.29: MALDI-TOF spectrum of Pt-TPTBPF-benzoyl-Cl in a alpha matrix with the corresponding isotope pattern (upper pictures)

10.4.4 compound 9

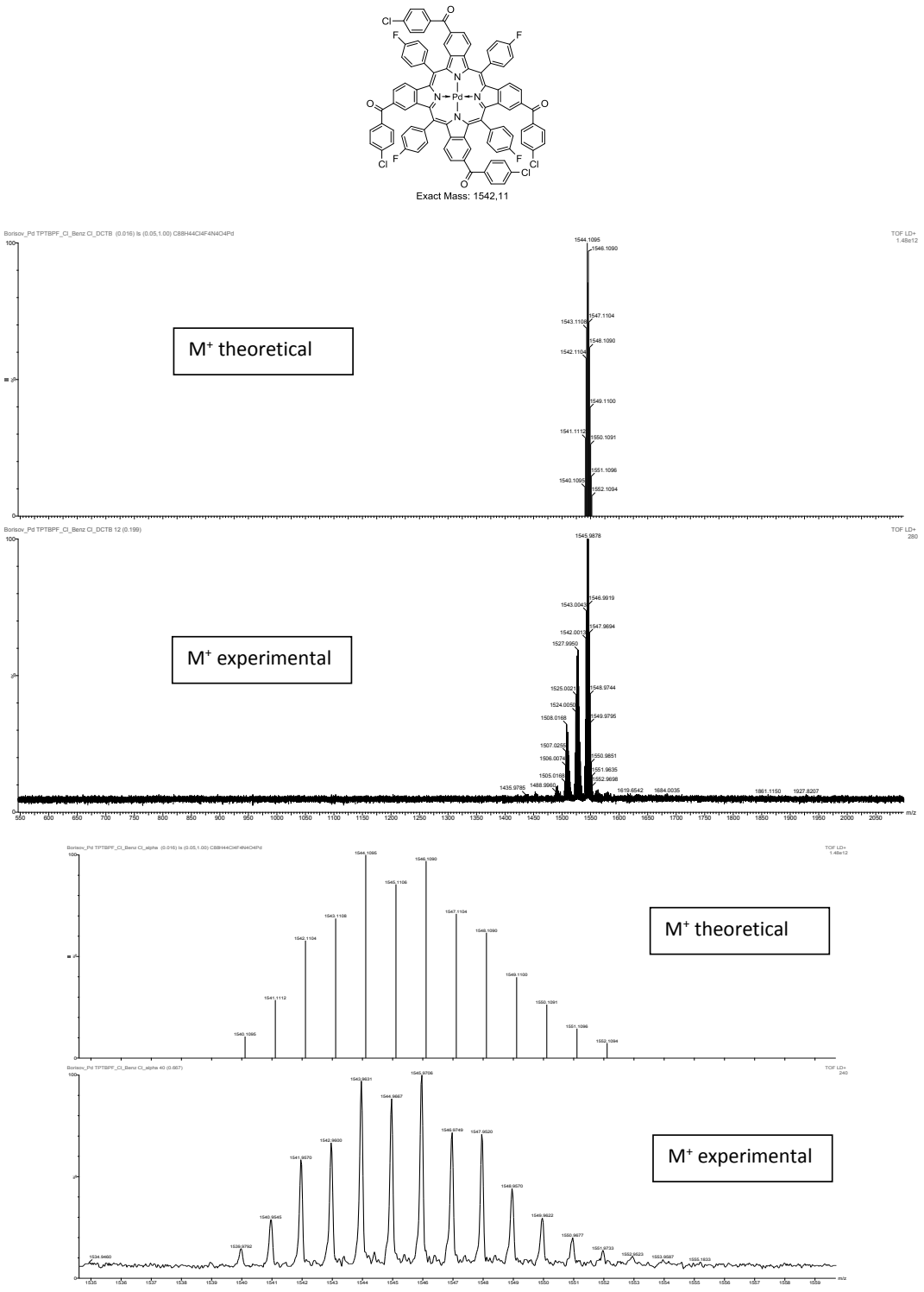

Figure 10.30: MALDI-TOF spectrum of Pd-TPTBPF-benzoyl-Cl in a DCTB matrix with the corresponding isotope pattern (upper pictures)

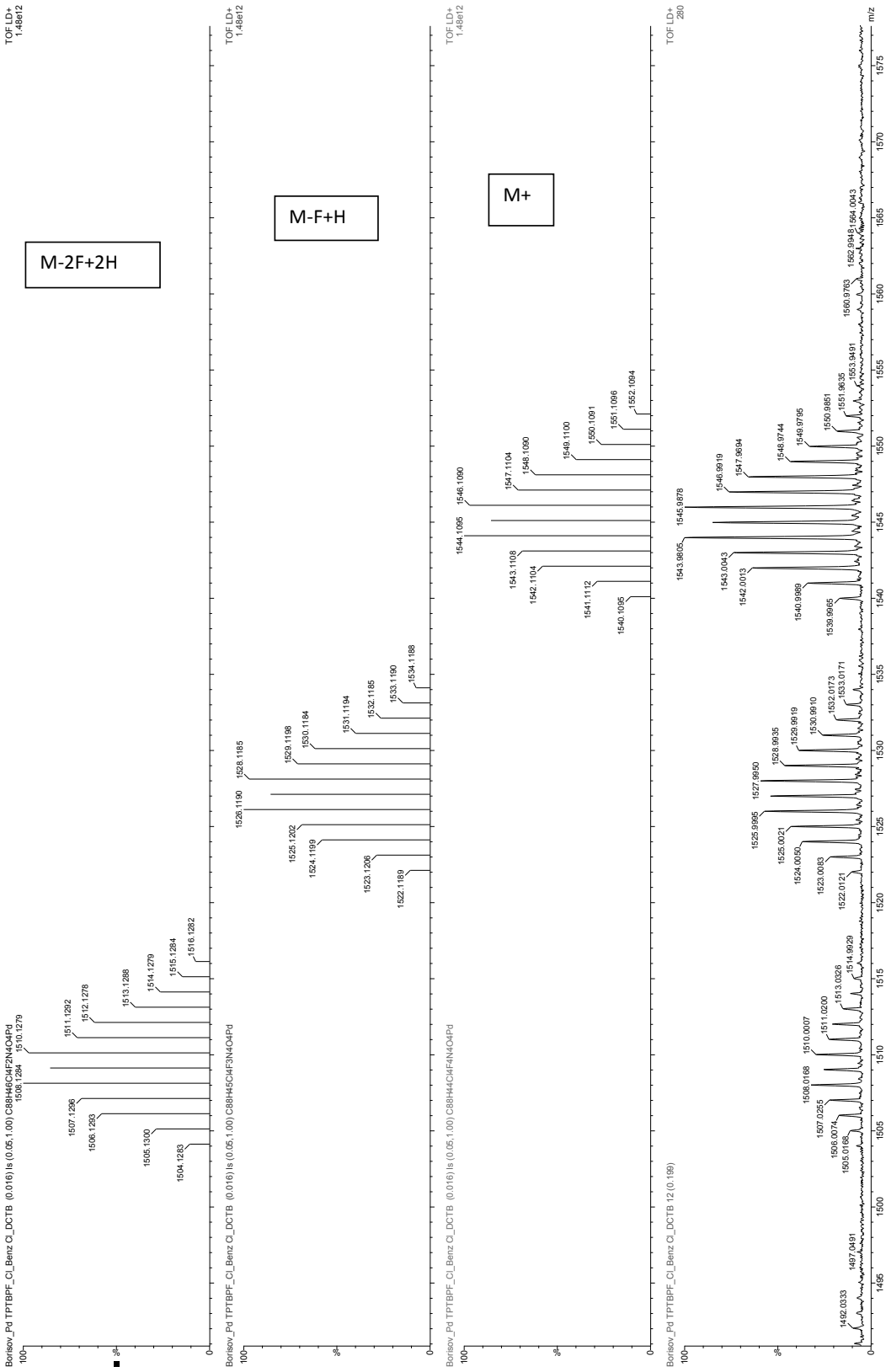

Figure 10.31: Detailed MALDI-TOF spectrum of Pd-TPTBPF-benzoyl-Cl in a DCTB matrix with the corresponding isotope pattern (upper 3 pictures)

10.4.5 Attempted synthesis of Zn – $bEHS_2$ – Pc

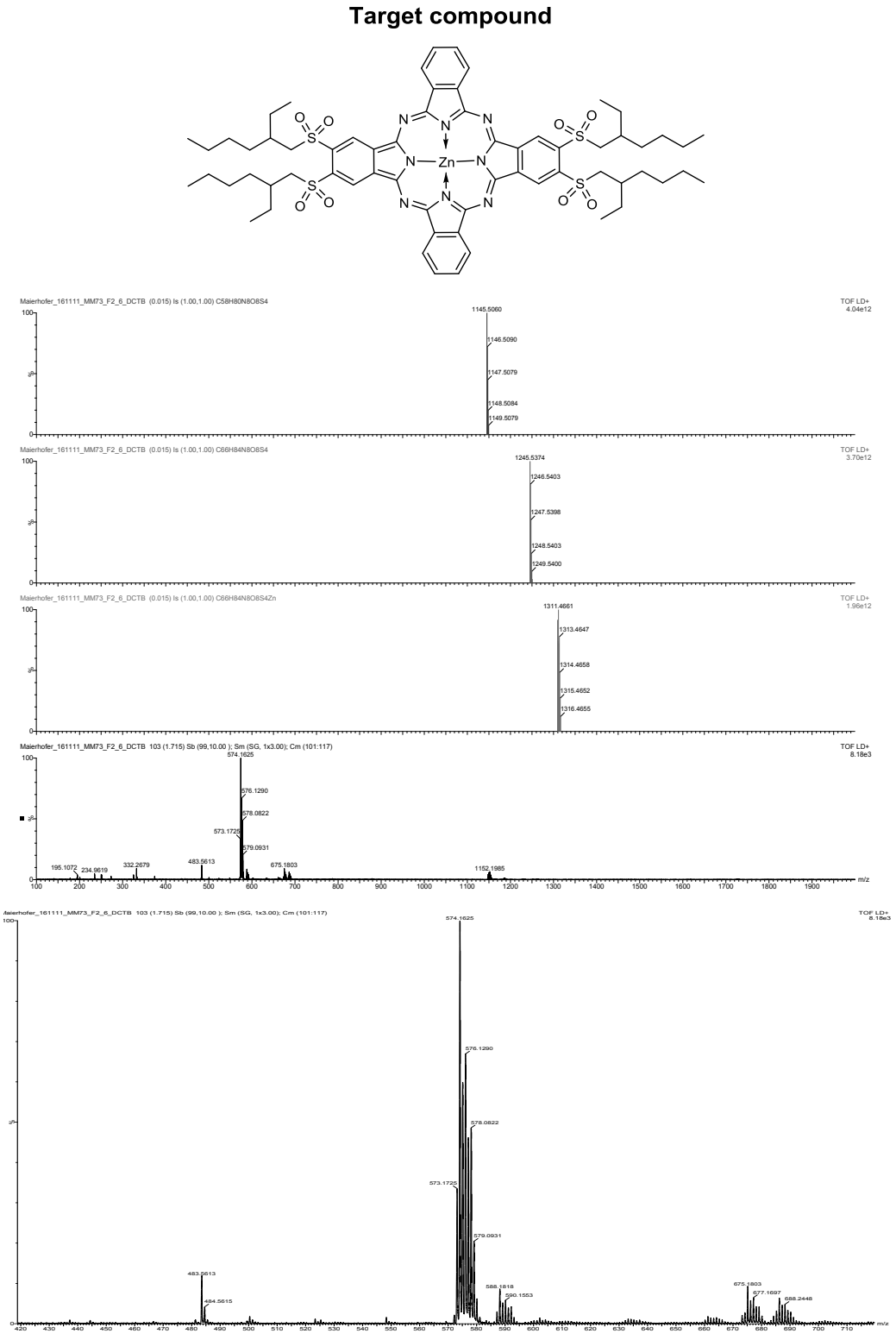

Figure 10.32: MALDI-TOF spectrum of attempted synthesis of Zn – $bEHS_2$ – Pc in a DCTB matrix with the corresponding isotope pattern (upper 3 pictures) for different substitution possibilities

10.5 Supporting information: synthetic considerations

In this section the detailed experimental procedures for each unsuccessful experiment can be looked up.

10.5.1 Compound 3

Here are the different synthetic approaches for the synthesis of compound **3** which are shown in figure 5.2 on page 47 listed. Also the direct synthesis of the nitrile **3** from the ester **1** was tried (see figure 5.3 on page 48).

Reaction A

This synthesis was performed analogously to [116]
Pyridazine-4,5-dicarboxamide (100 mg, 602 µmol, 1.00 eq) was added to 1.5ml (16.3 mmol, 27.0 eq) of $POCl_3$ in a Schlenk flask under Ar atmosphere and stirred for 5 h at 110 °C. The reaction turned to a green-brown color. A mini-workup was conducted. The excess of $POCl_3$ was quenched with saturated $NaHCO_3$. The red-brown solid was indissoluble in DCM, THF, EtOAc or Et_2O. The ^{1}H-NMR data did not show any expected product signals.

Reaction B

This synthesis was performed analogously to [133]
Pyridazine-4,5-dicarboxamide (60.0 mg, 360 µmol, 1.00 eq) was dissolved in 4 ml of a 1+1 mixture of H_2O and acetonitrile in a Schlenk flask. $Pd(OAc)_2$ (4.05 mg, 18.1 µmol, 0.05 eq) was added as catalyst. Due to solubility problems 1 ml of DMF was added after 1 h of stirring at RT. The reaction mixture was heated to 82 °C and stirred for 24 h. After mini-workup which is descried in Reaction A (10.5.1) no product spot could be observed with TLC (silica-gel, DCM:EtOAc 5+1).

Reaction C

This synthesis was performed analogously to [133]
Reaction C is the same one as B (10.5.1) with one difference: as catalyst $PdCl_2$ was used. This reaction does not lead to the desired product.

Reaction D

This synthesis was performed analogously to [134]
$AlCl_3$ (80.3 mg, 602 µmol, 2.00 eq) and NaI (270 mg, 1.81 mmol, 6.00 eq) were stirred in 8 ml of

abs. acetonitrile in a Schlenk flask under Ar atmosphere at RT (yellow solution). After 30 min of stirring pyridazine-4,5-dicarboxamide (50.0 mg, 300 µmol, 1.00 eq) was added. The reaction mixture was heated to 84 °C. This caused a color change to orange. The solution was stirred for 1.5 h at this temperature. After mini-workup which is descried in Reaction A (10.5.1) no product spot could be observed with TLC (silica-gel, DCM:EtOAc 5+1).

Reaction E

This synthesis was performed analogously to [135, 136]
Pyridazine-4,5-dicarboxamide (50.0 mg, 300 µmol, 1.00 eq) was dissolved in 3 ml abs. DMF in a Schlenk flask under Ar atmosphere. Cyanuric chloride (138 mg, 750 µmol, 2.50 eq) was added at 0 °C. The solution was stirred for 15 h at RT. The reaction turned to a yellow color. After mini-workup which is descried in Reaction A (10.5.1) the ^{1}H-NMR data did not show any expected product signals.

Reaction F

This synthesis was performed analogously to [137]
$AlCl_3$ (45.0 mg, 338 µmol, 1.12 eq) and KI (151 mg, 910 µmol, 3.02 eq) were stirred in 7.5 ml of a 5+1 mixture of H_2O and acetonitrile in a Schlenk flask at RT. Before adding pyridazine-4,5-dicarboxamide (50.0 mg, 300 µmol, 1.00 eq) the solution was stirred for 30 min at RT. Then the reaction was heated to 80 °C and stirred for 7 h (yellow solution). After removal of the solvent under reduced pressure the residue was diluted with 10 ml H_2O and the product extracted with DCM ($3 \cdot 20$ ml). The red organic layer was treated with 5% aq. NH_3 (color change to light yellow). The organic layer was washed with 20 ml H_2O, dried over Na_2SO_4. The solvent was removed under reduced pressure. The ^{1}H-NMR data did not show any expected product signals.

Reaction G

This synthesis was performed analogously to [138]
Pyridazine-4,5-dicarboxamide (50.0 mg, 300 µmol, 1.00 eq) was dissolved in 3 ml abs. DMF in a Schlenk flask under Ar atmosphere. $SOCl_2$ (55 μl, 750 µmol, 2.50 eq) was added dropwise at 0 °C. The solution was stirred for 15 h at RT. The reaction turned to a yellow color. After mini-workup which is descried in Reaction A (10.5.1) the ^{1}H-NMR data did not show any expected product signals.

Compound 3: direct synthesis ester to nitrile

This synthesis was performed analogously to [130]
NaO^tBu (77.2 mg, 803 µmol, 1.80 eq) was dried in a Schlenk flask under Ar atmosphere. After drying 2 ml abs. THF and DIBAl-H (760 μl, 760 µmol, 1.70 eq) were added at 0 °C and the reaction mixture was stirred for 1 h at RT. Then diethyl pyridazine-4,5-dicarboxylate (100 mg, 446 µmol, 1.00 eq) predissolved in 3 ml of abs. THF were added dropwise at 0 °C to the solution (color change to red). The reaction was stirred for 4 h. 3 ml of 25% aq. NH_3 and I_2 (453 mg, 1.78 mmol, 4.00 eq) were added at 0 °C (color change to orange). The reaction mixture was stirred for 3 h at RT. The reaction was poured onto 20 ml of a saturated solution of Na_2SO_3 and the product was extracted with EtOAc (3*100 ml). The organic layer was dried over Na_2SO_4. The solvent was removed under reduced pressure. The ^{1}H-NMR data did mainly show signals of the substrate and not of the desired dinitrile.

10.5.2 Porphyrin modification by Friedel-Crafts acylation

target compound: Pt-TPTBPF-naphthalen-1(4H)-one

In a Schlenk flask Pt-TPTBPF (10.0 mg, 9.40 µmol, 1.00 eq) was dissolved in 1,2-dichlorobenzene (5 ml) under Ar atmosphere (green solution). 2-(Chloromethyl)benzoyl chloride (27.0 µl, 185 µmol, 20.0 eq) and $AlCl_3$ (20.0 mg, 150 µmol, 16.2 eq) were added to the solution. The reaction mixture was heated to 130 °C and stirred for 30 min. The reaction progress was monitored via absorption spectroscopy (solvent: $CHCl_3$, 1 drop of EtOH). After 30 min, another 20 eq 2-(chloromethyl)benzoyl chloride and 16.2 eq $AlCl_3$ were added. The reaction mixture was heated to 160 °C for 30 min. The reaction progress was detected via absorption spectroscopy. The green soltuion was cooled down to RT. In the work-up reaction mixture was treated with EtOH:H_2O (1+1, each 20 ml) and stirred for 10 minutes to neutralize the excess of $AlCl_3$. After addition of DCM, the organic layer was washed with dest. H_2O, dried over Na_2SO_4 and the solvent was removed under reduced pressure. Finally the crude product was purified via flash column chromatography (silica-gel, cond. toluene, gradient elution starting from DCM:Tol 1+10 ending with DCM:THF 3+1), yielding a dark green solid.

target compound: Pt-TPTBPF-DBr-naphthalene

In a Schlenk flask Pt-TPTBPF (10.0 mg, 9.40 µmol, 1.00 eq) was dissolved in 1,2-dichlorobenzene (5 ml) under Ar atmosphere (green solution). α, α, $\acute{\alpha}$, $\acute{\alpha}$-Tetrabromo-o-xylene (78.0 mg, 185 µmol, 20.0 eq) and $AlCl_3$ (40.0 mg, 300 µmol, 32.4 eq) were added to the solution. The reaction mixture was heated to 130 °C and stirred for 30 min. The reaction progress was monitored via absorption spectroscopy (solvent: $CHCl_3$, 1 drop of EtOH). A significant change in the absorption spectrum was observable. The reaction mixture was cooled to RT. In the work-up reaction mixture was treated with EtOH:H_2O (1+1, each 20 ml) and stirred for 10 minutes to neutralize the excess of $AlCl_3$. DCM was added, the organic layer was washed with dest. H_2O, dried over

Na_2SO_4 and the solvent was removed under reduced pressure. A new absorption spectrum shows that Pt-TPTBPF is partly reformed. Finally the raw product was purified via flash column chromatography (silica-gel, cond. CH, gradient elution starting from CH:DCM 12+1 ending with THF:MeOH 5+1), yielding no desired product, only Pt-TPTBPF could be observed. Absorption spectra were measured in toluene.

target compound: Pt-TPTAPF

In a Schlenk flask Pt-TPTBPF (10.0 mg, 9.40 µmol, 1.00 eq) was dissolved in 1,2-dichlorobenzene (5 ml) under Ar atmosphere (green solution). α, $\acute{\alpha}$-Dibromo-o-xylene (97.0 mg, 370 µmol, 40.0 eq) and $AlCl_3$ (40.0 mg, 300 µmol, 32.4 eq) were added to the solution. The reaction mixture was heated to 130 °C and stirred for 45 min. The reaction progress was monitored via absorption spectroscopy (solvent: $CHCl_3$, 50 µmol of EtOH). The green soltuion was cooled down to RT. In the work-up reaction mixture was treated with EtOH:H_2O (1+1, each 20 ml) and stirred for 10 minutes to neutralize the excess of $AlCl_3$. After addition of DCM, the organic layer was washed with dest. H_2O, dried over Na_2SO_4 and the solvent was removed under reduced pressure.

TLC: R_f= 0.18 (silica-gel, CH:DCM 15+1)

For the second step the green solid (14.0 mg, 9.27 µmol, 1.00 eq) of step one was dissolved in 6 ml abs. toluene in a Schlenk flask. DDQ (34.0 mg, 148 µmol, 16.0 eq) was dissolved in 2 ml abs. toluene and added dropwise to the stirring solution. The reaction mixture was heated to 105 °C and stirred for 1 h. Reaction progress was monitored via absorption spectroscopy (solvent: toluene).

target compound: Pt-TPTtBuBPBr-2-benzoyl-Br

In a Schlenk flask Pt-TPTtBuBPBr (5.00 mg, 3.23 µmol, 1.00 eq) was dissolved in 1,2-dichlorobenzene (5 ml) under Ar atmosphere (green solution). 2-Bromobenzoyl-chloride (9.00 µl, 64.0 µmol, 20.0 eq) and $AlCl_3$ (10.0 mg, 75 µmol, 23.0 eq) were added to the solution. The reaction mixture was heated to 130 °C and stirred for 30 min. The reaction progress was monitored via absorption spectroscopy (solvent: $CHCl_3$, 50 µl of EtOH). After 30 min another 20.0 eq of 2-bromobenzoyl-chloride and 23.0 eq of $AlCl_3$ were added. The reaction mixture was again stirred for 30 min. Then the reaction mixture was cooled to RT. Reaction mixture was treated with EtOH:H_2O (1+1, each 20 ml) and stirred for 10 minutes to neutralize the excess of $AlCl_3$. After addition of DCM, the organic layer was washed with dest. H_2O, dried over Na_2SO_4 and the solvent was removed under reduced pressure. Finally the crude product was purified via flash column chromatography (silica-gel, cond. CH, gradient elution starting from CH:DCM 15+1 ending with EE:MeOH 10+1) yielding a dark green solid.

Yield: 5.00 mg (40%)

TLC: R_f= 0.59 (silica-gel, CH:EE 20+1)

$\lambda_{max}(CHCl_3)$: 441 nm (1.00), 573 nm (0.08), 613 nm (0.44), 625 nm (0.46)

For the second step the green solid (5.00 mg, 2.19 µmol, 1.00 eq) of step one was dissolved in 5 ml abs. NMP in a Schlenk flask under Ar atmosphere. 1-Dodecylamine (8.13 mg, 44 µmol, 20.0 eq) was added to the green solution. The reaction mixture was heated to 130 °C and stirred for 2 h. For monitoring the reaction progress absoprtion spectra (solvent: toluene) as well as TLC (silica-gel, CH:EE, 7+1) were investigated but no product could be observed.

10.5.3 New Porphyrin with thiadiazole as main building block

target compound: Pt-TPTBPF-(1,2,5-thiadiazole)

5,6-Dicyanobenzo[c]-1,2,5-thiadiazole (1.60 mg, 8.61 µmol, 4.00 eq), 2-(4-fluorophenyl)acetic acid (1.99 mg, 12.9 µmol, 6.00 eq) and zinc-4-fluorophenylacetate (800 µg, 2.15 µmol, 1.00 eq) were mixed together and sealed in a small capillary. The capillary was put onto a 280 °C heating block and heated to 320 °C. After 30 min absorption spectrum was taken (solvent: toluene). No specific porphyrin signals could be observed. This reaction was also conducted with two other reaction conditions. First the starting temperature was increased to 320 °C and ending at 340 °C. Another approach was conducted with Ar atmosphere. Also the reaction time screening was investigated (20, 30 and 40 min). None of the described reaction conditions worked for this type of precursor.

10.5.4 Highly soluble Porphyrin and Phthalocyanine dyes for J-aggregates

zinc(II)-di(4,5-bis((2-ethylhexyl)sulfonyl)-phthalocyanine: $Zn-bEHS_2-Pc$

This synthesis was performed analogously to [122]
$Zn(CH_3COO)_2 \cdot H_2O$ (57.1 mg, 260 µmol, 5.00 eq) and 4,5-bis((2-ethylhexyl)sulfonyl)phthalonitrile (50.0 mg, 104 µmol, 1.00 eq) and phthalonitrile (13.3 mg, 104 µmol, 1.00 eq) were dissolved in a Schlenk flaks under Ar atmosphere in 5 ml abs. DMF giving an orange solution. After adding 3 drops of DBU as catalyst a color change occurred (red solution). The reaction was heated to 155 °C and stirred for 16 h. The reaction progress was monitored absorption spectroscopy (solvent: toluene). The dark green solution was cooled to RT and precipitated into a 3+2 mixture of H_2O:MeOH. The product was extracted with DCM:EtOAc 1+1 ($3 \cdot 100$ ml), the organic layer was dried over Na_2SO_4 and the solvent was removed under reduced pressure. The crude solid product was further purified via flash column chromatography (silica-gel, cond. CH, CH:EE 3+1) yielding no pure fraction of solid green product. The MS spectra showed no desired product.

10.5.5 Pt(II) complexes supported by tetradentate N_2O_2 chelates: Diphenyphenanthroline system

$dBAN_2O_2$–dpp: published method for bipyridyl system

This synthesis was performed analogously to [126]
4-Bromo-N,N-dibutyl-3-methoxyaniline (82.3 mg, 261 µmol, 5.80 eq) was dissolved in 1 ml abs. Et_2O in a Schlenk flask under Ar atmosphere. The solution was stirred at RT. 7.00 mg Li metal pieces (1.01 mmol, 22.0 eq) were added and the reaction (yellow solution) was heated to 40 °C for 2 h. In a second Schlenk flask 4,7-diphenyl-1,10-phenanthroline (15.0 mg, 45.1 µmol, 1.00 eq) was dissolved in abs. toluene (1.5 ml) under Ar atmosphere. The in situ generated Li-species was added with a syringe to the 4,7-diphenyl-1,10-phenanthroline solution and the reaction mixture was heated first to 50 °C (remove the Et_2O) then to 110 ° for 24 h. The reaction was poured into H_2O (10 ml) to hydrolyze the products. The organic layer was separated and stirred with MnO_2 (161 mg, 1.85 mmol, 41.0 eq) for 24 h at RT. After filtration the organic orange layer was dried over Na_2SO_4, the solvent was removed under reduced pressure. Absorption spectra were taken in toluene and TLC (silica-gel, CH:EE, 5+1) was conducted but no product could be observed.

$dBAN_2O_2$–dpp: metal-halogen exchange with nBuLi

This synthesis was performed analogously to [126]
4-Bromo-N,N-dibutyl-3-methoxyaniline (82.3 mg, 261 µmol, 5.80 eq) was dissolved in 1 ml abs. THF in a Schlenk flask under Ar atmosphere. The soltuion was cooled to -75 °C. n-Butyllithium solution (108 µl 270 µmol, 6.00 eq, 2.5 M in hexanes) was added drop-wise via a syringe (color change yellow to orange). The reaction mixture was stirred for 30 min. To confirm that the metal-halogen exchange was successful a mini work-up was conducted. A sample of the orange solution (20 µl) was added to a NH_4Cl solution for exchanging the lithium atom by a hydrogen atom. The product was extracted with DCM, the organic layer was dried over Na_2SO_4. To confirm the metal-halogen exchange the solution was measured via GC-MS.

In a second Schlenk flask 4,7-diphenyl-1,10-phenanthroline (15.0 mg, 45.1 µmol, 1.00 eq) was dissolved in abs. toluene (1.5 ml) under Ar atmosphere (colorless solution). The in situ generated Li-dbutMeOA was added drop-wise with a syringe at 0 °C to the 4,7-diphenyl-1,10-phenanthroline solution. The reaction mixture was first heated to 70 °C (to remove the THF) and then to 110 °C. The reaction was stirred for 24 h (green solution). In the work-up the reaction was poured into H_2O (10 ml) to hydrolyze the products.

The organic layer was divided into two vials (A and B). Solution A was stirred with MnO_2 (161 mg, 1.85 mmol, 41.0 eq) for 24 h at RT. After filtration the organic orange layer was dried over Na_2SO_4, the solvent was removed under reduced pressure. To solution B DDQ (9.70 µl, 72.2 µmol, 3.00 eq) was added and stirred in the dark at RT for 24 h. Absorption spectra were taken in toluene and TLC (silica-gel, CH:EE, 5+1) was conducted but no product could be

observed. NMR measurements also showed no product formation.

$dBAN_2O_2$−dpp: metal-halogen exchange with tert-BuLi

This synthesis was performed analogously to [126, 139]
4-Bromo-N,N-dibutyl-3-methoxyaniline (54.8 mg, 175 µmol, 5.80 eq) was dissolved in 1 ml abs. THF in a Schlenk flask under Ar atmosphere. The soltuion was cooled to -78 °C. tert-Butyllithium solution (241 µl 349 µmol, 11.6 eq, 1.45 M in pentane) was added drop-wise via a syringe (color change yellow to orange). The reaction mixture was stirred for 30 min. The in situ generated isobutan/isobuten was removed from the system via a gas bubbler and Ar counterflow. To confirm that the metal-halogen exchange was successful a mini work-up was conducted. A sample of the orange solution (20 µl) was added to a NH_4Cl solution for exchanging the lithium atom by a hydrogen atom. The product was extracted with DCM, the organic layer was dried over Na_2SO_4. To confirm the metal-halogen exchange the solution was measured via GC-MS.

In a second Schlenk flask 4,7-diphenyl-1,10-phenanthroline (10.0 mg, 30.1 µmol, 1.00 eq) was dissolved in abs. toluene (1.5 ml) under Ar atmosphere (colorless solution). The in situ generated Li-dbutMeOA was added drop-wise via a cannula system with N_2 gas pressure at 0 °C to the 4,7-diphenyl-1,10-phenanthroline solution. The reaction mixture was first heated to 70 °C (to remove the THF) and then to 110 °C. The reaction was stirred for 24 h (yellow solution). In the work-up the reaction was poured into H_2O (10 ml) to hydrolyze the products. The organic layer was separated and for oxidation MnO_2 (107 mg, 1.23 mmol, 41.0 eq) was added to the solution. The reaction mixture was stirred at RT for 24 h. After filtration the solvent was removed under reduced pressure. TLC (silica-gel, CH:EE, 5+1/1+1/1+5) showed no product formation.